AA Technical Memorandum ERL ARL-159

THE NOAA-ERL-ARL SOLAR UV RADIATION AND CLIMATE RESEARCH PROJECT

PROGRAM DESCRIPTION AND PROGRESS REPORT

Lawrence C. Puga
Richard F. Donnelly
Joan Barrett
Glenn Falcon
Karl Pfendt
David Stevens
Meiqing Gao

Air Resources Laboratory
Silver Spring, Maryland
November 1987

noaa NATIONAL OCEANIC AND ATMOSPHERIC ADMINISTRATION / Environmental Research Laboratories

NOAA Technical Memorandum ERL ARL-159

THE NOAA-ERL-ARL SOLAR UV RADIATION AND CLIMATE RESEARCH PROJECT

PROGRAM DESCRIPTION AND PROGRESS REPORT

Lawrence C. Puga
Richard F. Donnelly
Joan Barrett
Glenn Falcon
Karl Pfendt
David Stevens

Sun-Climate Staff
Boulder, Colorado

Meiqing Gao

Cooperative Institute for Research in Environmental Sciences
University of Colorado at Boulder

Air Resources Laboratory
Silver Spring, Maryland
November 1987

UNITED STATES DEPARTMENT OF COMMERCE

C.William Verity
Secretary

NATIONAL OCEANIC AND ATMOSPHERIC ADMINISTRATION

Environmental Research Laboratories

Vernon E. Derr,
Director

NOTICE

Mention of a commercial company or product does not constitute an endorsement by NOAA Environmental Research Laboratories. Use for publicity or advertising purposes of information from this publication concerning proprietary products or the tests of such products is not authorized.

For sale by the National Technical Information Service, 5285 Port Royal Road
Springfield, VA 22161

TABLE OF CONTENTS

The NOAA-ERL-ARL Solar UV Radiation and Climate Research Project

Program Description and Progress Report

Lawrence C. Puga, Richard F. Donnelly, Joan Barrett,
Karl Pfendt, David Stevens, Glenn Falcon
Sun-Climate Staff, Air Resources Laboratories, NOAA ERL
Boulder, Colorado 80303

and

Meiqing Gao*
Cooperative Institute for Research in Environmental Sciences
University of Colorado
Boulder, Colorado 80303

Progress of the Solar UV Radiation and Climate Research Project, which studies temporal variations in solar UV irradiance, the effects of those variations on stratospheric ozone and temperature, and any subsequent changes in global climate and weather patterns, is discussed. The last report of this nature was published in February, 1984; this report concentrates on research conducted since that report which has not been previously published in other formats. Changes in the goals of the program due to completed research and changes in personnel are also reviewed.

A series of analyses conducted to extensively compare the NIMBUS-7 observed UV to Ca II K plage modeled UV, 10830A ground based observations, and the Ca II K plage index for short-term variations; their similarities remain questionable over the long-term such as an entire solar cycle. In addition, an extended analysis of NIMBUS-7 observed UV for many wave-lengths between 171 and 285nm shows the common characteristics for all the wavelengths; the 13- and 27-day power spectra for these wavelengths are also examined. The NIMBUS-7 UV observations are also studied by looking at the Si II lines with the Al I con-tinuum removed, the Mg II center to wing ratio, the Al I edge ratio, a comparison with observations of the SME satellite, measurements of UV half-widths for various wavelengths, a comparison with Ca K full disk measurements, and through a table of UV data availability. A number of short-comings in the analysis methods used by the Sun-Climate staff are scrutinized and found to have no serious influence on our final results.

The studies discussed in this report represent a great deal of research which has not previously been published by the Sun-Climate staff over several years, thus there is a certain amount of discontinuity from chapter to chapter which we acknowledge but do not consider detrimental; we believe it to be inherent in this type of report.

---

* *Visiting Scientist from the Institute of Geophysics, Academia SINICA, Beijing, China.*

1. INTRODUCTION TO THE SOLAR UV RADIATION AND CLIMATE RESEARCH PROJECT

1.0 Background

The Solar UV Radiation and Climate Research Project started as a new initiative in FY80, as part of NOAA's Climate Program where monitoring of the temporal changes in the solar radiation input to the atmosphere and researching the atmospheric effects of those changes are goals of the NOAA climate program (Fleming, R.J., 1982). The solar ultraviolet (UV) radiation is not just part of the effects caused by the total solar irradiance (S); UV flux variations alone have been hypothesized to cause climate variations through inducing stratospheric changes that then couple into the troposphere. For examples, UV induced changes in stratospheric ozone modulate the atmospheric transmittance at visible wavelengths, which changes the heating in the lower troposphere; also UV induced changes in stratospheric temperature modulate the upper boundary of planetary waves, which may lead to changes in regional climate, etc. (Herman and Goldberg, 1978).

Project work in the start-up year FY80 was dominated by small outside contracts, granting funds to the Cooperative Institute for Research in Environmental Sciences for support of a Research Associate, and the sole member of the project, Dr. R.F. Donnelly resigning as the Ionospheric Physics Group Leader of the Space Environment Laboratory in order to devote more time to the new project (Donnelly, 1981). In FY80 - FY84, the project's work involved the following main areas: (1) analysis of available solar UV measurements to prepare for the analysis of future measurements from the solar backscatter UV (SBUV/2) monitors on the NOAA satellite series, (2) modeling the temporal variations of solar UV spectral irradiance to understand why the observed variations occurred, to estimate the corresponding effects of wavelengths not included in the observations and to provide a link between solar physics research of spatially resolved structures on the sum and solar- terrestrial studies of the temporal variations of the full-disk solar UV flux, (3) development of improved UV spectroradiometers for rocket-flight measurements for use in recalibrating drifting satellite instruments, and (4) studies of the literature of the atmospheric effects of solar UV radiation (Donnelly et al., 1984).

In FY83, the project moved from the NOAA Space Environment Laboratory to the NOAA Air Resources Laboratory for the following reasons: (1) to be located near scientists researching the stratosphere and climate change, (2) to be located near our sister project, Dr. Kirby Hanson's Ground-Based Solar Radiation Project and (3) to insulate the project staff from undesirable side effects during the aftermath of large budget reductions in the Space Environment Laboratory's research program.

The first SBUV/2 instrument was launched on NOAA 9 in December 1984, as part of a joint NASA/NOAA program to monitor the global distribution of ozone as a function of altitude, latitude, longitude and time. Other groups within NOAA have the primary responsibility for analyzing the ozone data. NOAA-NESDIS monitors the telemetry from the NOAA SBUV/2 instrument and conducts routine processing of the data. These same instruments measure daily the solar UV spectral irradiance in the 160-400 nm range with a 1 nm bandwidth and 0.15 nm wavelength step. The staff of the Solar UV Radiation and Climate

Research Project are the only NOAA group processing and analyzing the solar UV irradiance measurements from the NOAA satellites from the NESDIS-generated raw data tapes onward. The first raw data were delivered from NOAA-NESDIS to us in mid 1985.

1.2 Project Objectives

The purpose of the Solar UV Radiation and Climate Research Project is to answer the following questions:

(1) What are the temporal variations of the solar UV spectral irradiance in the wavelength range 100 - 400 nm?

(2) What are the stratospheric effects of the observed UV variations?

(3) What influence on the troposphere and climate do these stratospheric effects induce?

To answer these questions, the project includes: (1) analysis of solar UV spectral irradiance observations from the NOAA-9 and NIMBUS-7 satellites, (2) analysis of observations and modeling of the stratospheric effects of the solar UV flux variations, and (3) theoretical research of coupling of these stratospheric effects into the troposphere. Currently, we are behind our goals for analyzing the solar UV irradiance measurements from the NOAA-9 satellite because of complications in the observations that require study, the development of appropriate corrections and then revision of the data analysis. Therefore we have increased our effort on the NOAA-9 data analysis to meet this challenge. This increased effort has been achieved through phasing out our work on developing UV spectroradiometers for rocket-flight measurements and through slowing down our build-up of staff and contractors to work on the third question listed above. Because numerous other scientists have recently conducted much research on the second question above, we have mainly tried to encourage and keep abreast of their literature (see J. Geophys. Res., 92, D1, 795-914, 1987). Our present work on the third question is still in the literature research stage and our current main emphasis is to build up our staff and contractors in this area, through graduate level training of Larry Puga and grants to CIRES and other organizations for research on stratosphere- troposphere coupling.

The last report in this series (Donnelly et al., 1984) reviewed the following: (1) some of the first observations and also theoretical model results of the stratospheric effects of solar UV variations, (2) the early results of studying the UV measurements from the NIMBUS-7 satellite, (3) models of solar UV temporal variations, (4) design and development of UV spectroradiometers and (5) detailed results of studies of the temporal evolution of Ca-K plages and the CMD dependence of the sunspot number.

1.3 Project Personnel

Several personnel changes occurred in fiscal-years 1984-1986. Larry Puga converted from a COOP student employee to a full time meteorologist in the summer of 1984 after graduating with a B.A. degree from the University of

Northern Colorado. Thomas Repoff, mathematician and statistician, departed to work in industry in December 1984. He made a major contribution to the numerical analyses of the solar UV irradiance measurements that are now used extensively by all members of the group. Joan Barrett, computer analyst, joined the group in April, 1985, and has helped greatly with the analysis of solar UV measurements from the NIMBUS-7 and NOAA-9 satellites. Dr. Judith Lean left CIRES in June, 1986. Her research completed the group's main work on modeling the temporal variations of the solar UV flux, contributed our most important results to date with respect to the total solar irradiance (Foukal and Lean, 1986), and contributed the first results from UV spectroradiometer laboratory tests. The UV spectroradiometer development work is now being closed out due to decreasing funding and the loss of key personnel. Mathematics Aide, Wanda Busby, departed in June, 1985, after graduating from Metro State University with a B.A. in Mathematics. She contributed greatly to the analysis of EUV measurements from the AE-E satellite. Karl Pfendt and David Stevens joined the group in May, 1986, and have already contributed greatly to extensive studies of six years of NIMBUS-7 data. Meqing Gao, from the Institute of Geophysics, Beijung, China, joined the group as a visiting scientist in July, 1986.

1.4 Collaborations and Relations to Other Organizations

Table 1.1 lists the staff and various collaborating groups currently involved with the NOAA-ERL-ARL Solar UV Radiation and Climate Project. The collaborations usually involve several members of the Sun-Climate Staff, so the alignment of rows of staff and collaborators does not designate a sole collaborative link. Don Heath has provided solar UV measurements from NIMBUS-7, for November 7, 1978, through October 29, 1984. NIMBUS-7 measurements are the main data we have analyzed over the past five years. These data are from the SBUV instrument, which is the predecessor of the SBUV/2 instrument now flying on NOAA-9 and scheduled to fly on future NOAA satellites. The SBUV/2 measurements are now our main data source. Walter Planet is our main contact in NOAA NESDIS for the SBUV/2 data. Gary Rottman of LASP has permitted us to study solar UV irradiance measurements from the SME satellite.

1.5 Future Project Plans

We have recently completed analyses of six years of NIMBUS-7 measurements of the solar UV spectral irradiance and are now writing several papers about those results. We are also currently analyzing more than a year of SBUV/2 UV measurements from the NOAA-9 satellite and expect to publish the 1986 Mg II center-to-wing ratio this year. We have completed our comparisons of the temporal variations of solar extreme ultraviolet radiation with those of solar UV radiation and have only to complete one more paper on the average dependence of active region emission as a function of the solar central meridian distance of the region. Because of our loss of key staff, Dr. J.L. Lean, and because of delays in the program, the UV spectroradiometer development for rocket-flight calibrations has been phased out as an in-house activity. The largest remaining unknown in our research of whether variations in the solar UV flux affect climate is to determine the coupling between the UV induced stratospheric changes and the troposphere.

In FY88 and FY89, most of the group's effort will be spend on analyzing the SBUV/2 measurements of solar UV spectral irradiance from the NOAA satellites, while building up our staff and contractors for research on stratosphere-troposphere coupling. In FY90 and thereafter, the project should consist of two nearly equal parts, namely: (1) the analysis of SBUV/2 measurements of the solar UV spectral irradiance as a function of wavelength and time, and (2) modeling the stratospheric and tropospheric effects of these UV changes.

1.6 Outline of this Report

Many of the research results derived from this project have been published in science journals and will not be reviewed in this report, except to list the references in Chapters 6 and 8, and to briefly summarize their main results in Chapter 7. The main purpose of the rest of this report is to document the project's research that has not been published elsewhere, either because: (1) the work involves too many details to be appropriate for a science journal that aims at a wider audience but is appropriate for a technical memorandum aimed at the small group of scientists involved in research of the temporal variations of the solar UV flux and its atmospheric effects, or (2) the work is too small or isolated in subject to support a separate journal paper but is appropriate for one section of a technical memorandum.

Chapter 2 discusses research aimed at identifying deficiencies in our current model of the temporal variations of the solar UV spectral irradiance and ways for improving the model to correct for these deficiencies. Chapter 3 discusses the results of several analyses of NIMBUS-7 measurements of the solar UV flux. Chapter 4 discusses several problems identified in previous analyses and tests that were conducted to determine whether the numerical analyses performed the way one would expect. Chapter 5 discusses Larry Puga's studies of the literature on stratospheric effects of solar UV flux changes and coupling of such effects into the tropospheric.

The first three appendices report development and calibration results for the UV spectroradiometers designed for rocket-flight measurements of the solar UV flux, including the phasing out of this part of the project and suggestions for possible further uses of these instruments. The fourth appendix documents the comparison of solar UV fluxes with the occurrence of coronal holes.

TABLE 1.1 Staff and Collaborations of the Solar UV Radiation and Climate Research Project

Current Staff	Research Areas	Collaborators	Collaborative Studies
Richard F. Donnelly	Project Leader Solar UV Radiation Solar-Terrestrial Physics	Donald F. Heath NASA GSFC P.I. for SBUV NIMBUS-7	Analyses of NIMBUS-7 measurements of the temporal variations of solar UV spectral irradiance.
		Walter Planet NOAA NESDIS	Analysis of SBUV/2 measurements from NOAA-9 satellite.
Joan Barrett	Computer Analyses	Gary Rottman LASP, U. of Colorado	Comparison of NIMBUS-7 and SME measurements.
Glenn Falcon	Electronics Development UV Spectroradiometers	Henry Kostkowski (Contractor) Spectroradiometry Consulting, Charlotte Hall, Maryland	Design, development, and calibration of UV spectroradiometers.
Meiqing Gao	Visiting Scientist Solar Cycle Radiation	O.R. (Dick) White (Contractor) Solar Physicist Mancos, Colorado	Full-disk Ca-K line measurement over solar cycle 21.
Karl Pfendt	U. of Colorado Student Computer processing and analyses.		
Larry Puga	Stratospheric Effects of solar UV Variations Stratosphere-Troposphere Coupling Solar Radiation Variation	Prof. Douglas N. Yarger Meteorology Dept. Iowa State University	Stratospheric Effects
David Stevens	U. of Colorado Student Computer processing and analyses		

2. STUDIES OF OBSERVED AND MODELED UV IRRADIANCE AND SOLAR INDICES

L.C. Puga

The study of climatic changes linked to the variations of solar UV irradiance necessitates having an extended set of data that can confidently be expected to show the actual UV variations. The satellite measurements necessary for the study of long term UV variations have been accurately recorded for less than a solar cycle. Although these measurements are the most valuable source of data there is for these type of studies, the short length of time they have been made and uncertainties in their accuracy means they must be supplemented with other measurements of solar variability which closely imitate the UV. Comparisons of the NIMBUS-7 satellite measured UV, modeled UV calculations from ground based Ca K II Plage observations, and other solar indices such as the 10.7cm Radio Flux (F10.7), and the Sunspot Number (R) have begun to complete an overall picture of the UV variability over time as well as showing the complex nature of physical processes on the sun.

2.1 Solar Processes which may effect the Plage - Modeled UV

Significant differences in the values of modeled Ultraviolet flux versus observed UV flux requires a close look at the various events on the solar surface that may affect the UV flux and/or the various parameters used in calculating the modeled UV. Several things might affect either one of these values; plages which dominate the solar surface but do not have a uniform intensity, solar flares of significant intensity, sunspots, coronal holes and filaments may all cause differences between the two sets of data.

2.1.1 Plages

Large plages on the solar disk are often given a high intensity value by observers. This intensity value may correspond to some small percentage of the plage but not the entire area it covers. Because of this, the use of Area times Intensity in the model calculations may cause over-estimation of peaks in the modeled UV flux values, for example on days where large plages with an intensity value greater than or equal to 3.0 dominate the solar disk at the time of the peak are used to determine if this is true.

Graphs of the NIMBUS-7 and Modeled 205nm UV flux (meaning the model of Lean et. al., 1982) together for the period 10/7/78 through 8/31/82 show when the modeled UV flux obviously over-estimates the peak variation in the measured flux. Pre-peak and post-peak minima for times when the modeled data over-estimated the observed UV were averaged to provide one minimum which was used in the simple formula,

$$\frac{\text{MODELED MAX. FLUX}}{\text{MODELED MIN. FLUX}} - 1 \Big/ \frac{\text{OBSERVED MAX. FLUX}}{\text{OBSERVED MIN. FLUX}} - 1$$

to show the ratio of short-term variations between the modeled and the observed 205nm UV flux. These ratios are shown in table 2.1.1A, along with the plage information used in the comparison. The plage information was found using Solar Geophysical Data (SGD) reports to see if there were large plages dominating the solar disk on days the modeled UV flux reached its peak. Plages qualified as large enough to be of importance for this comparison when the area of at least one plage on the day in question equaled or exceeded 4000

TABLE 2.1.1A

PLAGES ASSOICATED WITH MODELED OVER-ESTIMATION OF UV FLUX (AREA ≥ 4000, INTENSITY ≥ 3.0)

RATIOS OF MODELED PEAK VARIATION TO NIMBUS-7 OBSERVED PEAK VARIATION

DATE OF MODEL PEAK	JULIAN DATE	MAIN PLAGE AREA	MAIN PLAGE INTENSITY	MAIN PLAGE I.D.#	ADDITIONAL LARGE PLAGE FOR DATE	FLUX MAX./FLUX MIN (MODELED)	FLUX MAX./FLUX MIN. (OBSERVED)	RATIO MODEL FLUX / OBS. UV FLUX	DIFFERENCE IN % VAR. MODEL/OBS.
12-4-78	338	6200	3.5	15687	NONE	0.0325	0.044	0.73/1	-1.15
2-20-79	51	8500	3.0	15830	15823,5300,3.5	0.042	0.021	2/1	2.1
3-18-79	77	11000	3.0	15877	NONE	0.0297	0.017	1.75/1	1.27
6-5-79	156	6600	3.0	16052	16046,4500,3.0	0.049	0.0395	1.24/1	0.95
"	"	----	---	-----	16051,6500,3.5	-----	------	------	----
"	"	----	---	-----	16058,4800,3.5	-----	------	------	----
7-6-79	187	4000	3.5	16123	16122,4000,3.0	0.0495	0.0401	1.23/1	0.94
"	"	----	---	-----	16117,4000,3.0	-----	------	------	----
8-25-79	237	5300	3.5	16239	16241,4500,3.0	0.0392	0.0229	1.71/1	1.63
9-25-79	268	10600	3.5	16298	16325,5000,3.5	0.033	0.0348	0.95/1	-0.18
11-13-79	317	9000	3.5	16418	16413,5300,3.0	0.069	0.048	1.44/1	2.1
"	"	----	---	-----	16421,5400,3.0				
"	"	----	---	-----	16426,5300,3.0	-----	------	------	----
12-9-79	343	9500	4.0	16478	NONE	0.092	0.064	1.44/1	2.8
5-6-80	127	5800	4.0	16182	NONE	0.039	0.016	2.44/1	2.3
6-21-80	173	8100	4.0	16918	16911,5600,4.0	0.093	0.047	1.98/1	4.6
"	"	----	---	-----	16923,6200,4.0	-----	-----	------	----
"	"	----	---	-----	16927,5400,4.5	-----	-----	------	----
10-9-80	283	7300	3.5	17188	17181,4500,3.5	0.079	0.021	3.76/1	5.8
"	"	----	---	-----	17187,6200,3.5	-----	-----	------	----
12-4-80	339	5900	4.0	17310	17304,5100,4.0	0.061	0.030	2.03/1	3.1
"	"	----	---	-----	17301,4800,3.5	-----	-----	------	----
12-14-80	349	10300	3.5	17331	NONE	0.043	0.029	1.48/1	1.4
7-27-81	208	6000	4.5	17760	NONE	0.036	0.026	1.38/1	1.0
10-19-81	292	7700	3.5	17923	17926,4500,4.0	0.046	0.021	2.19/1	2.5
"	"	----	---	-----	17906,4000,3.0	----	-----	------	----
11-12-81	316	5400	3.5	17989	18004,5300,3.5	0.059	0.031	1.90/1	2.8
12-9-84	343	4300	4.0	18055	NONE	0.079	0.055	1.44/1	2.4
2-1-82	32	5600	4.0	18176	18189,5000,3.0	0.070	0.040	1.75/1	3.0
6-18-82	169	11800	4.0	18422	NONE	0.069	0.019	3.63/1	5.0
7-18-82	199	10000	4.5	18474	18473,8000,3.0	0.107	0.068	1.57/1	3.9
"	"	----	---	-----	18484,5800,4.0	-----	-----	------	----
"	"	----	---	-----	18485,6200,3.5	-----	-----	------	----
"	"	----	---	-----	18493,4000,3.5	-----	-----	------	----
8-10-82	222	15000	4.5	18511	18519,4000,3.0	0.108	0.068	1.59/1	4.0

Mean Ratio = 1.80/1 Median Ratio = 1.65/1

millionths of a solar hemisphere, and the intensity value equaled or exceeded 3.0. Every case we used where the modeled peak variations exceeded those of the observed UV flux had at least one plage on the day of the modeled peak that met these requirements. There were two cases which were selected where the ratio was less than unity (observed peak variation exceeded modeled peak variation) even though the graphs originally indicated the opposite was true. These two particular periods also had large plages on the day that the modeled UV reached its peak value.

This indicates that there is very likely a relationship between the occurrence of these large plages with the over-estimation of actual peak 205nm UV flux variation by the modeled UV. There does not appear to be a dependence on whether the minimum to minimum time is around 13 days or 27 days; both time periods have large and small ratios even though a 27 day variation might be expected to show greater variation. These large plages may also explain why out of 22 cases, seventeen of them had the modeled UV flux peaking before or after the observed UV flux peak by one or two days, since the model will likely peak on the day the plage reaches it's largest area and intensity. More conclusive answers could be found by requiring that the Area X Intensity value of all qualifying plages make up 75% (or some high percentage) of the total Area X Intensity value for all plages occurring on that day, instead of just visually determining that they dominate the solar disk; still, it appears there is a causal relationship between very large plages and the over estimation of the 205nm UV flux by the model.

The previous problem shows that the peak variation ratio is a measure of short-term differences in the modeled and observed UV flux, so the peak variation ratio of the 205nm UV was determined for the entire data set according to dates picked from graphs showing the temporal variations of the flux values. These values are more accurate that the initial values listed in table 2.1.1A because the computations are made directly from the data tape, eliminating rounding errors, etc., that were present previously. These ratios, listed in table 2.1.1B, and graphs of the data, can now be used in conjunction with the SGD prompt reports and other data sources to examine the influence of solar flares, sunspots, and coronal holes on the modeled UV flux.

2.1.2 Solar Flares

Solar Flares occur irregularly on the solar disk, so any effect of their occurrence on the UV irradiance should be irregular as well, and fairly simple to spot in the daily scans made by the NIMBUS-7 satellite. NIMBUS-7 observations are taken in several scans which last several minutes each. A class M soft X-ray flare that peaked on 10/14/84 was used to determine if there was any noticeable effect on the NIMBUS-7 observed UV that needs to be compensated for in the UV model. A comparison of NIMBUS-7 scans taken before, during and after the flare event showed no noticeable change in the UV flux. If there is an effect from flares it would have to be in the range of 0-3% not to be visible in the NIMBUS-7 flux measurements, our conclusion is that flares have no appreciable effect on the full-disk UV flux as measured by the NIMBUS-7 satellite.

2.1.3 Sunspots

The effects of sunspots on the peak variation ratio of modeled 205nm UV flux/observed 205nm UV flux was determined by using times when the percentage

TABLE 2.1.1B PEAK VARIATION RATIOS OF MODELED 205 nm UV OVER NIMBUS-7 MEASURED 205 nm UV

JULIAN DATE MIN TO MIN	PEAK VARIATION RATIO
1978	
328-350	0.88
1979	
19 - 31	1.40
31 - 55	2.12
55 - 74	1.72
71 - 83	1.53
83 - 100	0.60
100 - 111	1.35
111 - 126	1.22
126 - 139	0.84
139 - 153	1.66
153 - 166	1.24
166 - 197	1.18
197 - 221	0.77
221 - 245	1.52
245 - 270	1.31
274 - 301	0.93
303 - 331	1.42
331 - 358	1.46
1980	
27 - 41	0.60
41 - 53	1.28
53 - 69	1.20
69 - 80	0.95
80 - 96	0.98
96 - 109	1.57
109 - 122	0.87
122 - 136	2.03
136 - 160	1.16
160 - 187	1.96
187 - 218	1.23
217 - 240	1.17
240 - 268	2.20
268 - 279	0.93
279 - 296	3.81
296 - 320	1.62
320 - 333	0.77
333 - 344	2.02
344 - 360	1.45

JULIAN DATE MIN TO MIN	PEAK VARIATION RATIO
1981	
6 - 18	0.84
18 - 54	1.37
54 - 81	1.28
81 - 91	1.53
81 - 114	1.19
89 - 114	1.37
114 - 142	1.32
142 - 157	0.56
157 - 190	1.54
190 - 202	1.29
202 - 218	1.40
218 - 128	0.69
268 - 257	0.60
257 - 270	1.61
270 - 284	0.65
284 - 298	2.19
298 - 327	1.75
327 - 354	1.48
1982	
14 - 49	1.50
49 - 82	0.83
82 - 94	0.85
94 - 109	1.05
109 - 135	0.76
135 - 163	1.99
163 - 179	2.57
190 - 209	1.66
209 - 235	1.58

Mean Ratio = 1.36

Median Ratio = 1.32

variation in the solar constant due to sunspot blocking was ≥ 0.15 (Hoyt and Eddy, 1982), and checking the peak variation ratio at that time. Table 2.1.3A lists all the time intervals found and the corresponding peak variation ratio.

TABLE 2.1.3A

Large Sunspot Area on the solar disk. (dates are approx.)	Modeled UV Flux dates Min,Max,Min	Observed UV dates Min,Max,Min	Peak Var. ratio Model/Observed
1978			
334,346,355	319,346,357	320,338,358	0.806241
1979			
43,49,60	34,51,57	31,36,55	2.125138
150,162,170	152,156,167	153,158,166	1.245862
230,237,245	221,237,243	221,237,245	1.527462
310,317,325	303,317,332	303,317,331	1.421165
1980			
90,99,110	94,102,111	96,105,109	1.574567
135,145,155	137,146,156	136,146,160	1.162417
305,313,325	293,297,320	296,310,320	1.625130
1981			
198,210,214	201,208,216	202,208,218	1.406158
278,291,298	281,292,297	284,291,298	2.195279
305,313,325	297,316,328	298,304,327	1.756951
335,347,355	328,343,354	327,344,354	1.483193

Mean Ratio = 1.54 Median Ratio = 1.45

Eleven out of the twelve cases in which the solar constant changed at least 15% due to sunspot blocking have the modeled UV flux over-estimating the actual UV flux. The entire set of peak variation ratios in Table 2.1.1B has a mean value of 1.36 compared to 1.54 for this subset; this is a significant difference. There is only one value when the observed UV flux is under-estimated by the modeled UV in this subset, compared to 18 out of 63 in the larger data set, so it is reasonable to conclude that large sunspots are affecting the size of the peak variation ratio. This might be explained by the large sunspot area, which is associated with plages, causing an over-estimation of the plage area, and so an over-estimation of the UV by the model; the intensity (brightest part of plage) is systematically too large relative to plage average at the beginning of episodes of activity, i.e., at times of large spots; the sunspot darkening at UV wavelengths may not be negligible, or some combination of these three possibilities.

2.1.4 Coronal Holes

The study of coronal holes does not find any concrete evidence that the presence of coronal holes affects the UV flux values estimated by the model. It does, however, suggest there might be a relationship; out of the sixty-three solar rotations that were studied for the NIMBUS-7/Modeled UV flux comparison, there were eighteen rotations where the model under-estimated the peak value of the observed flux and five cases where the peaks were separated

by about thirteen days. There is no evidence that there were large plages affecting the model that caused this though it is possible a large number of plage remnants was a contributing factor since only two of the five cases correspond to times where large plages dominated the solar surface. This suggests that something such as coronal holes might be responsible for these differences; our complete study is presented in Appendix 4.

2.1.5. Filaments

Because filaments are abundant on the solar surface, tend to wander somewhat and are not always clearly identifiable, it was difficult to do an accurate study of whether they affect the UV peak variation ratios. If they were to effect the ratios, given their great abundance, it would probably be their absence that would produce the most identifiable effect. The H-alpha synoptic charts were used to try and identify days when filaments were absent from the center of the solar disk, since that is the area represented by the charts, (the dates on the chart represent central meridian passage of a particular Carrington longitude). The days when no filaments were present did not have any unusual ratios; from this quick study it is not evident that there is any affect of filaments on peak values of the UV.

2.2 Comparisons of 13 and 27 day periodicities in the Ca II K Plage Index and the 10830 Data

Strong thirteen and twenty-seven day periodicity in the years 1978-1979 (Donnelly 1985) has led to further investigation into the strength of these variations and where they occur within the 11 year solar cycle. 10830A data provided by Jack Harvey for the years 1974-1984 were used with the plage index computed by the World Data Center (WDC) for 1958-1983 to study these short term variations. If close agreement can be shown to exist between these two data sets of occurrence and strength of these short term variations, then this would indicate that the plage index is useful as an indicator of short term UV variations, since there already is evidence that the 10830A data shows short term UV variations fairly well (Donnelly et. al., 1985).

To remove the long term variations and any anomalous points from the data sets, they were least-squared fit in a time series analysis using a twelfth order polynomial (Heath et al., 1984). The residuals provided a data set that clearly show the short term variations of the order of days to weeks. The data sets were processed in two year windows, with the last year and first year of consecutive data sets being the same so there would be a one year overlap in the windows. The Harvey 10830A data were analyzed for the years 1974 to 1984; 1974 through 1976 were then discarded because the large number of missing data in those years could not be compensated for in the analysis. The Ca K II Plage index values were processed from 1958 to 1983 in the same manner.

Time series graphs and power spectra of the two data sets indicate there is strong thirteen and twenty-seven day periodicity in both data sets. These periodicities are caused by the 27-28 day rotation rate of the sun and regions of activity on the sun roughly 180^{o} apart. Cross correlation analysis shows fairly good symmetry, except where there are large amounts of data missing.

There is a lag of about one day in the Harvey 10830A data behind the plage index. A closer look at the power spectra indicates that the thirteen and twenty-eight day periodicities are not exactly at those periods for any given two year window. Periods for the twenty-eight day variability can range up to 1.2 days either side of the 28 day value, and for the thirteen day periodicity the actual period can be up to .5 days either side of the 13 day value. The changes in power spectra strength for these two periods over time indicate some long term rise and fall in twenty-eight and thirteen day variability that is related to the long term variability of the solar output produced by the changes in the strengths and positions of regions of activity on the sun.

A complex demodulation analysis (Heath et al., 1984) was performed on the detrended data to show more clearly where the thirteen and twenty-seven day variabilities were strongest and weakest over time. The values of 13.35 days and 27.70 days were chosen as the periods to be checked in this analysis because they are the best representation of the data set as a whole even if they differ slightly from the values in individual two year windows as a result of the increase or decrease in solar rotation rate at the latitudes where the regions of activity dominate. Heath et al. (1984) have indicated through their analysis of several Ultraviolet wavelengths that the thirteen day periodicities are not harmonics of the twenty-eight day period, and each represents a different behavior on the sun.

The graphs in figure 2.2.1 are graphs showing the complex demodulation amplitude values for both data sets and both periodicities for the years 1977 through 1983. For each data set there are two nearly overlapping lines visible on parts of the graphs because of the one year overlap in the two year windows; they do not always agree because there is an edge effect in the complex demodulation analysis at both the beginning and end of the data set. Those values closest to the middle of the analysis window are the most accurate, so there is a consistent data set of very accurate amplitudes because of the overlap. Graph 1 shows the amplitude of the 27.70 day periodicity in the 10830A and plage index for the years 1977 to 1984. There is a great deal of similarity in the overall shape of the graphs, which indicates that both are experiencing similar 27.70 day effects. The graph also shows that the plage index rises faster and peaks sooner than the 10830A data, and then falls off faster; this may be an indication of a deficiency in the plage index. So while the graph shows that the two data sets are experiencing 27.70 day periodicity in much the same way, nearly the same time and to about the same extent, the plage index data does not maintain that periodicity as long as the 10830A data and tends to show greater amplitude changes in minor dips and rises.

Graph 2 shows the 13.35 day periodicity for the two data sets for the years 1977 through 1983. Although this graph shows a small amount of the similarities apparent in the 27.70 day periodicity, they are restricted to a slight similarity in general shape and the relative amplitude of peaks that correspond to each other. One main reason for using the plage index as a proxy for chromospheric variations is its good match in 13-day to 27-day power ratios (Figure 7 of Donnelly, Hinterregger and Heath, 1986); graph 2 shows that even though the power ratio is similar how that 13-day power is distributed over a two year interval is only roughly similar. The dissimilarities in graph 2 between the two are important, however, these two are much more similar in their 13-day periodicity than are the other measures of solar activity that have been recorded for many years, the sunspot number

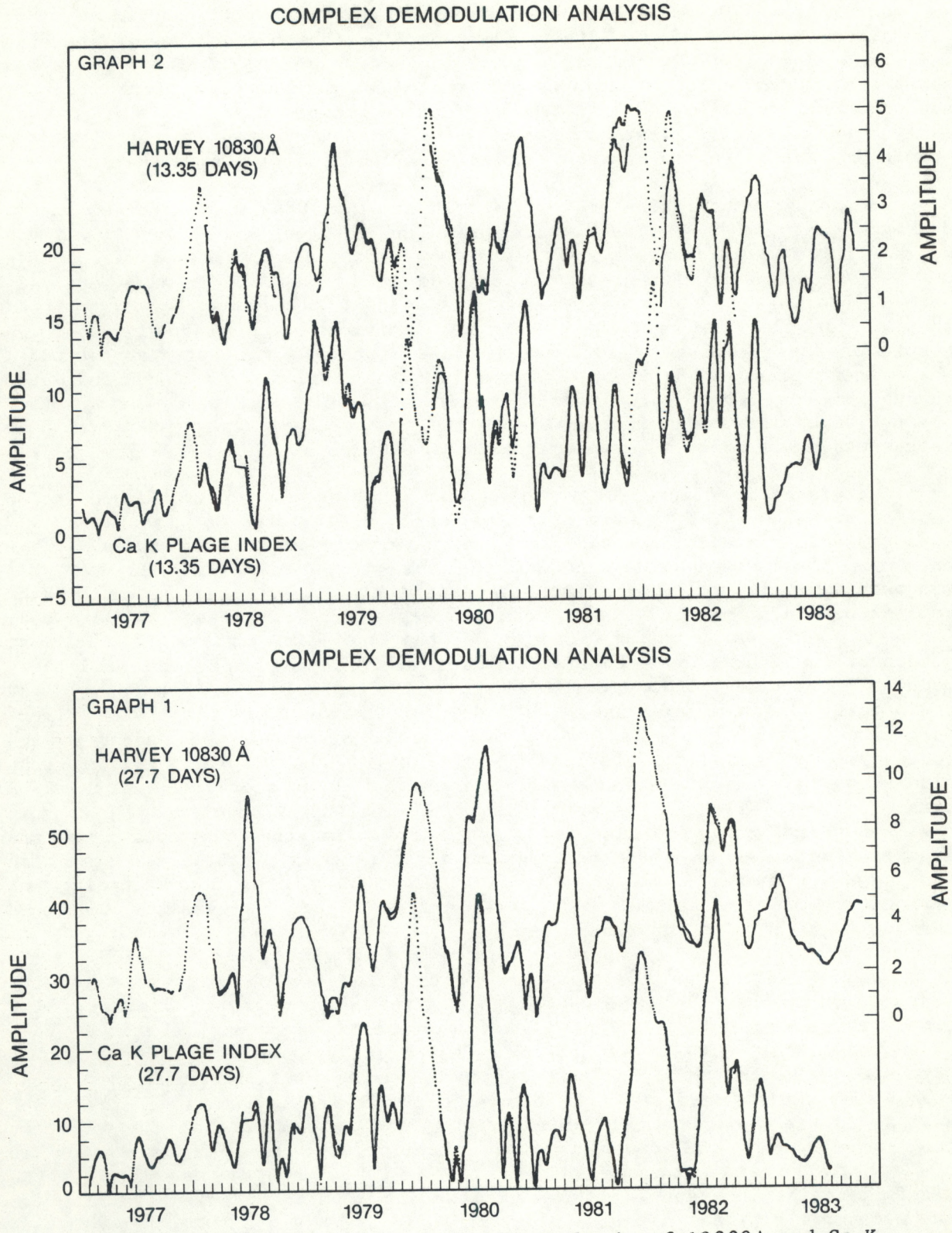

FIGURE 2.2.1 Complex demodulation analysis of 10830A and Ca K Plage index data, for 13.35 and 27.70 day periodicities, 1977 through 1983.

or 10.7cm solar radio flux, with respect to either chromospheric UV fluxes or the 10830A flux (see figures 4.7- 4.9, Donnelly et al., 1986). There is an obvious difference in widths of a number of major peaks, the peaks are often nearly 180° out of phase, and the Ca K plage index also often has its peak in any given rise after the 10830A data. The size, position and intensity of the plages, particularly the large plages that are a disproportionate amount of the Ca K plage index, may affect the thirteen day periodicity more adversely than the twenty-seven day periodicity because of the smaller portion of the solar disk involved.

Figures 2.2.2 and 3 are of the same complex demodulation analysis values as the graphs in figure 2.2.1 but have the two different periodicities for the same data set graphed together. Figure 2.2.2 shows the comparison between the 13.35 day and 27.70 day values for the 10830A data set. Except for one notable example, the periodicities are very consistent in their behavior relative to what the other periodicity is doing at the same time. Whenever the 27.70 day values are at a major peak (and even most of the minor peaks), the 13.35 day values are nearly 180° out of phase- i.e., near or at a minimum value whether coming down to the minimum or just starting to rise from it. The one time when this is clearly not the case occurs at the end of 1981, beginning of 1982 when both periodicities have a major peak which reach their maximum value about the same time. Even in this case, however, the peaks are slightly off and of such large magnitude it would be more surprising if they did not overlap. The 13.35 day peak dies out more rapidly than the strength of the 27.70 day periodicity, and reaches a minimum and another maximum just in about the time the 27.70 day periodicity is falling to its minimum values.

Figure 2.2.3, the 13.35 day and 27.70 day complex demodulation values for the Ca K plage index, do not show the clear relationships apparent in the 10830A data. Although there are only two cases when major peaks occur at the same time in these sets of values, (12/79-1/80 and July 1980), there is a fairly strong tendancy for peaks in one period to be matched approximately by a minimum in the other- i.e., approaching, at, or rising from a minimum. In this way there is fairly good agreement between the data sets; the 13.35 day period tends to be out of phase with the 27.70 day period, usually somewhere near 180° out of phase for both the 10830A and Ca K plage index.

Taking into consideration that the measurements that create these data sets are taken at different locations, at different times, with different instruments and using different observing methods the correlation of the data sets is still not as good as would be expected. The 10830A data are direct measurements while the Ca K plage index is computed from values for plage area and intensity, which are determined from human observations. This tends to lessen the degree to which they would agree because of the difficulty in being consistent with the plage observations. The Ca K plage data, which were used to model the UV, needs to be studied further before it can be used to approximate short and intermediate term ultraviolet variations, based on the agreement with the 10830A data, which has been shown to be in good agreement with the 205nm UV (Donnelly et al. 1985). A further look at the Ca K plage index data back to the beginning of the data set in 1958 is the next step in determining whether the approximation of UV variations can be made for times occurring before UV measurements were made.

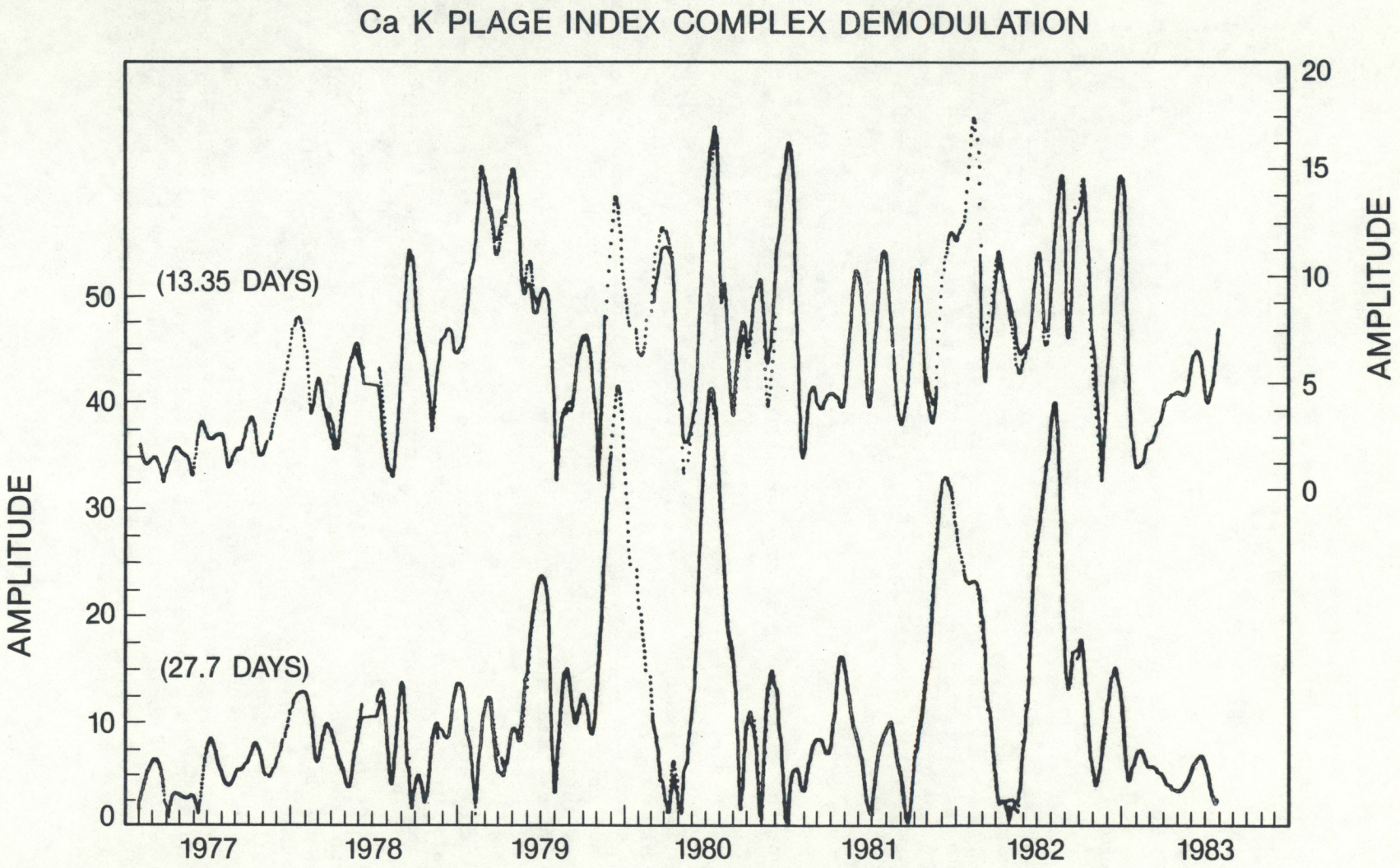

FIGURE 2.2.2 Ca K Plage index complex demodulation for thirteen and twenty-seven day periodicities.

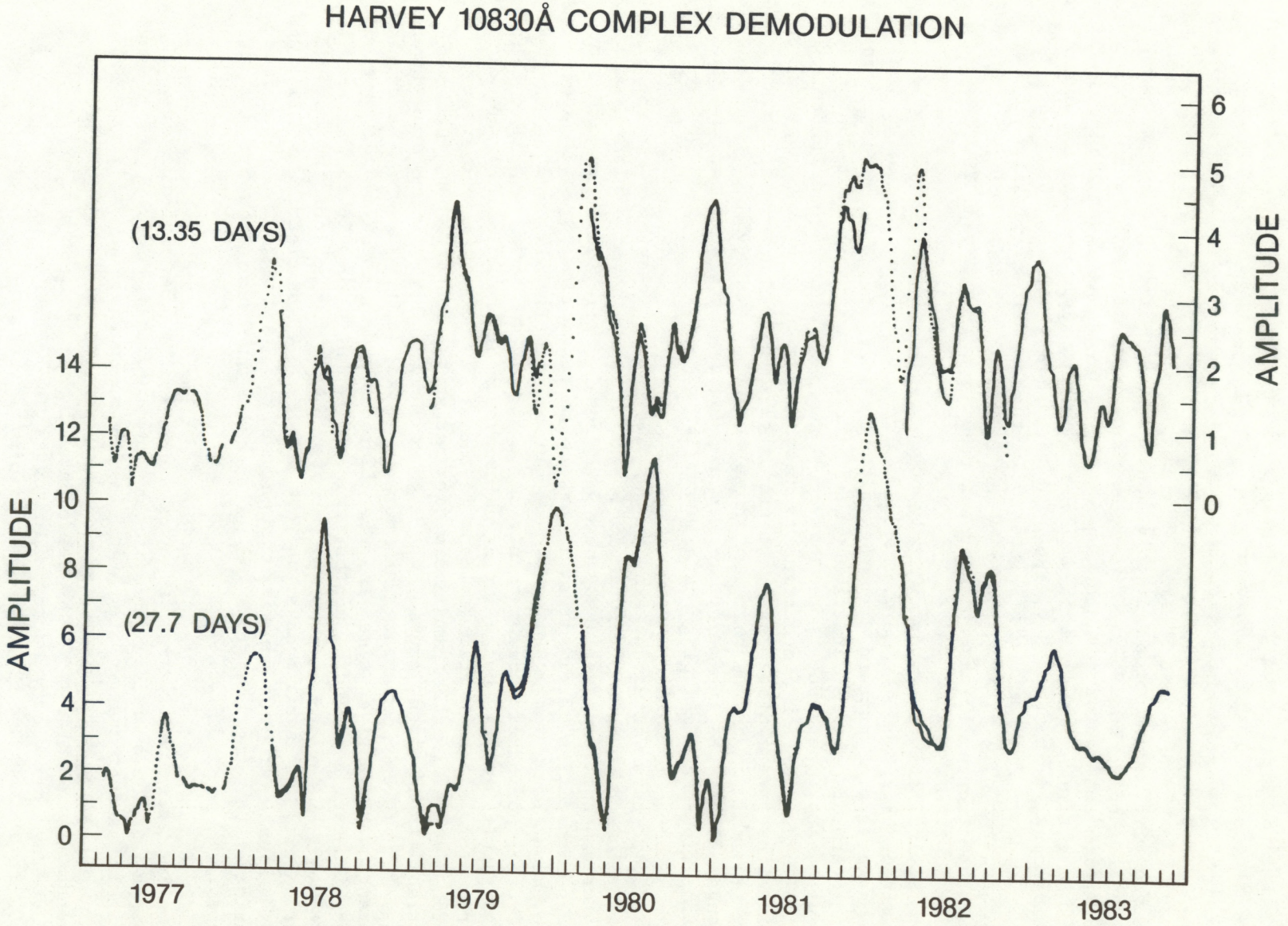

FIGURE 2.2.3 Harvey 10830A data complex demodulation for thirteen and twenty-seven day periodicities.

2.3 13-Day and 27-Day periodicity in the Plage Index, 1958-1983

Figures 2.3.1 and 2.3.2 are graphs of the complex demodulation values for the periods 13.35 and 27.70 days for the Ca K plage index from 1958 to 1968 and 1968 to 1978 respectively. Each graph contains both of the periodicities in it for the ten year period, so that comparisons can be made as to their behavior together over time. The complex demodulation values were also graphed with the smoothed monthly sunspot number for nearly two full solar cycles beginning in 1967. This comparison is graphed in figures 2.3.3 and 2.3.4 with one period on each graph. Note the strong fluctuations in 13 and 27-day periodicity in 1958-1959, the strong episode of 13 and 27-day periodicity in Sept. to Nov. 1960 and throughout 1969 and that those for 27-days in late 1979, mid 1980, late 1981, the beginning and last half of 1982 are stronger than in solar cycle 20 and comparable to the largest of cycle 19, but that stronger 13-day episodes occurred in cycles 19 and 20 than in cycle 21.

Several things are immediately obvious when figures 2.3.1 and 2.3.2 are examined. First of all, both the 13.35 day and 27.70 day periodicities follow the same general pattern, showing fair agreement over the entire comparison for intermediate term variations; i.e., those covering several months up to a couple years. There does not, however, appear to be any clear pattern in the 13.35 day periodicity occurring at greater strength at any particular time within the intermediate term variations relative to the behavior of the 27.70 day periodicity during that same time period. In addition the long term trends between the two periodicities also agree quite well for the entire 26 year period that Ca K plage data is available.

Short term variations exhibit the same characteristics as in the previous look at the years 1978 through 1983, except that they are clearer and other features become apparent when these additional earlier years are studied. The two periodicities rarely if ever peak at the same time; when it appears that they might peak at the same time one period, usually the 13.35 day, drops as the other periodicity peaks then rises again as the other begins to fall off; this results in twin peaks during major events of the 13.35 day periodicity in particular, although it is evident in the 27.70 day periodicity as well. The 13.35 day variability maintains its strength longer than the 27.70 day variability at times, causing the two to occasionally be nearly in phase, but they are more often near 180^{o} out of phase. They tend to alternate in strength at any given time, that is, if the peaks in the 27.70 day periodicity are high over a period of months, then the peaks in they 13.35 day periodicity are lower and vice-versa. The ratio of 27.70 day periodicity to 13.35 day periodicity at their peaks would illustrate this clearly. All this is additional evidence that although the two periodicities are caused by variations in the same physical presence on the sun, they are two distinct behaviors.

To determine if there is consistency in how the periodicities vary with respect to the overall output of the sun, they were compared to the smoothed monthly sunspot number from late in 1964 through 1980. Figures 2.3.3 and 2.3.4 illustrate this comparison. Both periodicities reflect the long term trends of the solar cycle as represented by the sunspot number, although the 27.70 day periodicity better illustrates the larger rise in the cycle from 1977 to 1983. The 13.35 day periodicity is strongest as the solar cycle is declining and rises to that peak after the 27.70 day periodicity which more

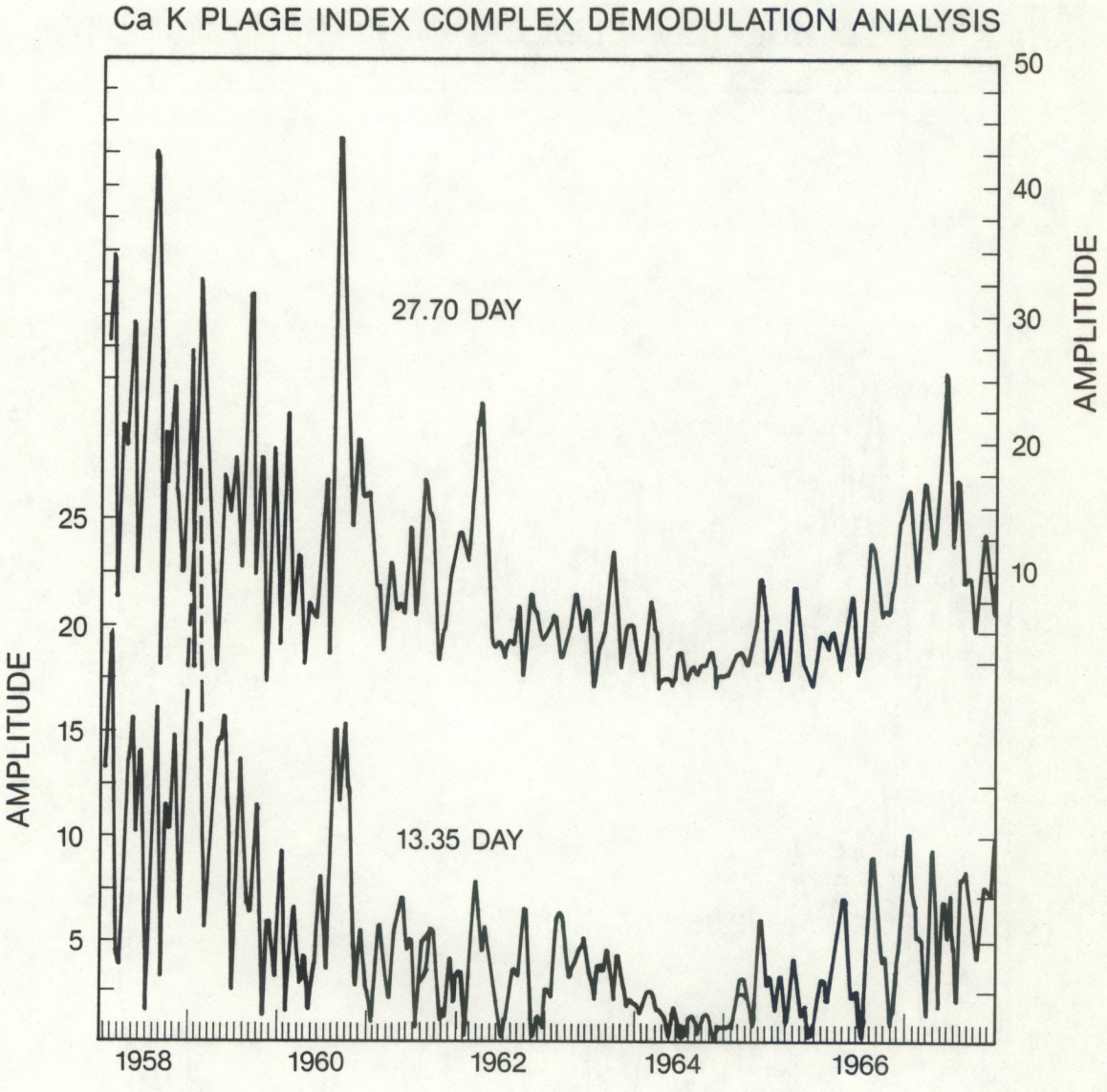

FIGURE 2.3.1 Ca K Plage index complex demodulation for thirteen and twenty-seven day periodicities, 1958 through 1967.

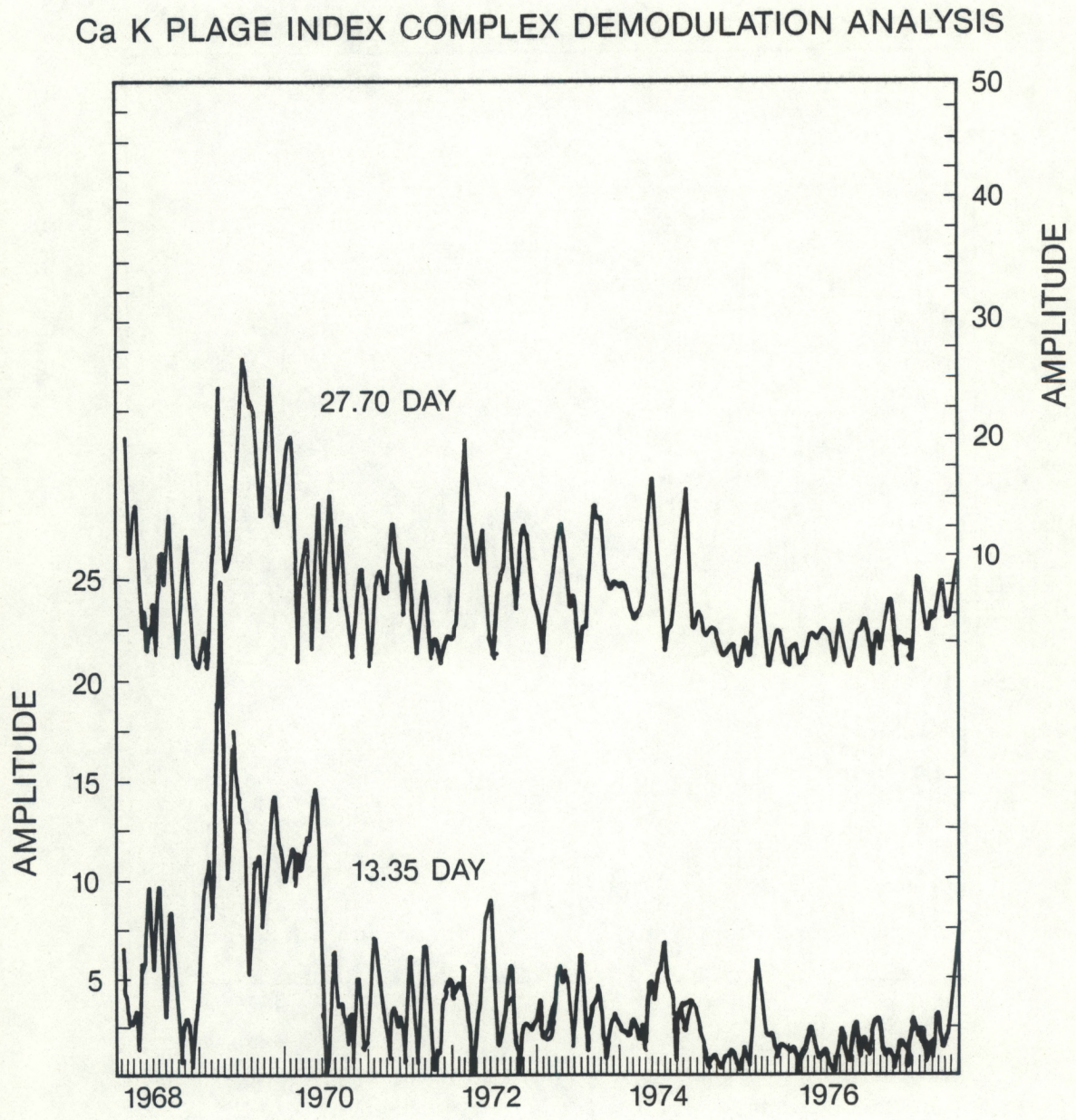

FIGURE 2.3.2 Ca K Plage index complex demodulation for thirteen and twenty-seven day periodicities, 1968 through 1977.

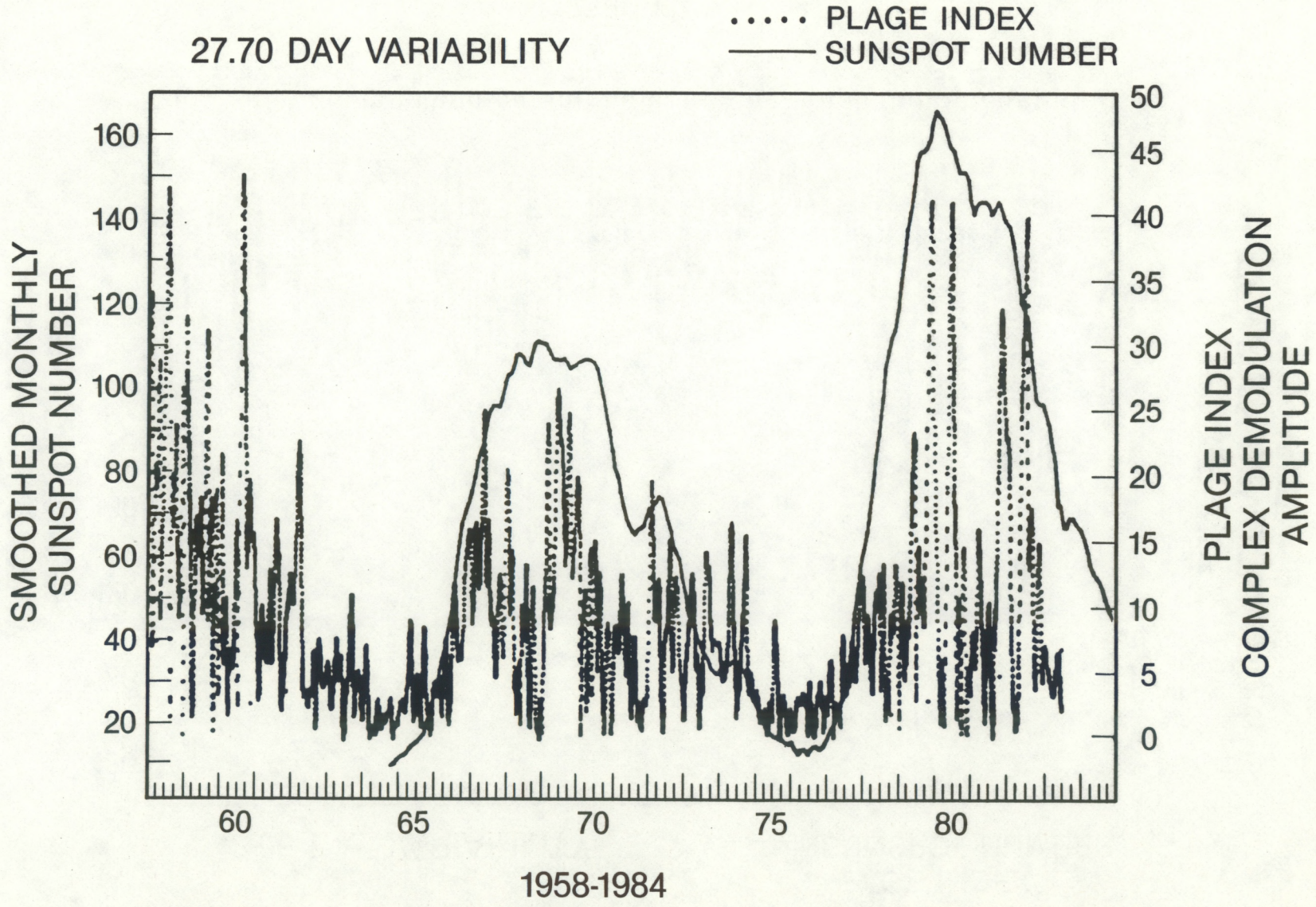

FIGURE 2.3.3 27.70 Day variability in plage index, with the smoothed monthly sunspot for the years 1958 through 1984.

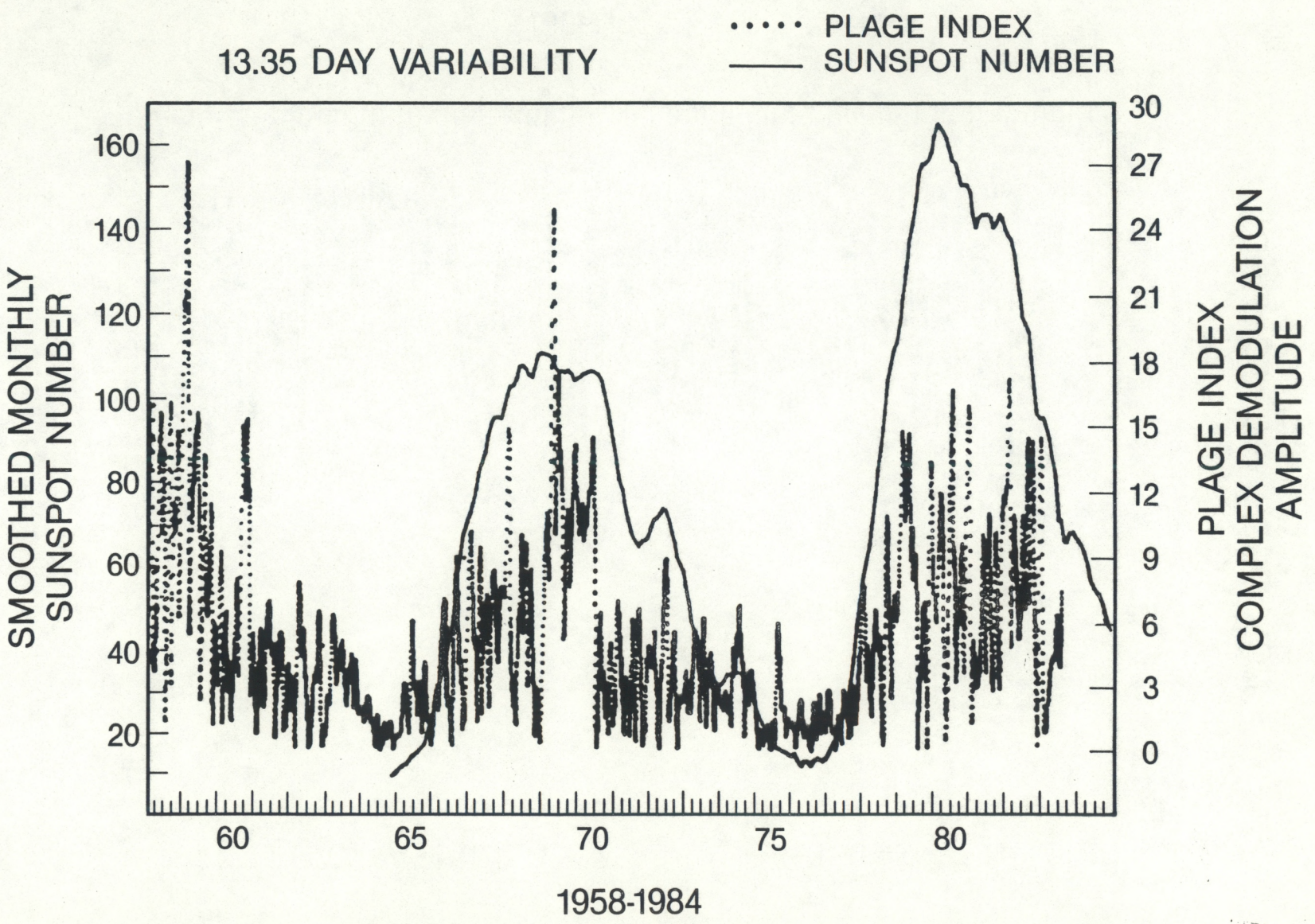

FIGURE 2.3.4 13.35 Day variability in plage index, with the smoothed monthly sunspot for the years 1958 through 1984.

closely follows the solar cycle in that respect. Within the major rise and fall with the sunspot number, both periodicities exhibit variations that cover several years so that there may be three smaller peaks within the major peak. These smaller peaks are greater in the early part of the solar cycle for the 27.70 day periodicity and later in the cycle for the 13.35 day periodicity.

The 13.35 and 27.70 day periodicities are fairly consistent in how they vary over time and with respect to each other for both the Ca K plage index and the 10830A data. These similarities should allow a crude approximation of UV variations over the short-term, at least for the 27-day variations. In order to take advantage of the similarities revealed in these more sophisticated statistical methods, additional analysis in the form of a simple linear regression might give a simple equation which would allow a tentative value for previously unknown short term UV variations.

2.4 Modeled UV 13 to 27-day Power Ratios, and their Relationship to Center to Limb Variations

The effect of the center to limb dependence on the contribution of plage emissions to the UV irradiance is studied by estimating the UV flux for the time period November 7, 1978 to November 2, 1980, and then comparing the modeled UV wavelengths to observations of the UV irradiance made by the SBUV experiment on the NIMBUS-7 satellite . The UV flux is calculated from a model which uses World Data Center (WDC) recorded Ca II K plages to estimate the variations of the solar irradiance at UV wavelengths. Time series analysis yields power spectra of the two data sets that give ratios of thirteen to twenty-seven day variability that are related to the average variation of the center to limb function through the chromosphere and photosphere.

2.4.1 Short-term Variation of the UV wavelengths

One way to easily calculate average variation of the center to limb function is by separating the short term variations from the long term variations and then using the short-term variations of about 27-days (one solar rotation period) and about 13-days (one-half a solar rotation period) to see the effects of varying the center to limb function. The removal of the long term trends by using the residuals from a 12^{th} order polynomial fit to represent the short-term variations allows a close look at the strengths of thirteen (13.35) and twenty-seven (27.70) day periodicities. Figure 2.4.1A shows the observed UV of the 2800A Mg II absorption line (the core of this line is enhanced in the plage data), the modeled UV using the center to limb coeffecients which most closely estimate 13 and 27 day periodicity similar to that seen in the observed 2800A UV, and the 10.7cm radio flux which is often used as a proxy for variations in the UV. This figure clearly indicates the 10.7cm radio flux does not do an adequate job of representing the <u>short-term</u> variations in this wavelength of the UV. The observed and modeled UV on the other hand, show many distinct similarities in their short-term variations; the relative amplitude of rotational variations in the two data sets closely resemble each other, the same is true of the half-rotational variations. The persistence of regions of activity through several rotations is also in good agreement for the observed and modeled UV, while the 10.7cm radio flux shows very little persistence at all. The strengths of the rotational and half-rotational modulation for each individual data set is shown in figure 2.4.1B,

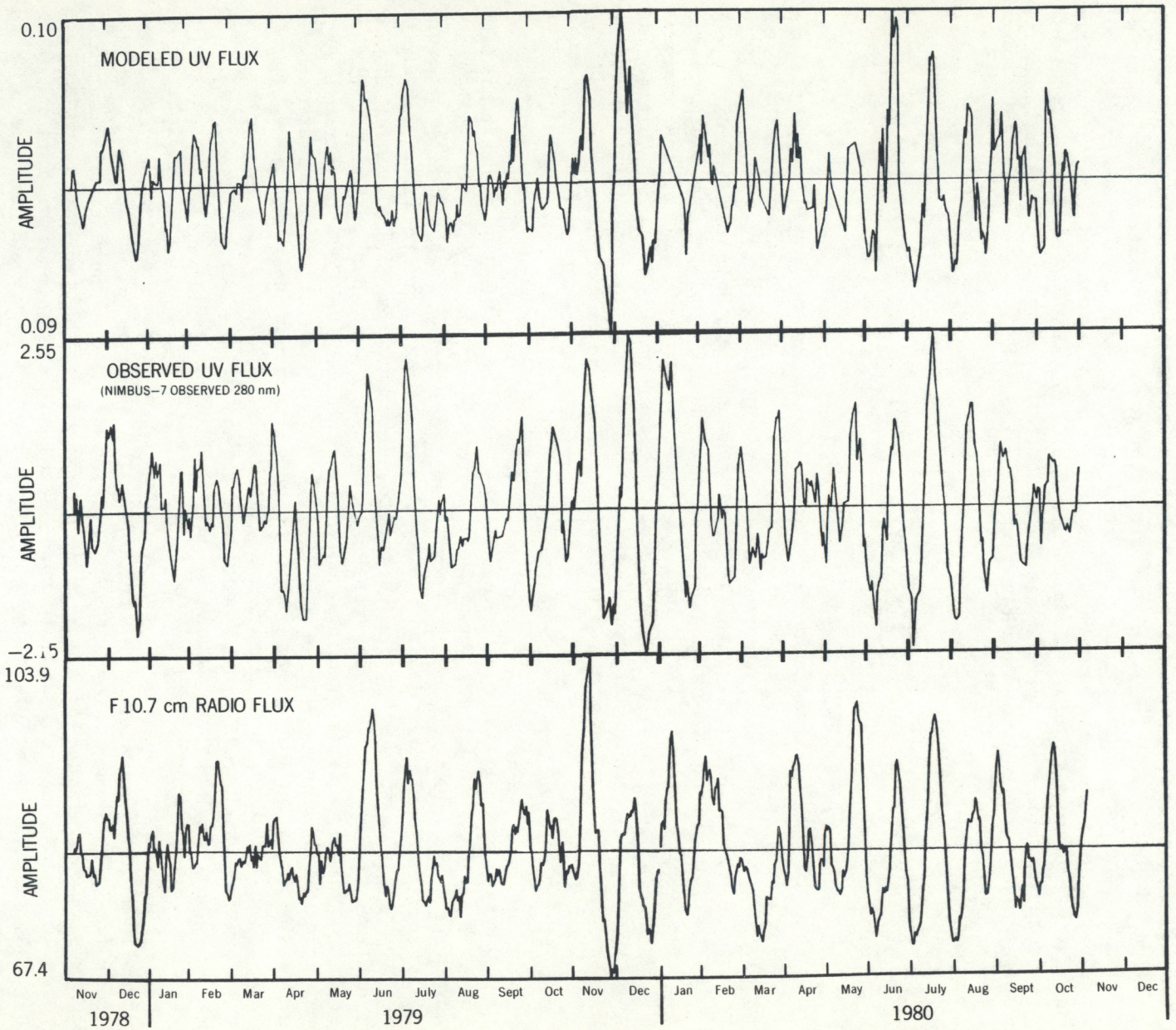

FIGURE 2.4.1A Timeseries of modeled UV flux, NIMBUS-7 observed UV flux, and the 10.7cm Radio flux after the long-term trends were removed by using a 12^{th} order polynomial fit to represent the long-term trends.

COMPLEX DEMODULATION

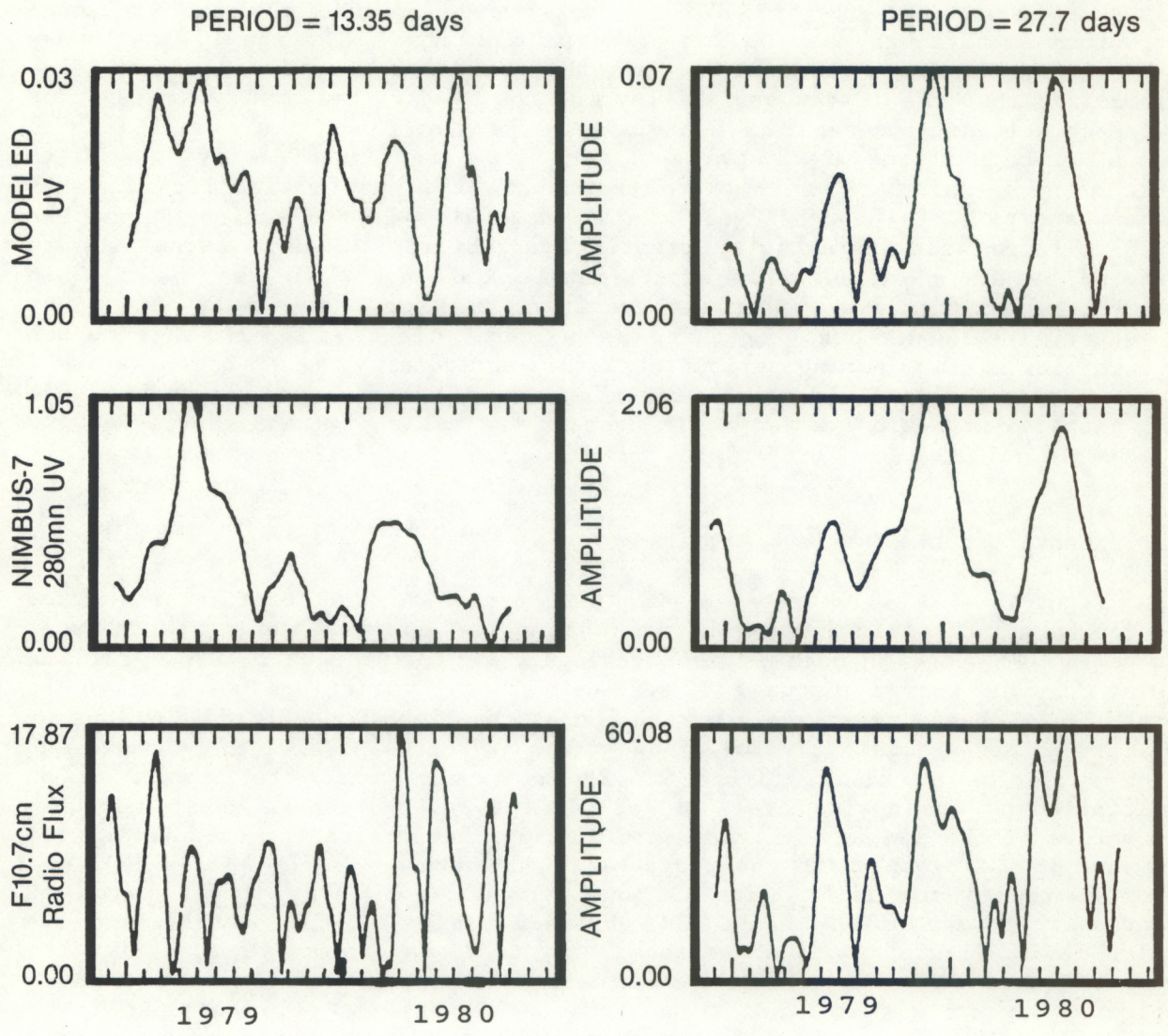

FIGURE 2.4.1B Complex demodulation graphs of 13.35 and 27.70 day periodicities for the modeled UV flux, NIMBUS-7 observed UV flux and the 10.7cm solar radio flux. The complex demodulation shows the strength of the each periodicity over time, for the time period of November 1978 to December 1980. Most obvious is the disagreement of the 10.7cm radio flux to either of the UV values.

where a complex demodulation of the data sets shows there is a remarkable similarity in the 27-day variability between the observed and modeled UV. The complex demodulation shows even more emphatically the differences in short-term variations between the UV wavelengths, and the 10.7cm flux. The thirteen day variability for the two UV data sets have somewhat the same relative structure even though they do not agree particularly well; the 10.7cm 13-day variability bears no resemblence to the UV at all. This figure also emphasizes that the 13-day variability and the 27-day variability are in fact representative of two separate behaviors on the sun, the 13-day variability is not a harmonic of the 27-day variability. Large regions of activity such as that seen on December 8, 1979 are the cause of 27-day variability as they rotate and persist through several rotations. This is one region on the sun with a large area of activity creating variability; 13-day variability is created by areas of activity approximately 180^{o} apart on the sun. When neither of these areas are at the center of the sun, but are at the limbs together, they contribute together to the total plage emission; this causes the shallow minimum during periods of 13-day periodicity. Each of these areas acts independently of the other, for this reason it is important to know how the plage contribution varies as it crosses the solar disk and approaches the limb.

2.4.2 Center to Limb Average Variations

Figure 2.4.2A illustrates a number of center to limb coefficient curves where the heliocentric angle is shown in degrees from the center of the sun; curves 1, 2, and 4 through 10 are previously determined coefficients for the quiet sun UV flux. Curves 11, 12 and 13 are variations we created to drastically change the plage contribution at the limbs and at middle values of 0, curve 3 has a constant value of one which is representative of no center to limb variation at all. Figure 2.4.2B shows the center to limb function multiplied by the cosine of to include the foreshortening created by the curvature of the sun; this figure more clearly illustrates the deep curves 11, 12, and 13 which emphasize the plage emissions between 0 and 45^{o} and fall off rapidly toward the limb. The UV was then modeled using these curves to represent the variation of the WDC observed plages as they transversed the solar disk. Figure 2.4.2C shows the 13-day to 27-day ratios of power for the various curves as well as for a number of special cases. The model uses a weighting function that tends to enhance the 27-day variation because it is related to the intensity of an active region, and those which contribute to the 27-day variation are the largest and brightest. For a number of the curves, (3,10,11,12, and 13), this weighting function was removed from the model; for these curves the superscript "a" represents the model run with the weighting function in, the superscript "b" is the ratio for the model run without the function. In all five cases the removal of the weighting function caused the strength of the 13-day variability to increase. In addition to these special runs there were several other cases of note; the ratios for A1, A2, and A3 are for predetermined curves for the quiet sun which for the sake of clarity are not shown in Figure 2.4.2A or 2.4.2B, but fall between curves 9 and 10. The ratios for 10^{c}, 10^{d}, and 10^{e} show the effects of simply making minor changes to the deepest curve which was already determined for the quiet sun; these were changes made in the first three center to limb coefficients for that curve to emphasize the contribution of the middle of the curve. The other three curves were created to emphasize different sections of the solar disk. Figure 2.4.2D illustrates ratios for the EUV and the UV at selected

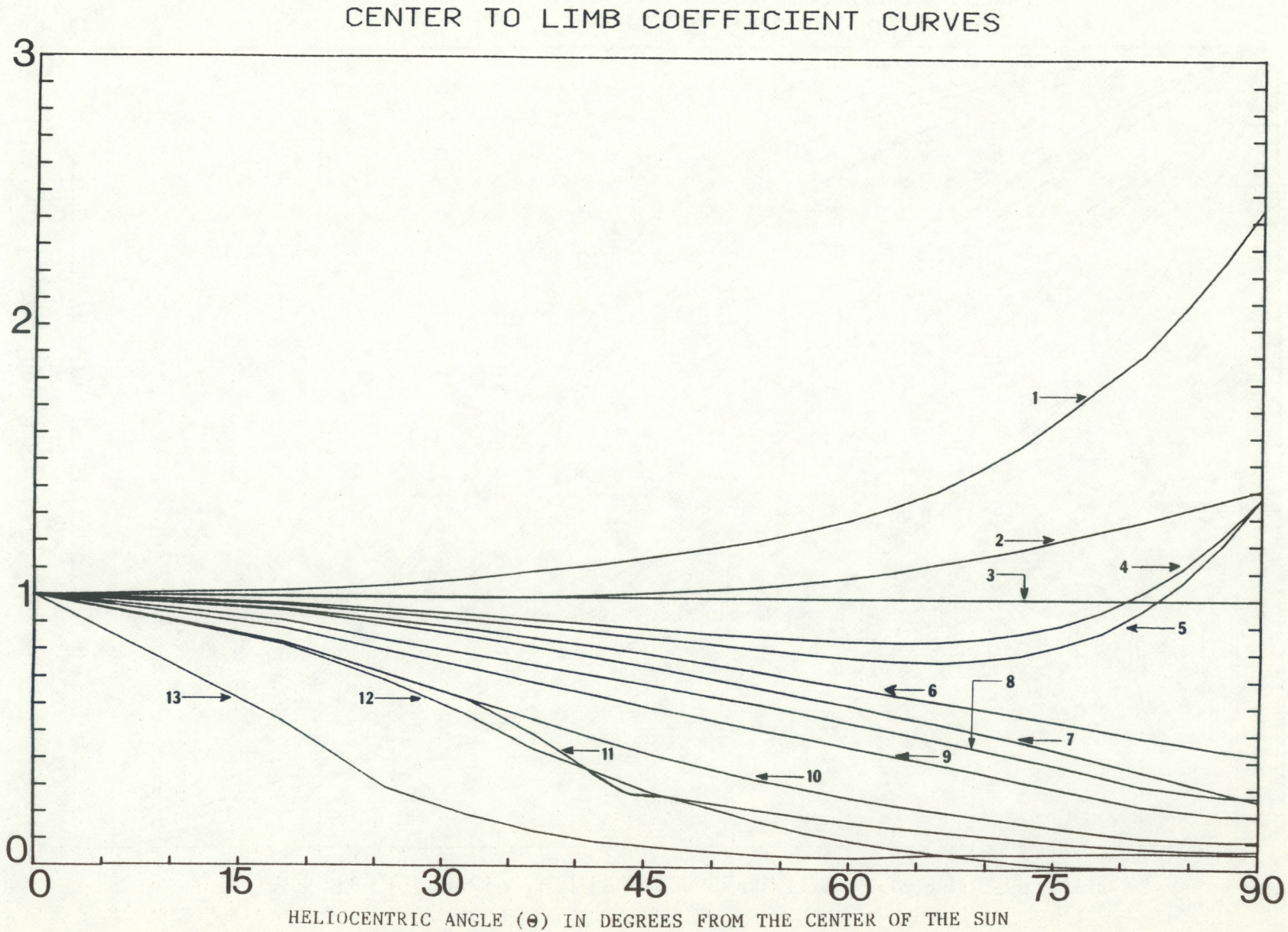

FIGURE 2.4.2A Center to limb coefficient curves for modeling the UV flux, including previously determined coefficient values (Samain, 1978) and new estimates used to improve the accuracy of the model. (Nov. 1978 to Dec. 1980)

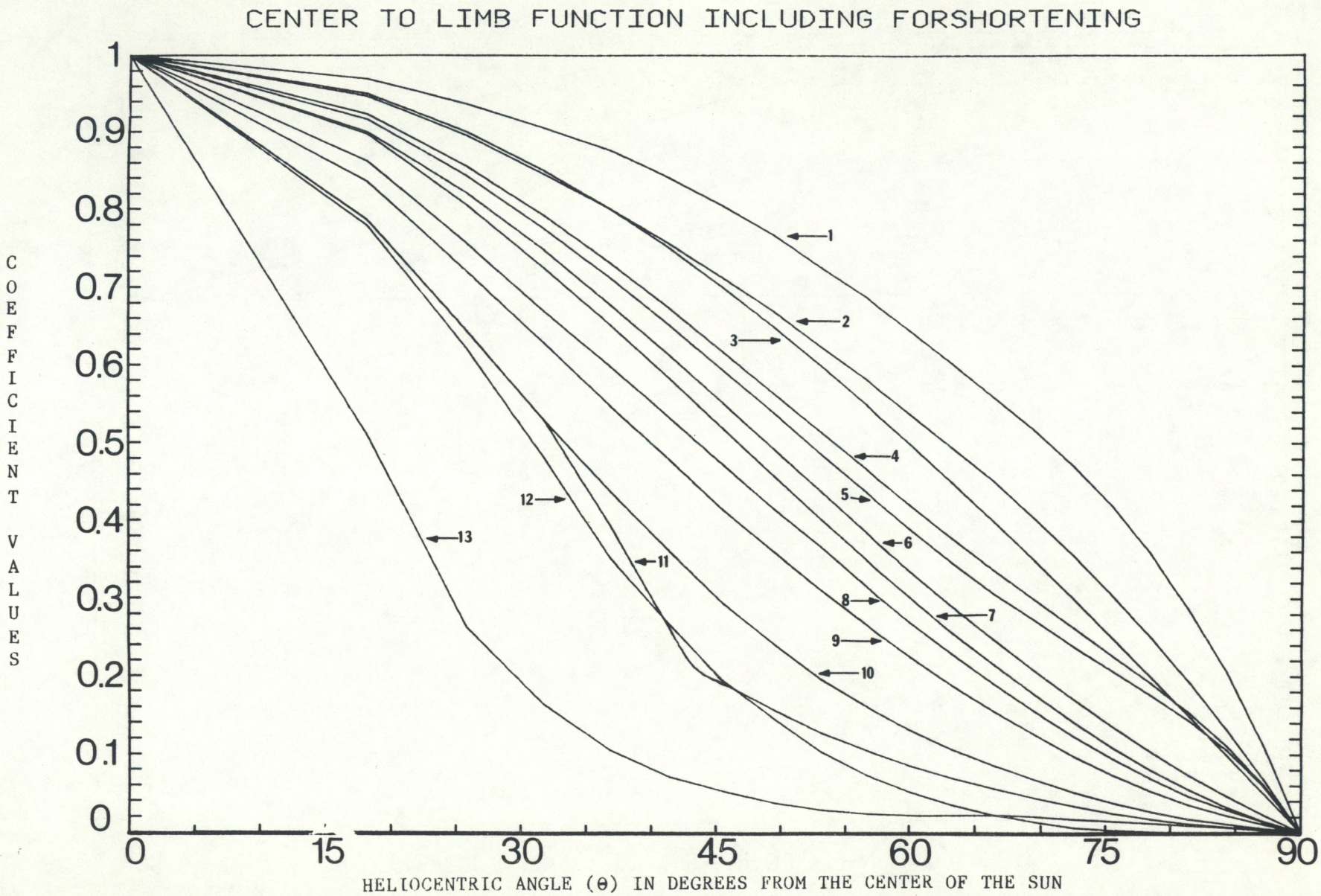

FIGURE 2.4.2B Center to limb coefficient curves for modeling the UV flux, including previously determined coefficient values (Samain, 1978) and new estimates used to improve the accuracy of the model, where the coefficient values have been multiplied by cosine 0 to include foreshortening effects. (11/78 through 12/80)

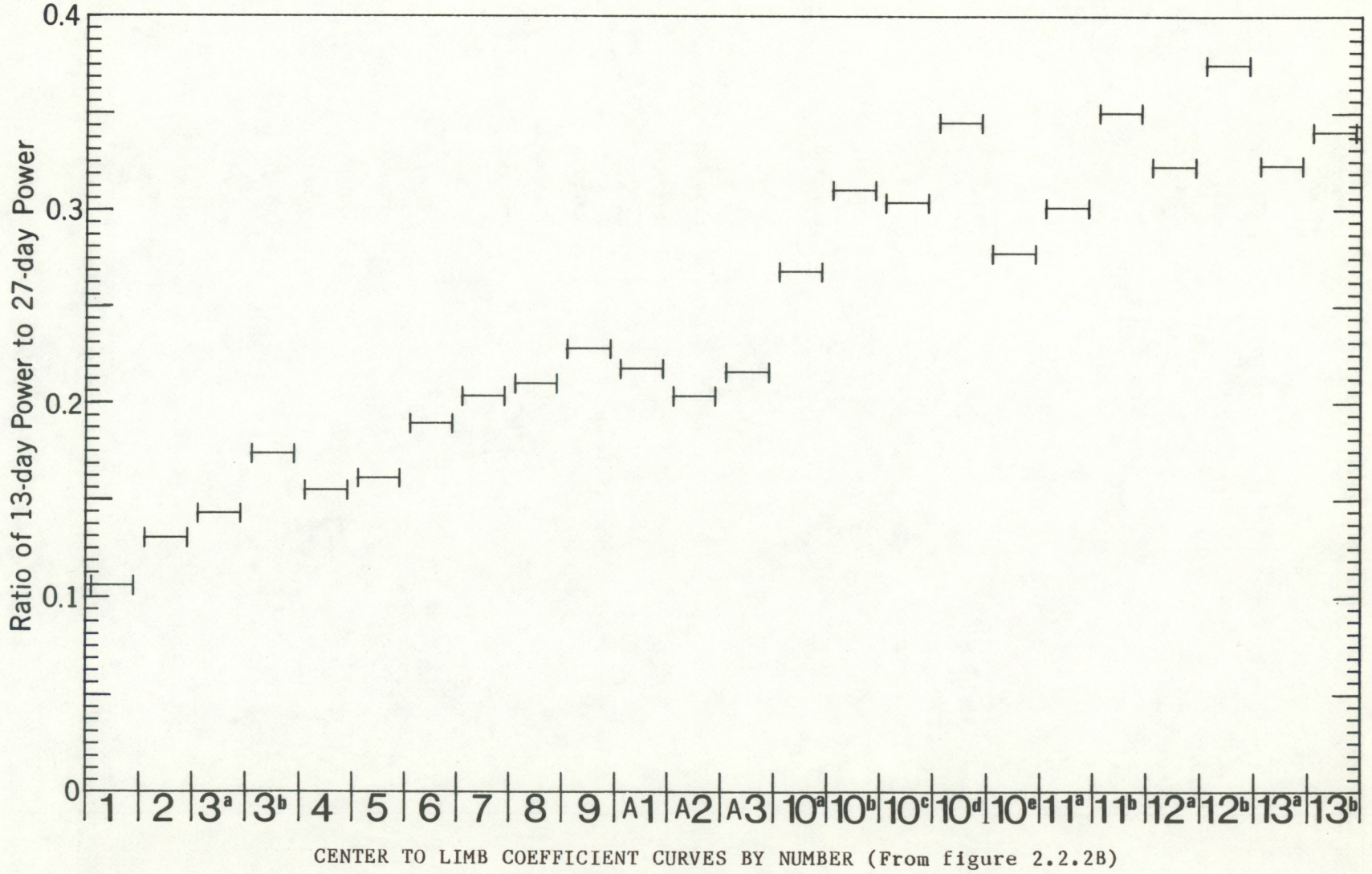

FIGURE 2.4.2C Ratios of power from modeled UV flux values computed using the center to limb coefficients illustrated in figure 2.4.2B. (November 1978 through December 1980)

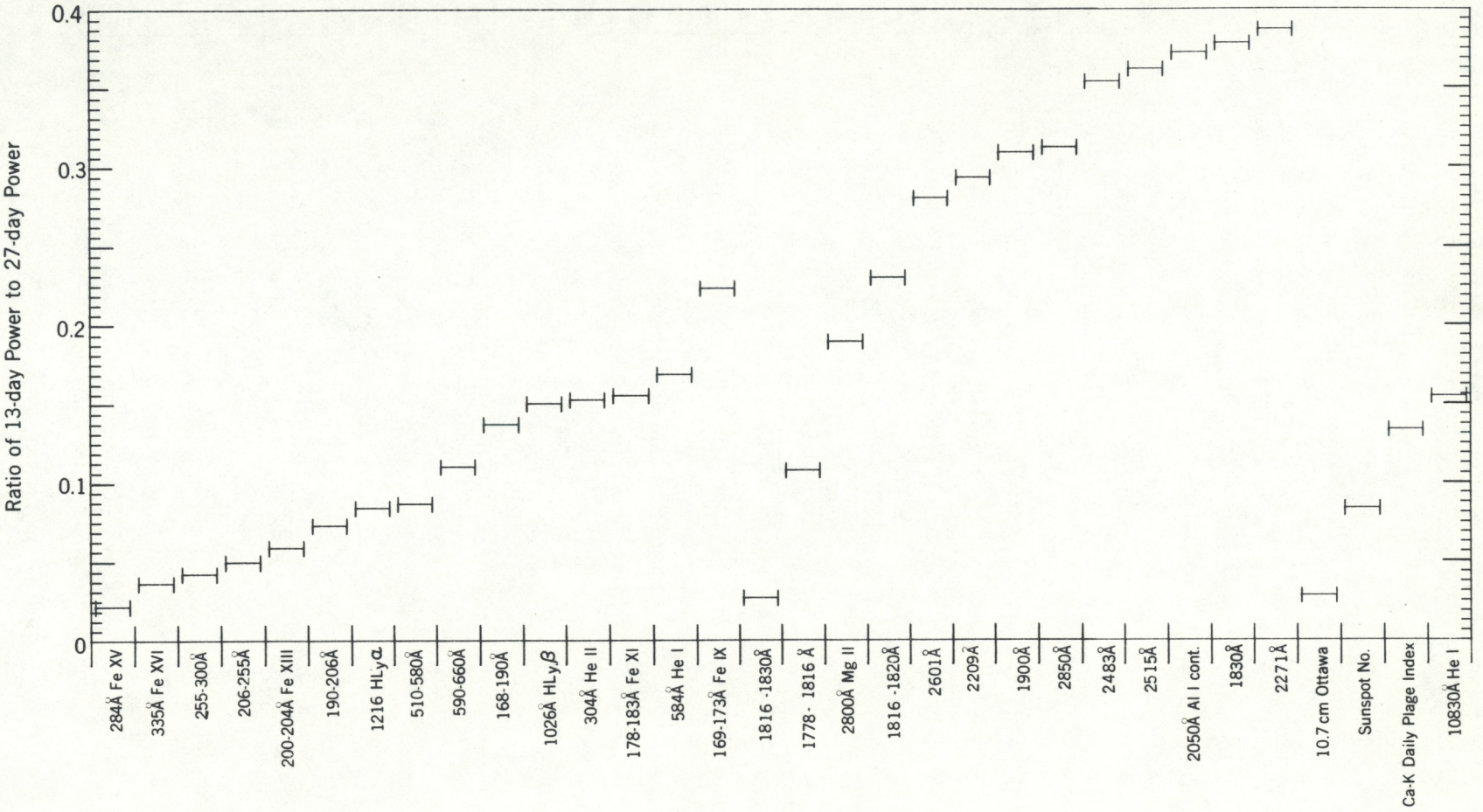

FIGURE 2.4.2D Ratios of power for the EUV, UV and four common indices of solar variability. (November 1978 through December 1980)

wavelengths and for four common measures of solar activity for the same November 7, 1978 to November 1, 1980 time period after long-term trends have been removed from the data. This figure in conjunction with figure 2.4.2C indicates which average center to limb variation best explains a number of the EUV and UV wavelengths.

Conclusions

- The quiet sun curves do not explain all the center to limb variation seen in the short-term variations caused by the plages in the modeled UV.

- The fairly small number of EUV and UV wavelengths which have ratios similar to those created by the various center to limb curves suggests that along with the center to limb variation there might possibly be another component in the short-term variations in the UV, or that the rotational persistence of the model is insufficient.

- Since the ratios found using curve 12 are the highest, it is likely that center to limb curves very near this one are likely to produce the highest ratios of 13-day to 27-day power, and thus curves below this one are probably not useful for the UV we are interested in which have high ratios.

- The lack of 13-day to 27-day ratios of power above .35, even though a number of ratios for the UV exceed .40 (not shown), suggests there might be something besides the center to limb variation contributing to the short term variations.

2.5 Harmonic Content and the Full-Disk Filter Effect

R.F. Donnelly and D. Stevens

We do not like to call the 13-day periodicity a second harmonic of the 27-day periodicity because it does not rise and fall in phase with the 27-day quasi-periodicity and its period is slightly less than half that of the 27-day periodicity. However, because the 27-day solar-rotational variations are not pure sinusoids, there must exist harmonics of the 27-day periodicity and these related harmonics are examined below. Solar physicists tend to wonder whether the 13-day periodicity in UV fluxes implies that certain modes of solar oscillations or global ringing tend to enhance the emergence of solar activity about 180° apart in solar longitude. Perhaps there are preferential modes, but it is important to realize that full-disk flux measurements have certain filter effects related to the CMD dependence of the active-region emission that strongly influence the strength of their rotation related periods. These filter effects are also discussed below.

Figure 6.1 of Donnelly et al. (1986b) shows empirical estimates of the average dependence of active-region emission on the solar central meridian distance (CMD) for the solar 10.7 cm radiation, 1-8Å soft X-ray emissions, the sunspot number and UV flux. Figures 6.2 - 6.4 of that report show the temporal variations corresponding to these CMD dependencies for the following cases: (a) one plage, (b) two equal plages 180°apart in solar rotation, (c) one pair of equal plages separated longitudinally by two days of solar rotation, and (d) two such equal pairs where the mid-points of each pair were 180° apart. The temporal evolution of the plages was neglected. Real plages usually vary a lot over a solar rotation and the emergence of new plages in the same longitudinal vicinity are often slightly shifted in longitude. These evolutional variations and phase shifts during episodes of activity would greatly broaden and weaken the peak intensity of power-spectra lines at the higher harmonics. In other words, the power in the harmonics for Figures 6.2 - 6.4 is higher than would occur in real solar data.

The time series for Figures 6.2 - 6.4 were analyzed for daily-sampled data with the same numerical-analysis computer programs developed by T. Repoff that have been used for all of our power spectra analyses. The time series in Figures 6.2 - 6.4 were revised to a 32-day period rather than 28-days so that the even harmonies (16, 8, 4, and 2 days) would fit with the frequency grid used in Repoff's program; however, the results of these analyses for the more realistic plage-pair cases are presented in Table 2.5A, where the values given are 100% times the ratio of the peak power in the harmonic to that in the fundamental. The very low power in the harmonics for the case of two pairs of plages, where the centers of the pairs are 180° apart, shows that the UV CMD dependence for two equal peaks per rotation forms a near perfect 13-day sinusoid. The 27% power in the second harmonic for the UV CMD dependence for one peak per rotation is too low compared to the 13- to 27-day power ratios observed for photospheric UV fluxes in 1979-1980. The higher observed ratios come from episodes of predominantly 13-day periodicity. On the other hand, from the complex demodulation analyses, the ratio of 13- to 27-day power during episodes of strong 27-day variations tends to be less than 5% for photospheric

UV fluxes. These lower observed values are probably the consequence of the quasi-periodic nature of the observations, i.e., the rise and fall of 27-day periodicity over a few months, rather than the constant plage results in Table 2.5A.

TABLE 2.5A Harmonic Content

	Percent Power Ratio			
	One Peak Per Rotation One Plage-Pair		Two Peaks Per Rotation Two Plage-Pairs	
CMD Dependence	Second Harmonic	Third Harmonic	Second Harmonic	Third Harmonic
UV	27	1.5	0.05	~0
Sunspot Number	13	0.3	1.2	0.05
10.7 cm, F10	2.2	<0.1	0.3	0.2
1-8Å X-Rays	4.3	4.5	36	4.4
Fundamental =	27-day Periodicity		13-day Periodicity	

The important results in Table 2.5A are the relative values. For example, the second harmonic for two pairs of plages (13 to 14 periodicity) is large only for the solar soft X-rays, which fits with the 6.7 day line occurring only in the power spectra for soft X-ray observations. Also, the second harmonic even for one plage pair is very weak for F10.

Figure 2.5.1 shows the case of three equal plages spaced one-third solar rotation apart (neglecting the latitude and B angle = 0). The 9-day modulation is there for the UV, but at 40% the peak-to-peak amplitude compared to the two-peaks per rotation case. For R and F10 the peak-to-peak modulation is quite small, far differently shaped than a sinusoid, and out of phase with respect to the UV signal. The soft X-ray modulation is the only case still near full strength and is now closer to a sinusoid than in the one-peak or two-peaks per rotation cases. It is still out of phase with the UV flux or plage data. There is no evidence for a distinct peak at 9 days in the power spectra for soft X-rays, EUV or UV observations (Figures 3.7 and 4.3, Donnelly et al., 1986b). From the viewpoint of random occurrence as a function of solar longitude, the chance of three nearly equal-strength peaks in the plage distribution as a function of solar longitude spaced nearly one-third solar rotation apart is very small compared to one main peak per rotation or even two peaks per rotation. Even if three peaks per rotation were a preferential mode for region emergence, as long as one of the peaks were stronger than the others then the 27-day periodicity would greatly dominate over any 9-day periodicity.

The main point we want to make here is that the full-disk flux has a filter effect caused by the breadth of an active region's CMD dependence at a particular wavelength that filters out higher modes. This can best be seen by the peak-to-peak amplitudes in Table 2.5B, where one peak means one plage per solar rotation, two peaks means two equal plages spaced 180° apart in solar

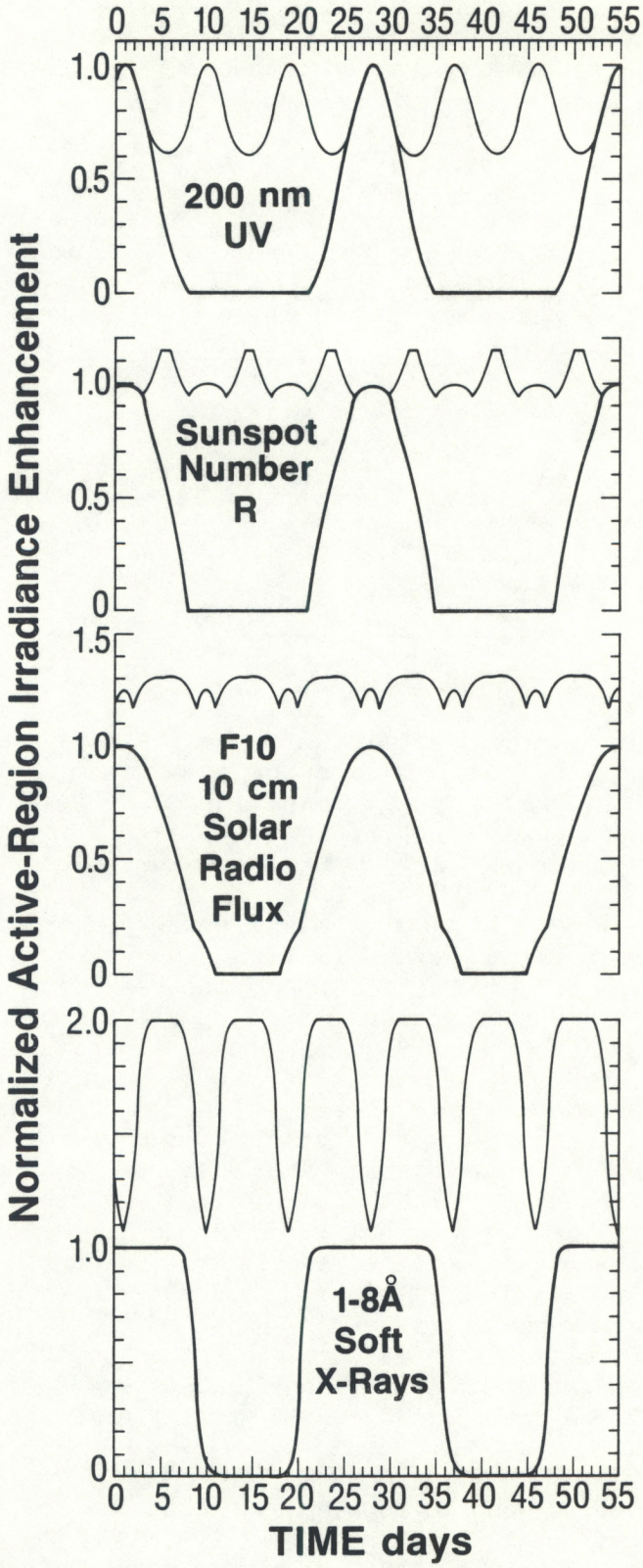

FIGURE 2.5.1 Periodicities in the 200nm UV, the sunspot number "R", the 10cm solar radio flux (F10), and the 1-8A soft X-rays caused by solar active region modulation.

longitude, three means three equal plages spaced 120° apart, and four means equal plages spaced 90° apart. If the CMD dependence for F10 were slightly raised at 90° to bring into agreement the lack of an observed 13-day peak, the higher modes would also decrease to near zero in Table 2.5B. Although the soft X-rays do not have a strong filter effect, they are very sensitive to temporal variations caused by solar flares and other fluctuations in the hot coronal cores of active regions, which causes a large broad-band background in their power spectra that can mask small lines in the spectra. The soft X-ray wave forms for the one-peak and two peaks per rotation cases are very non sinusoidal, which means they are rich in harmonics that would complicate the interpretation of lines like the 6.7-day line (fourth harmonic for episodes of one peak per rotation, second harmonic for episodes of four peaks per rotation?). In conclusion, full-disk flux data involve a low-pass filter effect. Spatially resolved data are more suited for studying special modes for solar ringing.

TABLE 2.5B Low-Pass Filter Effect

	Peak-to-Peak Amplitudes			
CMD Dependence	One Peak	Two Peaks	Three Peaks	Four Peaks
UV	1	1	0.38	0.02
Sunspot Number	1	1	0.20	0.45
10.7 cm, F10	1	0.29	0.13	0.03
1-8Å X-Rays	1	0.91	0.93	0.91

3. ANALYSIS OF SOLAR UV IRRADIANCE MEASUREMENTS FROM THE NIMBUS-7 SATELLITE

3.1 Short-Term Temporal Variations for 171-285 nm

G. D. Falcon and R. F. Donnelly

Heath et al. (1984) studied the autocorrelation and power spectra of the short-term variations of solar UV irradiance measurements from the NIMBUS-7 satellite at the following six wavelength groups: (1) 181.6-182.2nm, Si II lines (2) 200-205 nm, Al I continuum, (3) 279.8-280.2nm, Mg II H & K absorption lines, (4) 285.2 to 285.4nm, Mg I absorption line, (5) 393.3-393.7nm, Ca II K line and (6) 396.9-397.1nm, Ca H line. The results of similar analyses of the short-term variations of NIMBUS-7 measurements of the solar UV spectral irradiance are presented below for many more wavelengths in the 171-285 nm wavelength range during November 1978 through November 1, 1980. Slightly more than 500 days of valid measurements were obtained during this period for each of the frequency ranges considered. A thorough description of the NIMBUS-7 SBUV (Solar Backscattered Ultra Violet) experiment is given by Heath et al. (1975). Only short-term variations are studied here because the NIMBUS-7 data analyzed did not include corrections for long-term instrumentation drifts. Long and intermediate-term variations were removed by first fitting a twelfth-order polynomial to the two year data set then removing the polynomial values and analyzing the short-term variations of the residuals.

The 210-276 nm wavelength range has been neglected in most previous analyses because its percentage variation of the flux is considerably less than that below 210 nm, i.e. below the Al I absorption edge. However, because the average UV flux is much stronger at wavelengths longer than the Al I edge, the 210-276 nm flux change is very important in the computation of atmospheric effects. Specific frequencies used for this analysis were chosen according to their interesting characteristics in the spectrum of short-term fractional variations shown in Figure 3.1. NIMBUS-7 data at wavelengths of several local maxima and minima values in Figure 3.1 were analyzed and compared with each other and with previous results (Heath et al., 1984) for the key lines of Si II, Mg I, and Mg II, and just below the Al I continuum. In addition, several wavelengths, in the 171-205 nm range are included to cover wavelengths shorter than the Al I edge. See Table 3.1.

The autocorrelation function compares a time-varying data set to itself shifted in time by different amounts of time, or days of lag, thus revealing any repeated features in the data. Autocorrelation functions for six wavelengths in the range considered here are shown in Figure 3.2. The temporal variations at wavelengths of 190 nm, 205 nm, and 280 nm all show high autocorrelation values and similar values for corresponding days of lag, thus indicating similar rotational behavior. The 280 nm data involve major solar absorption lines and the 205 nm data involve the strong Al I continuum absorption just below the absorption edge. However the 190 nm data do not involve important lines or absorption edges, but is a rather common wavelength in the Al I continuum. The 220 nm and 248 nm autocorrelation values are very similar to each other in numerical values and skewed periodic variations. Figure 3.1 shows that the average fractional variations for short-term variations at these wavelengths is about the same for these two wavelengths. The autocorre-

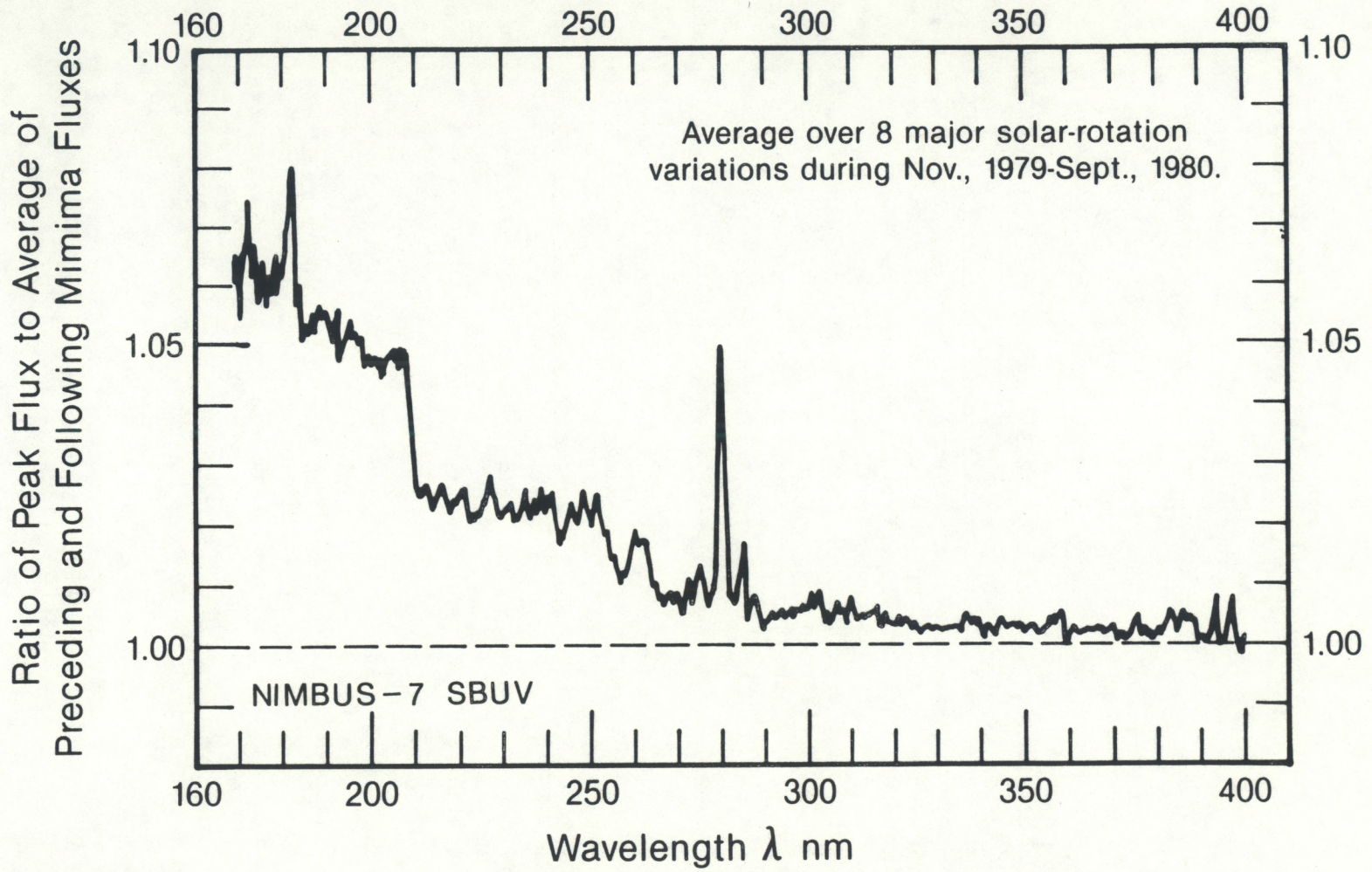

Figure 3.1 Average spectra of fractional variations caused mainly by the solar-rotation of major groups of active regions (Donnelly, 1985).

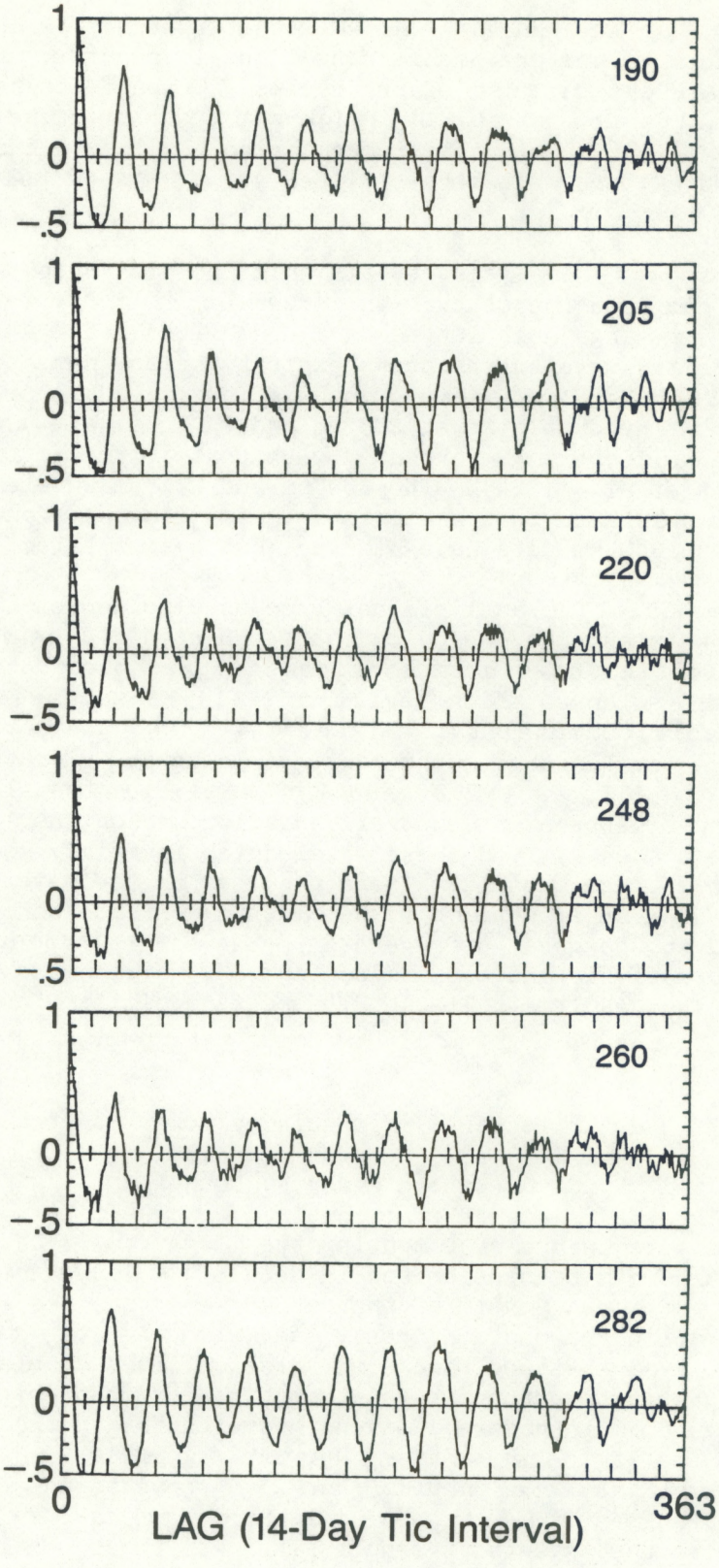

Figure 3.2 Autocorrelations as a function of days of lag for November 7, 1978 - November 1, 1980.

lation behavior for the 260 nm flux is least like any of the others in this set. The numerical values are smaller and there is considerably more irregularity in the valleys of most of the cycles. Compared to the diverse cross-correlation results for solar EUV and X-ray flux measurements found by Donnelly et al. (1986), the cross-correlation results (not shown) for the UV measurements studied here were very similar, very symmetrical and had no lag shifts.

The power spectra analysis reveals which portion of the total functional variance comes from each frequency. The power spectra for a few wavelengths in the 160-276 nm range are plotted on a normalized scale and shown in Figure 3.3. Each of the six wavelengths shown exhibit the dominant 27-day (actually 27.7 days) periodicity with some pronounced degree of 13 day (actually 13.35 day) periodicity. The data sets at 205 nm and 227 nm have the strongest 13-day periodicity and compare favorably with that of the Mg I line as reported previously (Heath et al., 1984). The 260 nm and 211 nm wavelengths have similar 13-day periodicities that are both smaller than that for the 205 nm data, and the 171 nm and 280 nm data have similar, but even smaller 13-day values.

Complex demodulation analysis has been used to depict the variation with time in a given wavelength's energy output for a specific periodicity. While several periodicities have been considered, the solar rotational period of 27.7 days and half solar rotation period of 13.35 days have been the values showing reasonable commonality. Figure 3.4 shows the complex demodulation analysis for five wavelengths in the range of interest. For the 27.7 day periodicity, the 171, 205, 248, 260, and 280 nm wavelengths all show remarkable similarity in their pattern of temporal variations. For the 13.3 day periodicity, the agreement among all of these wavelengths is fairly good, but not nearly so as for the 27.7 day result. These results for the wavelengths not previously analyzed are in agreement with those described before (Heath et al., 1984). Compared to the great differences in the complex demodulation results found for solar activity indices and coronal EUV wavelengths (Donnelly et al., 1985, 1986a,b), the results in Figure 3.4 are very similar from one wavelength to another.

3.2 Ratios of 13- and 27-Day Power Spectra

G.D. Falcon and R.F. Donnelly

The analysis technique of computing the 13-day to 27-day power ratio from the spectra results has been described in detail by Donnelly et al. (1986b). Some of the major conclusions of that study were that the 13-day periodicity is not simply a second harmonic of the 27-day periodicity, the ratio depends on the time interval analyzed, and some emission lines display ratios that are strongly photospheric in nature while others are chromospheric-like or similar to transition region in nature. Several wavelengths in the 160-285 nm region were studied to see if there were any resemblances to each other as to the major lines previously examined. Figure 3.5 presents these ratios. The upward pointing triangles indicate wavelengths which have relative maxima in Figure 3.1, while the inverted triangles indicate those wavelengths which have relative minima in that figure. See also Table 3.1. The unlettered dots between 170 nm and 196 nm represent wavelengths below the Al I 205 nm edge that are neither distinct local minima or maxima in Figure 3.1. The lettered dots

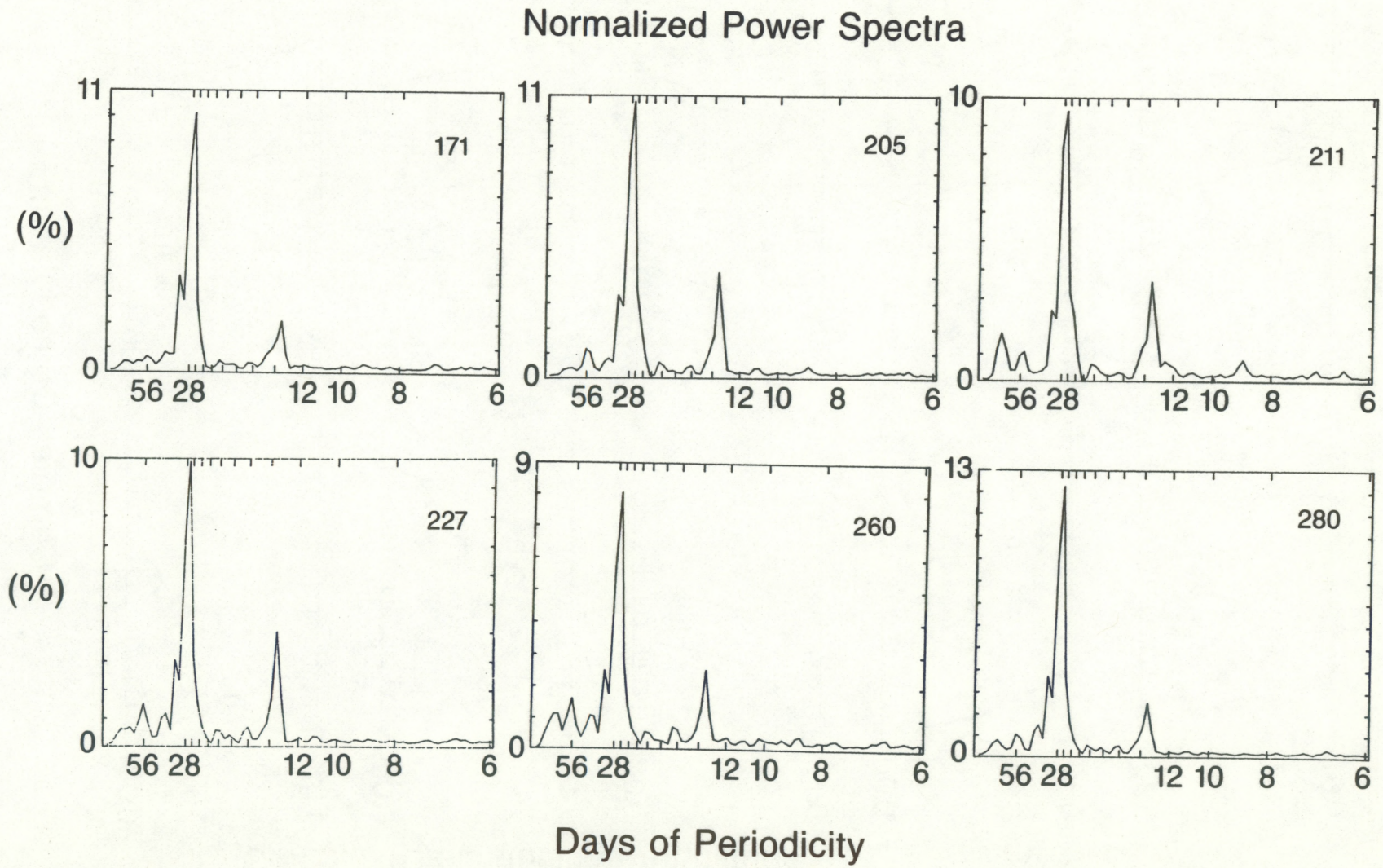

Figure 3.3 Power spectra for the short-term variations during November 7, 1978 - November 1, 1980, normalized so the sum over the frequency grid (periods from 2 to 512 days) is 100%.

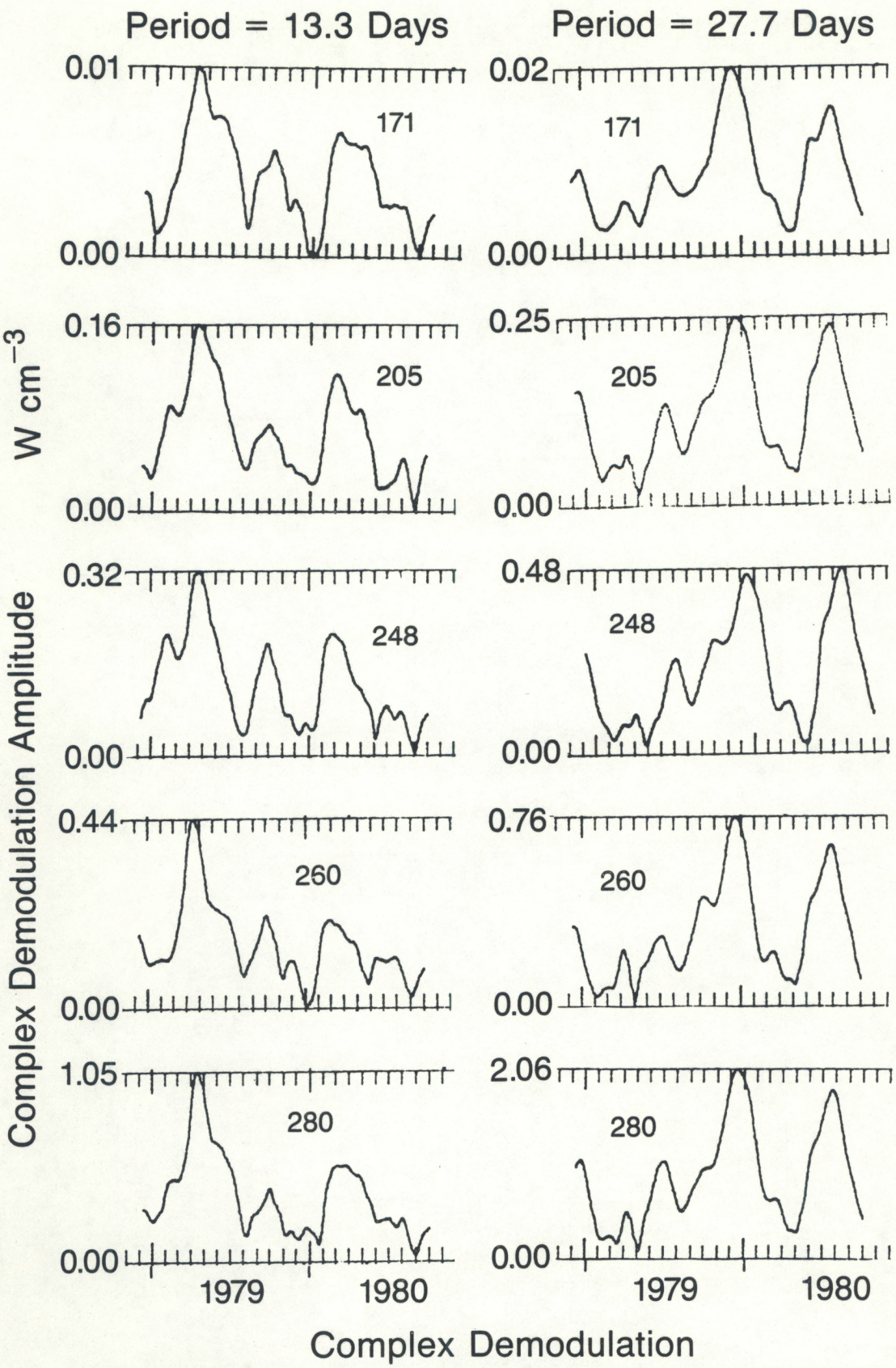

Figure 3.4 Complex demodulation amplitude for the sinusoidal signal strength for the two main solar-rotational periods.

will be discussed in the next section. The value for P_{12} in the formula in Table 3.1 represents a best estimate for a background continuum noise level which was removed from the line-plus-continuum values of $P_{13.47}$ and P_{27}.

Table 3.1. Ratio of 13-day Power to 27-day Power

Wavelength nm	Comments of Characteristics in Figure 4.1	$\frac{P_{13.47} - P_{12}}{P_{27} - P_{12}}$
171.0	local maximum, Fe II, I & Cr II emission lines	.1818
177.8	local minimum	.397
181.6 - 182.0	Si II lines, strong maximum	.230
183.0	local minimum	.378
187.6	A1 I continuum, Fe II emission lines	.423
190.0	A1 I continuum , Si III lines in sideband	.309
196.4	A1 I continuum	.439
205.0	A1 I continuum, near edge	.372
215.8	local maximum, Fe I, II, Ti II lines	.372
221.0	local maximum, Si I, A1 I, & Ni II lines	.293
223.2	local minimum, Mg I continuum	.443
226.6 - 227.2	local maximum, A1 I, Ni II & Fe I absorption lines	.387
243.2	local minimum	.423
248.4	local maximum, Fe I, II lines	.354
251.6	local maximum, Si I line	.362
257.0	local minimum, longer than Mg I edge	.511
260.2	local maximum, Fe II, Mg I lines	.280
271.4	local minimum	.426
275.2	local maximum, Fe I, II lines	.189
279.8 - 280.2	Mg II H & K major absorption lines, unresolved	.189
285.0 - 285.4	Mg I, strong absorption line	.312

The wavelengths 177 nm, 183 nm 187 nm, and 196 nm (the four highest dots of Figure 3.5) all have ratios much closer to that for Al I at 205 nm than to the ratios for the Si II and Mg II lines. The 190 nm wavelength has a value intermediate to those for Al I and Si II. Thus, these wavelength's emissions are probably more akin to the physical aspects of Al I emissions than to those of the closer wavelength of Si II. The large relative peak at 171 nm has a ratio of .182, similar to that of Si II (.230). The ratio for 275 nm, .189, is practically identical to that of the Mg II line at 280 nm (computed at 279-280 nm).

Most of the numerous wavelengths between the Al I and Mg II values have ratios similar to those of Al I and Mg I. Figure 3.1 shows the 256 nm wavelength to be in a weak amplitude region, so the power ratio would be more affected by noise problems than at nearby wavelengths of higher fractional variation. The same argument can be applied to a lesser extent to the ratios for the 243 nm, 271 nm, and the 223 nm wavelengths. However, that is not enough

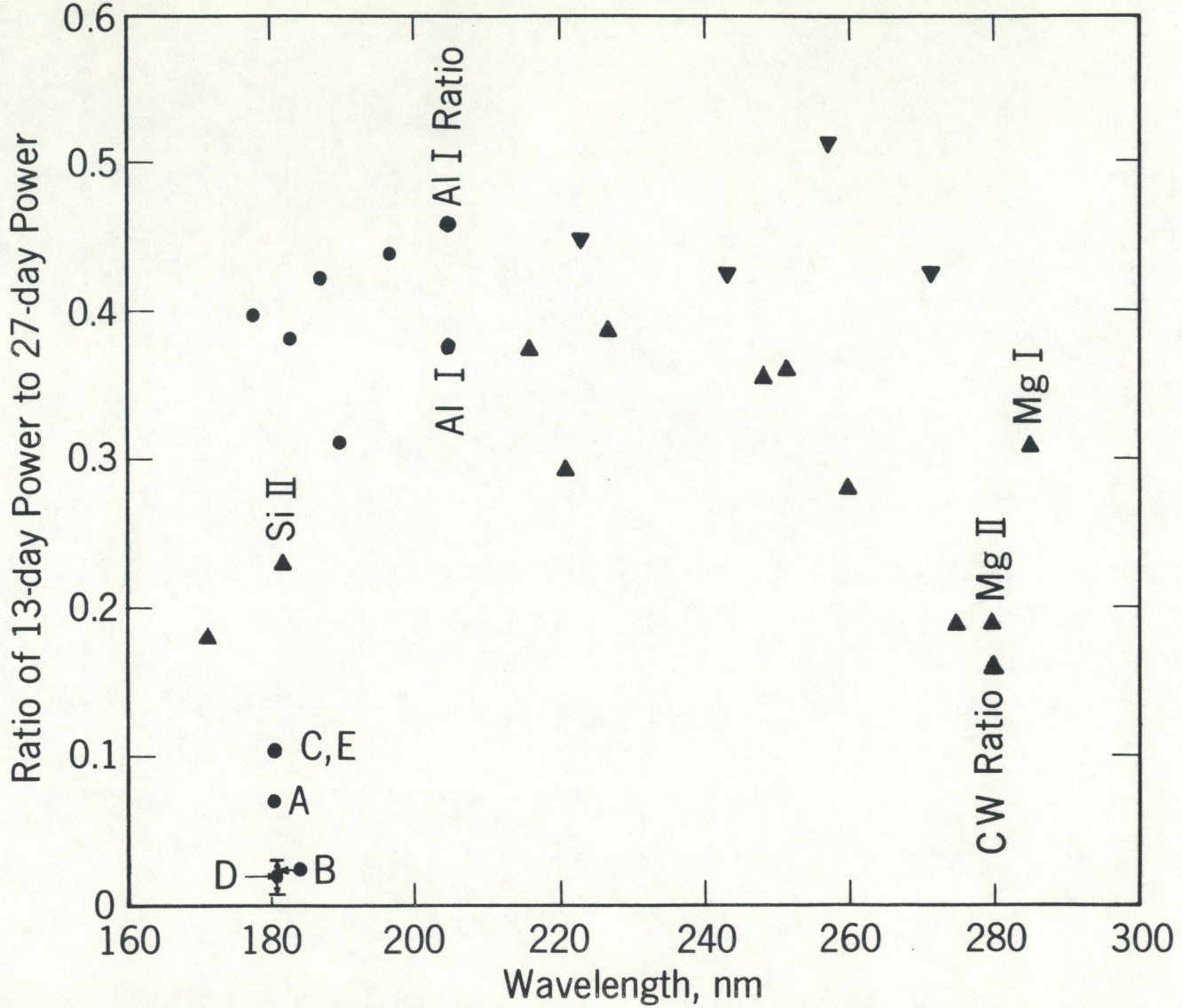

Figure 3.5 Ratio of 13-day to 27-day power as a function of wavelength. The upward pointed triangles correspond to local maxima with respect to wavelength in Figure 3.1, the downward pointed triangles are local minima, and the solid circles are neither distinct minima or maxima.

to explain the general pattern in Figure 3.5 that the downward pointed triangles all have higher ratios than the upward pointed arrows. In Table 3.1, the wavelengths corresponding to local maxima in the 210-271 nm range tend to involve lines that are partially from the chromosphere, like lines of Fe II, Ni II and Ti II, etc. We suggest that the peaks in Figure 3.1 tend to be caused partially by chromospheric lines while the local valley tend to be more predominantly photospheric emissions, e.g. influenced by the Mg I continuum in the 210-256 nm range, where the 13- to 27-day power ratio tends to be higher for the photospheric emissions than for those that are partially chromospheric.

3.3 The Si II Lines With The Al I Continuum Removed

G.D. Falcon and R.F. Donnelly

The purpose of this analysis is to determine the extent to which the background of the Al I emission continuum affects the flux at the wavelength of the Si II lines. The technique used was to select wavelengths slightly different from 182 nm to be used to study the characteristics of the nearby Al I background continuum values, and to see if these were more like the results for 205 or 182 nm. Additionally, these values close to 182 nm were used to estimate the background values at 182 nm to be subtracted from the total flux at 182, to see how much the resultant power-line ratio for the modified data at 182 nm differs from the unmodified ratio.

First, wavelengths of 177, 183, 187, 190, and 196 nm were chosen for comparing their short-term variations to those at 182 and 205 nm. Wavelengths of 177 and 183 nm were selected because these were the closest to the line at 182 nm that were on the roughly linear trend from the short-wavelength side (~205 nm) of the Al I edge through decreasing wavelength to 170 nm in Figure 3.1. The values at 190 and 196 nm were also on this line, but about halfway between 182 and 205 nm, and showed no prominance in Figure 3.1 of any sort. The flux at 187 nm was chosen in case that at 183 nm was still strongly affected by the 182 nm emission line. For the individual wavelengths used, 177, 183, 187 and 196 nm each had 13-day to 27-day power ratios much closer to that of Al I at 205 nm than to the ratio for Si II. The ratio for 183 nm in fact had a value, 0.378, nearly identical to that near the Al I edge. The ratio for 190 nm was about halfway between the Al I and Si II values, but still slightly closer to the value of Al I at 205 nm.

With respect to the complex demodulation analysis, the results for 177 nm are more nearly like those for 205 nm than those of 182 nm for the 13.3 day periodicity and about the same as those two reference sets for the 27.7 day periodicity. However, there is no significant difference in either the 13.3- or 27.7-day periodicity results between the reference wavelengths and the 183, 187, 190, and 196 nm results. In terms of 13- to 27-day power ratios, the flux for each of these five wavelengths had ratios closer to that of the Al I continuum at 205 nm, than for the combination of the Si II lines and Al I continuum near 182 nm, i.e. the unmodified data at 182 nm.

In determining the influence of the Al I background, flux values for five wavelengths or combinations thereof were subtracted, day-by-day, from the corresponding flux of the 181-182 nm measurements. These cases are defined in Table 3.2 and marked with the corresponding letter A - E in Figure 3.5. The important result in Table 3.2 and in Figure 3.5 is that all of the cases for

Si II with the Al I continuum removed involve much lower ratios of 13- to 27-day power. The Si II lines by themselves are nearly devoid of 13-day periodicity.

Table 3.2 Ratio of 13-day Power to 27-day Power

Case	Si II Flux with Al I Continuum Removed	$\frac{P_{13.47} - P_{12}}{P_{27} - P_{12}}$
A	$F(181.6\text{-}182.0,t) - \frac{F(183.0,t)+F(177.8,t)}{2}$	0.070
B	$F(181.6\text{-}182.0,t) - \frac{F(187.6,t)+F(177.8,t)}{2}$	0.030
C	$F(181.6\text{-}182.0,t) - F(177.8,t)$	0.108
D	$F(181.6\text{-}182.0,t) - F(183.0,t)$	0.027
E	$F(181.6\text{-}182.0,t) - F(187.6,t)$	0.107
	Mean for A-E	0.117
Δ	F(181.6-182.0,t), no Al I continuum removed	0.230

Figure 3.6 shows the autocorrelation function and power spectra for case B of the Si II line with the Al I background continuum removed. The autocorrelation function shows strong 27-day recurrence with a persistence comparable to the results for chromospheric EUV results (Donnelly et al., 1986b) but not as strong as for the photospheric Al I flux at 205 nm. The results in Figure 3.6 are fairly free of noise, which can be a problem in the small difference calculations for cases A to E in Table 4.2. The power spectra show a strong 27-day solar-rotational line but very little evidence of a line at 13.3 days, which means the computation of 13- to 27-day power ratios involves a small difference computation in the numerator when the background power continuum is removed. The error bars for case D in Figure 3.5 are an estimate of the uncertainly caused by the P_{12} estimate of the power-spectra continuum.

Before these results were obtained, the following viewpoint existed: The ratio of 13-day power to 27-day power was high (~1/3 for this same 2 year interval, Heath et al., 1984) for photospheric fluxes, like the Al I continuum and Mg I line. The results for UV lines partially emitted from the chromosphere, specifically the Mg II lines at 280 nm and Si II lines near 182 nm, were smaller (~1/6, Heath et al., 1984). EUV chromospheric (and base of the transition region) lines like H Lyman beta at 1026 A, He I at 584 A, and He II at 304 A, the ratios agreed with those for the UV Si II lines (including Al I continuum) and Mg II lines and were much higher than the results for coronal EUV lines (Donnelly et al., 1986a,b). However, the ratio for the chromospheric H Lyman alpha emission line, the strongest emission line in the solar spectrum, was distinctly lower than the rest of the chromospheric results (~1/12 for Nov. 1, 1978 - Nov. 1, 1980, Donnelly et al., 1986b). Now the UV result for Si II, after removing the Al I continuum, is also lower than the

other chromospheric EUV lines, which is important for the studies of average CMD dependencies of plages as a function of wavelength or source region.

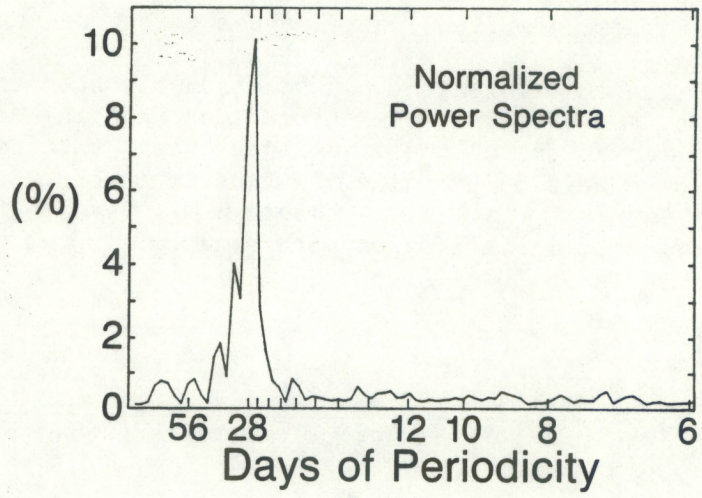

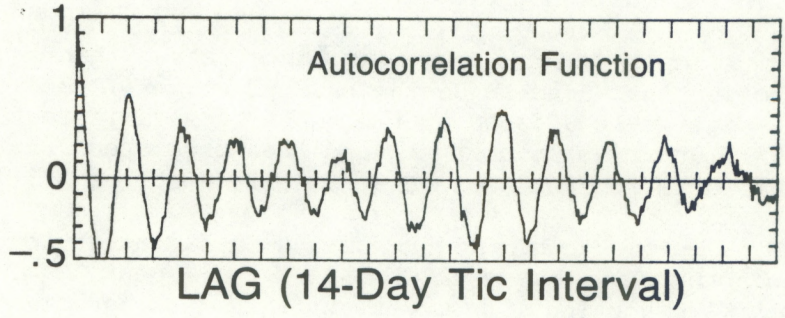

Figure 3.6 Autocorrelation function and power spectra for the Si II lines near 182 nm with the Al I background continuum via Case B in Table 3.2.

In summary, the five test wavelengths used in this analysis, all had 13-day to 27-day power spectra ratios closer to the Al I value than to the Si II value. But when used to estimate the "background" Al I continuum and subtracted from the flux at 181-182, the resultant ratios for these Si II lines were radically lower than either the Al I or older Si II values.

3.4 Mg II Center-to-Wing Ratio and Al I Edge Ratio

G.D. Falcon and R.F. Donnelly

It is known that there is significant long-term drift of the NIMBUS-7 instrument which provides these measurements but its quantitative value is not known. Heath and Schlesinger (1986) have used a technique whereby flux ratios at closely spaced wavelengths, where the instrument drift is assumed to be a slowly varying function of wavelength, can be used to better estimate the long-term flux variations. Wavelengths were chosen such that the solar flux variation is much stronger at one of the wavelengths than at the other one. Heath Schlesinger (1986) also developed scaling factors to account for an instrumentation drift that is nearly a linear function of wavelength. The analysis techniques used previously in this paper were repeated for their Al I and Mg II ratios (FR) defined as follows:

Mg II Center to Wing Ratio

$$FR(280nm,t) = \frac{F(279.8,280.0,\ 280.2nm,t)}{1/2[F(276.4,276.6,276.8,t) + F(283.2,283.4,283.6,t)]}$$

Al I Continuum Edge Ratio

$$FR(210nm,t) = \frac{F(208.6,208.8,209.0nm,t)/F(211.2,211.4,211.6nm,t)}{1/2\ \frac{F(203.4,203.6,203.8nm,t)}{F(206.0,206.2,206.4nm,t)} + \frac{F(213.8,214.0,214.2nm,t)}{F(216.4,216.6,216.8nm,t)}}$$

In each case, F is the average flux over the three wavelength steps listed. The denominator for FR(280nm,t) differs slightly from that of Heath and Schlesinger in that each F term includes three rather than two wavelengths, 276.4 and 283.6 nm were not used in Heath and Schlesinger (1986). This difference should have negligible effects on the short-term variations studied here. FR(280nm,t) and FR(210nm,t) were computed and then processed for the same analyses of short-term variations as those discussed in sections 3.1 and 3.2.

The ratio of 13- to 27-day power for the Mg II center-to-wing ratio was 0.16 slightly lower than the value of 0.189 for the peak of these chromospheric Mg II H & K absorption lines, yet still in good agreement with most of the chromospheric EUV emission lines (Donnelly et al., 1986a,b). The decrease from 0.189 for the peak to 0.16 for the center-to-wing ratio is analogous to the larger decrease for Si II at 182 nm. In other words, the small percentage variations of the far wings of the Mg II H & K lines near 277 and 283 nm, in the sharp valleys just next to the Mg II line in Figure 3.1, are the following: (1) not completely negligible in percent variation,(2) more photospheric, and (3) therefore stronger in their 13-day periodicity relative to their 27-day periodicity than is the center of the line. Consequently, removing the small signal in the wings via the center-to-wing ratio leads to the smaller value of 0.16.

The ratio of 13-day to 27-day power for the Al I edge ratio is 0.46, higher than the ratio of 0.372 at 205 nm, which is at shorter wavelengths than the absorption edge. Presumably the variations below the aluminum edge include variations from a combination of the aluminum continuum, the continuation of

the Mg I and any other continua from longer wavelengths, and numerous minor lines. The results for the aluminum edge ratio should be more purely a variation in the aluminum absorption with a reduced influence of the Mg I and other continua.

3.5 Comparison of SME and NIMBUS-7 205nm UV flux measurements

L. C. Puga

There has always been a difference in the absolute magnitude of UV flux measurements made by the SME and NIMBUS-7 satellites, but a difference in the short and long term variations has not been well investigated. Limitations on the availability of data for the same time periods make it impractical to attempt a comparison of long term variations at this time, (presently concurrent data is available only for ten months of 1982); a look at short term variations becomes the only alternative.

The wavelength of study was also predetermined since only the 205nm Al continuum was available for NIMBUS-7 SBUV observations made in 1982. The SME measurements at wavelengths 204nm, 205nm, and 206nm were used to create an averaged data set at 205nm; this was done to try to minimize interference from noise in the data. The data was then least-squared fit using a twelfth-order polynomial to remove the long term trends. The residuals from this procedure represent the short term varations (days and weeks) quite well.

Figure 3.5.1 shows the detrended data sets graphed over time; the twenty-seven day solar rotation period is obvious in both data sets and appears to be in fair agreement, the half solar rotation (13-day) variations of the two data sets show some large discrepancies in amplitude and time of peaks, though, and the SME data suffers from considerable noise which has an obvious detrimental effect on the short-term variations. Figure 4.5.2A, the power spectra for the two data sets, indicates that both have strong thirteen and twenty-seven day periodicity despite the noisy SME data.

Thirteen to twenty-seven day ratios of power, .3672 for the SME data and a value of .4535 for the SBUV data, indicate that the SBUV data has a higher percentage of thirteen day periodicity relative to the twenty-seven day periodicity than the SME. It is not likely that a difference in observation times or even the noise problems in the SME would account for that difference. The time period under consideration here is obviously too short, but that does not supply a ready explanation for the difference in the two ratios of power.

A complex demodulation analysis, graphically shown in Figure 3.5.2B, serves as further evidence that overall the twenty-seven day variations are in good agreement as to their time of occurence, but that there is a problem between the two data sets in the when we look at the thirteen day variations. Even the apparent agreement between the twenty-seven day variations loses much of its strength when the relative amplitudes and widths of the two different graphs are examined. The complex demodulation analysis shows that there are serious differences in the strengths of the twenty-seven day variations, and the amount of time they dominate the variations at this wavelength. Of course additional data and wavelengths must be studied extensively to confirm that the short-term variations in the two data sets do not compare favorably as this initial investigation indicates.

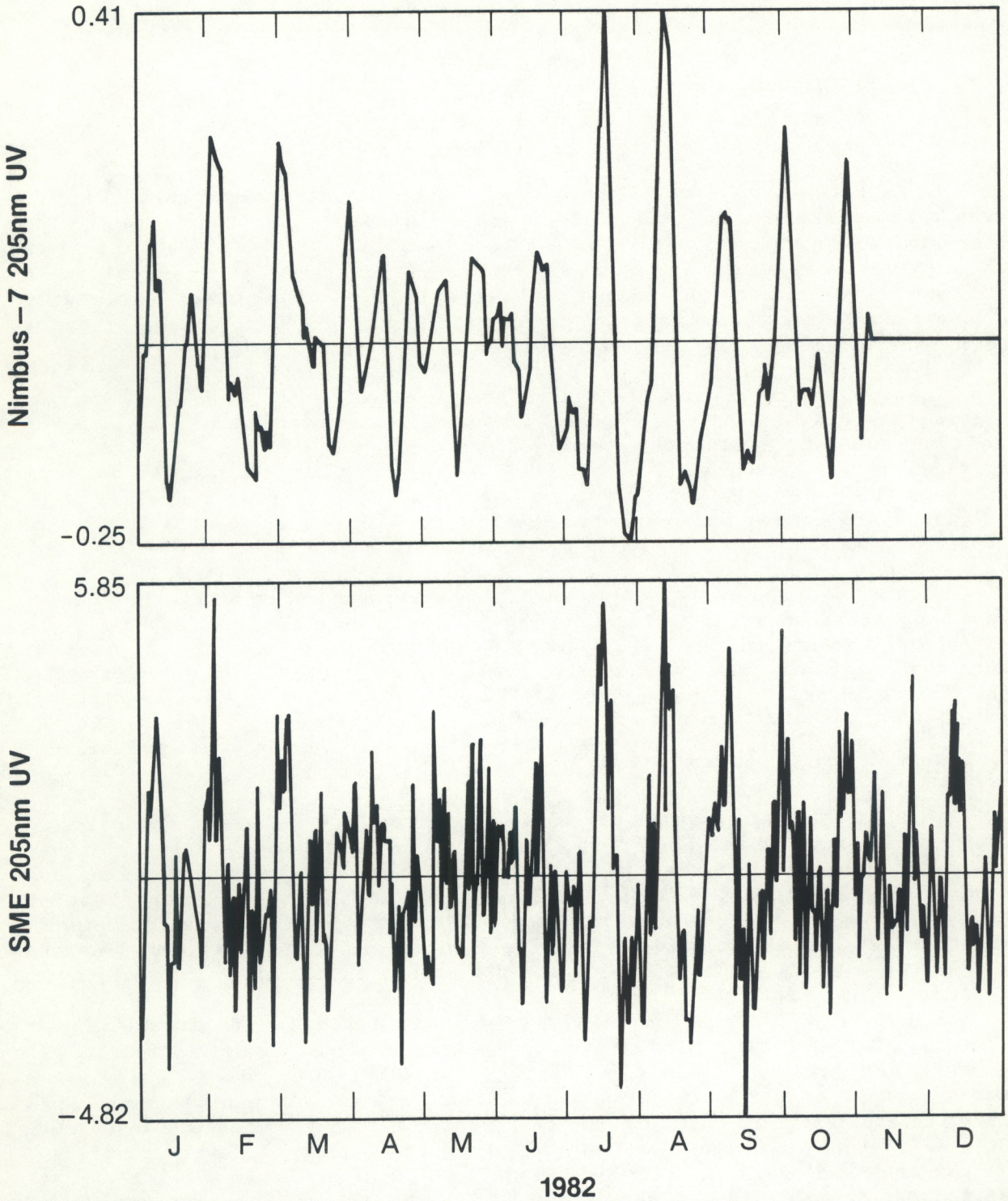

FIGURE 3.5.1 Short-term variations of the 205nm UV observed by the NIMBUS-7 and SME satellites, for 1982. The SME is actually an average of the three wavelengths 204, 205 and 206nm, while the NIMBUS-7 data is a single line measurement. The short-term variations are the residuals after a 12th order polynomial was fitted to the original and removed as the long-term and intermediate variations.

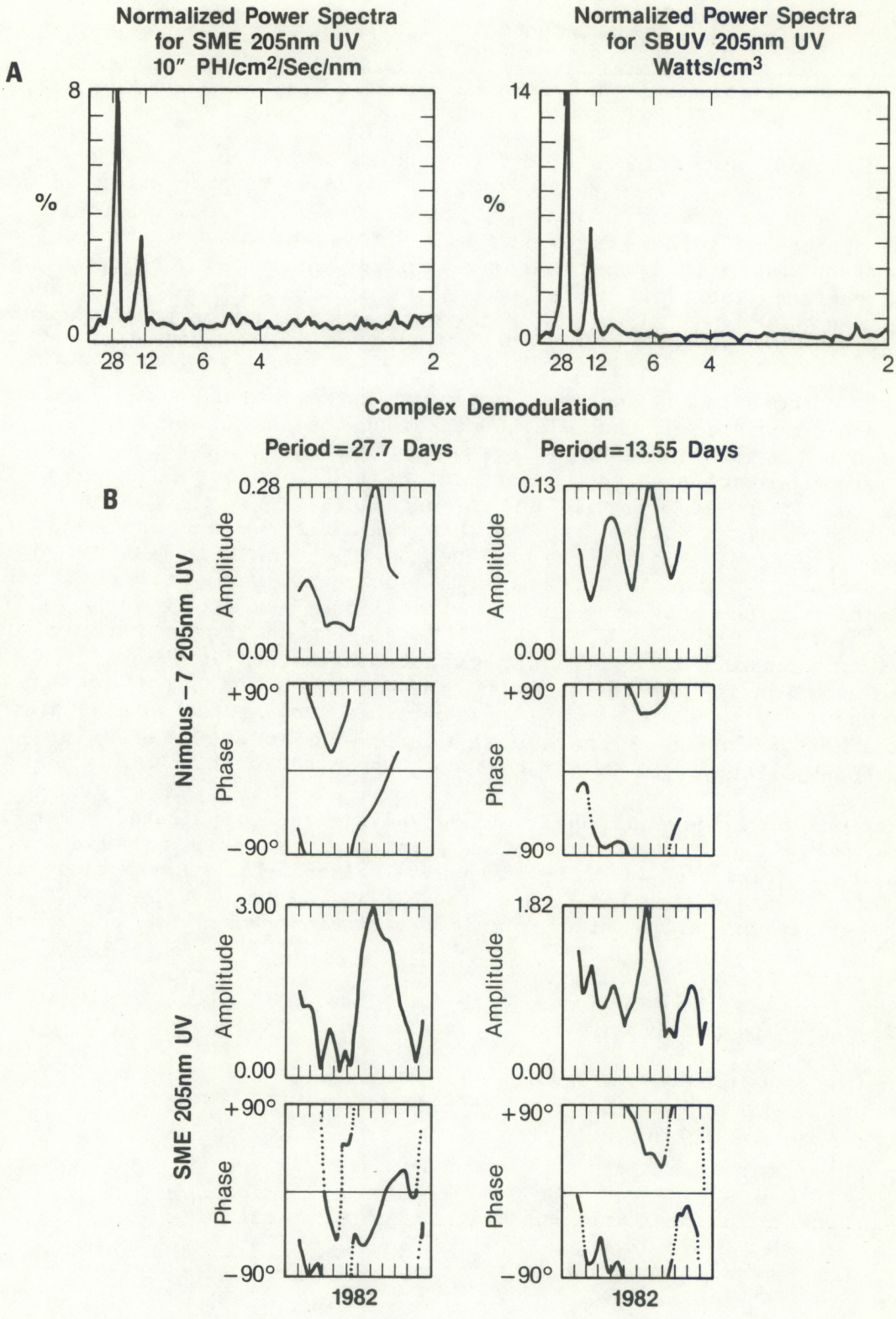

FIGURE 3.5.2 Power spectra and complex demodulation analysis for short-term variations of 205nm UV measured by SME and NIMBUS-7 satellites, for 1982.

3.6 Measurements of UV Half-Widths

K. Pfendt

The width of temporal variations for the solar UV flux were looked at in relation to the Ottawa 10.7 cm solar radio flux (F10). The variations studied were short term in nature; spanning several weeks. These types of temporal variations are caused primarily by the solar rotation of a distribution of active regions which is inhomogenous in solar longitude. The evolution of individual regions also adds to the temporal structures studied. The results were averaged over many solar rotations in order to minimize the influence of this effect.

The differences in the temporal widths may be used as a means of determining the central meridian distance (CMD) dependence of the active region's emission as a function of its source region temperature in the solar atmosphere. Two UV wavelengths were studied; a representative UV photospheric wavelength (the Al I continuum at 205 nm), and a representative UV chromospheric wavelength (the Mg II lines at 279.7 to 280.1 nm). These were compared against the coronal F10 flux, which is the most common full-disk flux measurement used to estimate the EUV flux. The time interval looked at, was that for which UV measurements from the SBUV experiment on the Nimbus-7 satellite are available: November 7, 1978 to October 29, 1984. This is a much longer interval than discussed in sections 3.1-3.4 and somewhat longer than used in section 3.5. It is also much longer than the two-year study of half widths of Donnelly et al., (1986b). These NIMBUS-7 data were obtained from new data tapes distributed by the National Space Science Data Center and World Data Center A for Rockets and Satellites, NASA GSFC, Greenbelt, Maryland 20771.

Variations of large amplitude, without having too complicated a temporal structure, were identified from time graphs of the data for use in the rotational half-width study. Half-widths were selected for study because width measurements at intensities too high or too low can become overly sensitive to instrument noise, or to any minor temporal variation caused by active region evolution.

Figure 3.7.1 shows a typical solar rotational variation. The half width in days was determined from this type of variation as follows:

1) The maximum value (Φ Max) was idenfied (at tMax) along with the preceding and following rotational minima (at t_{pmin}, and t_{fmin}).

2) Using linear interpolation between the two minima, the background flux level was removed from all observations between these minima.

3) The maximum value of the revised flux was again identified, in case the peak shifted during removal of the background.

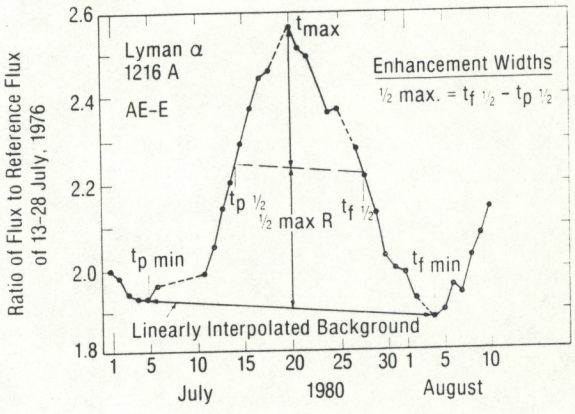

Figure 3.7.1

4) The flux level half way between this maximum and the background was then determined ($\Phi_{1/2}$ Max).

5) The immediately preceding and following times from the maximum, in which the intensity is at the half-max level between maximum and background, were determined by linear interpolation ($t_{p1/2}$, $t_{f1/2}$).

6) The half width in days is then computed from $t_{f1/2} - t_{p1/2}$.

The main problem in these analyses, was that of missing UV data. A quality factor scale was used to determine if an individual rotation had too much missing data to be considered a useful case for further study. If there was enough missing data at the rotational maximum, minima, or around the observations in which the half-width was scaled off, then the case was eliminated. Out of 48 variations originally identified from time graphs of the data, 15 cases were eliminated based on the quality factor scale, leaving 33 valid cases.

Table 3.7.1 shows the half-width results. Two different values for the mean are listed in this table. One mean involves no weighting, while the other mean has weightings based upon how much missing data there is according to the 205 nm quality factor. Cases with higher quality factors have a higher weighting.

TABLE 3.7.1 Half-Width Results (in days)

Statistical Parameter	205nm	280.1nm	10.7cm
Weighted Mean	8.91	9.62	10.0
Mean	8.78	9.65	9.79
Standard Deviation	2.3	2.5	3.3
Standard Error of the Mean	0.40	0.44	0.58
Median	8.60	9.20	10.2

The means and the median all give the result that of the three wavelengths studied, the coronal F10 half-width is the largest. The photospheric Al I continuum has the smallest half-width with the chromospheric Mg II half-width falling between the other two. For increasing depth into the solar atmosphere, the half-width of a rotational variation decreases in value.

Due to the magnitudes of the standard error of the mean values, caution should be used in quoting the mean values, especially since the chromospheric and coronal averages are so close to one another. However, the median results for the wavelengths, are not so close in value. **Since** the median is not as sensitive to abnormally small or large half-width cases as the mean is, the order of results as a function of location in the solar atmosphere can be viewed with a greater degree of confidence.

3.7 NIMBUS-7 Data Availability Tables

Joan Barrett

Measurements of the UV made by the NIMBUS-7 satellite SBUV instrument in the 160-400 nm range since 1978 are our primary source of UV data. The majority of work performed by the Sun-Climate group uses an average of the four daily scans to improve the signal to noise ratio. We have used four different computer tapes of data since 1982.

The group first received six months of data from November 1978 to April 1979 in 1982. The data for April 1979 to November 1979 was also received in 1982. In 1983 we began using a tape with two years of NIMBUS- 7 data covering the time period November 1978 to November 1980. In 1984 four years of NIMBUS-7 data for the 205nm wavelength values became available, and we began using this with the two years of data for all scans. In January 1986, archive data became available for a full 5 years of data from November 1978 to October 1984 with adjustments made for long-term variation in solar UV. Since all of the data sets had been used extensively in analysis work, a validation of the new data set was initiated to determine how it differed from previous sets.

The last three data sets were chosen for comparison (those received in 1983, 1984 and 1986). Daily average header information and scans were output for the two year data set received in 1983 and the new six year set received in 1986. The year, Julian day and data were then checked for complete data scans and repeating data. For the data received in 1984, only the 205nm line was available. Tables were then compiled for all three data sets, using 0 for days where no data was available, 1 for days with a complete data scan, and a 2 for days where two complete daily average scans were available. The attached table was generated by combining the three original tables. Parentheses indicate a difference in data availability between the two year tape and six year tape, and brackets indicate a difference in the five year 205 nm line and the six year tape.

The tables show a number of differences in data availability among the three data sets. In a few cases, editing of data has been performed to include points that were not available previously (ie., December 14, 1978, April 13, 1979). Some days show two daily average scans. These occur primarily in 1981 to 1984, with only one in 1979, which apparently was edited from the two year tape and five year data set. Since the great majority of these points follow a day showing no scans, it appears a timing problem on the satellite may have occurred, giving data from one day the next day's date. Since we were not sure of this, only the first scan values are being used in the data set. The most noticeable differences are those involving the fourth day editing throughout 1980 and 1981. Due to instrumentation problems, every four days a value had to be removed from the data set. These data values are included in the two year tape ending in November 1980, and although they are not present during 1980 in the 205nm line data received in 1984, they have not been removed from the years 1981 and 1982.

TABLE 3.7.1 Availability of NIMBUS-7 Solar Scan Data on the Six Years of Data Tapes

	1978								1979																1980												1981								
DAY	N O V	D E C	J A N	F E B	M A R	A P R	M A Y	J U N	J U L	A U G	S E P	O C T	N O V	D E C	J A N	F E B	M A R	A P R	M A Y	J U N	J U L	A U G	S E P	O C T	N O V	D E C	J A N	F E B	M A R	A P R	M A Y	J U N	J U L	A U G	S E P	O C T
1	0	1	1	0	1	1	1	0	1	1	0	1	1	1	1	1	1	1	1	[(0)]	1	1	(0)	1	1	0	1	1	1	[0]	1	1	[0]	1	1
2	0	1	1	1	1	1	1	1	1	1	1	[(0)]	1	0	0	1	1	1	0	1	1	(0)	1	1	0	1	1	0	0	1	1	0	1	1	[0]	1
3	0	0	1	1	1	1	1	1	0	1	1	0	0	0	0	1	(0)	1	1	(0)	1	1	(0)	1	1	1	1	1	[0]	1	1	1	1	1	1	1
4	0	1	0	1	1	1	0	1	1	0	0	1	0	1	1	(0)	[1]	[(1)	1	1	1	1	1	1	1	1	0	1	1	1	1	1	1	0	1	1	[0]
5	0	1	1	1	0	0	0	0	1	1	0	1	1	1	0	1	1	1	1	1	(0)	1	1	[(0)]	1	1	1	0	0	1	1	0	1	1	0	1	1
6	0	1	1	0	1	1	1	1	0	1	0	1	1	1	1	1	1	0	(0)	1	(0)	(0)	1	1	0	1	1	[0]	0	1	1	[0]	1	1	[0]	1
7	1	1	1	1	1	1	1	1	0	0	1	0	[0]	0	0	1	(0)	1	1	(0)	1	1	(0)	1	1	0	1	1	1	[0]	1	[1]	1	1	1	1
8	1	1	0	1	1	1	0	0	1	0	1	1	0	1	0	0	1	(0)	1	1	1	1	1	1	1	0	1	1	[0]	1	1	1	0	1	1	[0]
9	1	1	1	0	0	1	1	0	1	1	0	0	1	1	1	1	1	1	1	1	(0)	1	1	(0)	1	1	0	[1]	1	1	[0]	1	1	0	1	1
10	1	[(0)]	1	1	1	1	1	1	1	1	0	[(2)]	0	0	1	1	1	1	(0)	1	1	(0)	1	1	0	1	1	[0]	0	1	1	0	1	1	[0]	1
11	0	0	0	1	0	1	1	1	0	1	0	0	1	1	0	1	(0)	1	0	(0)	1	1	(0)	1	1	1	1	0	1	[0]	1	1	1	1	1	1
12	1	1	1	1	1	0	0	1	1	0	1	[(1)]	0	[(1)]	1	0	1	(0)	0	1	1	1	1	[1]	1	0	1	1	1	1	1	1	0	1	1	[0]
13	1	1	1	0	1	[(1)]	1	0	1	1	0	[(1)]	1	1	1	[1]	0	1	1	1	(0)	1	1	(0)	1	1	[0]	0	1	1	0	1	1	0	1	1
14	1	[(1)]	1	1	1	0	1	1	1	1	0	1	1	0	0	1	1	1	(0)	1	1	(0)	1	1	0	1	[1]	0	0	1	1	0	1	1	[0]	1
15	0	0	1	1	1	0	1	1	0	1	1	0	0	1	0	1	(0)	1	1	(0)	1	1	(0)	1	1	1	1	1	1	1	0	1	1	1	1	1
16	[(0)]	1	0	1	0	1	1	1	1	0	1	1	0	1	1	(0)	1	(0)	1	1	1	1	1	1	1	0	1	1	0	1	1	1	0	1	1	[0]
17	0	1	0	1	0	1	1	0	1	1	0	1	1	1	1	1	1	1	0	1	(0)	1	1	1	1	1	0	1	0	1	0	1	1	0	1	1
18	[(0)]	1	1	0	1	1	1	1	0	1	1	1	0	0	1	1	1	1	0	1	1	(0)	1	1	0	1	1	0	[0]	1	1	[0]	1	1	[0]	1
19	1	1	1	1	1	1	1	[(1)]	0	1	1	0	1	1	0	1	(0)	1	1	(0)	1	1	(0)	1	1	1	1	1	1	[0]	1	1	[0]	1	1	1
20	[(0)]	1	0	1	1	1	0	0	1	0	1	0	0	0	1	(0)	1	0	1	1	1	1	1	1	1	0	1	1	1	1	[0]	1	1	1	1	1
21	0	1	1	0	0	1	1	0	1	0	0	0	1	1	1	1	1	1	1	1	(0)	1	[1]	(0)	1	1	0	1	1	1	0	1	1	0	1	1
22	1	1	0	1	1	0	1	1	1	1	1	1	0	1	1	1	1	1	1	1	(0)	1	1	0	1	1	0	[0]	1	1	[0]	1	1	[0]	1	1
23	1	0	1	1	0	1	0	1	0	1	1	0	1	1	(0)	0	(0)	0	1	1	1	1	(0)	1	1	1	1	0	[0]	1	1	1	1	1	1	1
24	1	1	1	1	1	0	0	[(1)]	0	0	1	1	0	1	1	(0)	1	(0)	[1]	1	1	1	1	1	1	0	0	1	1	1	1	1	0	1	1	[0]
25	1	1	1	0	1	0	1	0	1	1	0	1	1	1	1	0	1	1	1	1	(0)	1	1	(0)	1	1	0	1	1	1	1	1	1	1	1	1
26	1	1	1	1	1	0	1	1	1	1	1	1	1	0	[1]	1	1	1	[(0)	1	1	(0)	1	1	[0]	1	1	0	0	1	1	[0]	1	1	[0]	1
27	1	0	1	1	1	1	1	1	0	1	1	0	1	0	(0)]	1	(0)	1	1	(0)	1	1	(0)	1	[1]	1	1	1	1	[0]	1	1	1	1	1	1
28	1	1	1	1	1	1	0	0	1	[0]	1	1	0	1	1	(0)	1	1	(0)	1	1	(0)	1	[1]	1	1	1	1	[0]	1	1	1	1	1	1	1
29	0	1	1		1	1	0	0	1	[1]	0	1	1	1	1	(0)	1	(0)	1	1	1	1	[1]	1	1	0	1	1	1	1	1	1	[0]	1	1	[0]
30	[(0)]	1	1		1	0	1	0	1	1	1	1	1	0	1		1	1	[(0)	1	1	(0)	1	1	0	1	1		1	1	0	1	1	0	1	1
31		1	1		1		1		0	1		0		1	(0)		(0)		1		1	1		1		1	1		0		1		1	1		1

TABLE 3.7.1 (Continued)

	1981								1982												1983												1984					
DAY	NOV	DEC	JAN	FEB	MAR	APR	MAY	JUN	JUL	AUG	SEP	OCT	NOV	DEC	JAN	FEB	MAR	APR	MAY	JUN	JUL	AUG	SEP	OCT	NOV	DEC	JAN	FEB	MAR	APR	MAY	JUN	JUL	AUG	SEP	OCT
1	0	0	1	0	0	[0]	1	0	1	1	0	1	1	1	1	0	1	0	0	0	2	1	1	1	1	1	0	0	0	1	1	1	1	1	1	0
2	1	1	1	1	0	1	0	1	1	[0]	1	1	[0]	0	1	1	1	1	0	0	1	1	1	1	1	1	1	1	1	1	0	1	1	1	1	1
3	1	[0]	1	1	1	1	1	1	0	[2]	1	0	1	1	0	1	1	1	0	2	1	0	1	1	0	2	1	1	1	0	1	1	0	1	0	1
4	1	1	[0]	1	1	1	0	1	1	0	1	1	0	0	1	0	0	1	1	0	1	1	1	1	1	1	0	1	0	1	1	1	1	1	0	1
5	[0]	1	1	0	0	1	1	0	[0]	1	0	0	0	2	1	1	0	0	0	1	1	0	0	0	1	1	1	1	1	1	0	1	1	1	1	1
6	1	1	1	1	1	0	[0]	1	[2]	1	1	1	1	0	1	0	1	1	1	1	0	1	1	0	1	0	1	1	0	1	1	2	1	0	1	1
7	1	[0]	1	1	1	1	[2]	1	0	1	[0]	0	0	1	0	1	1	1	0	1	0	0	1	1	1	1	1	0	1	1	0	1	1	1	1	0
8	1	1	[0]	1	1	[0]	0	1	1	0	1	1	0	0	1	0	0	0	1	0	2	1	0	1	0	1	1	1	1	0	0	1	1	1	1	0
9	[0]	1	[0]	0	0	[2]	1	0	1	1	0	[0]	0	1	0	1	1	0	0	0	1	1	1	1	1	1	1	1	1	1	1	1	1	1	0	1
10	1	1	1	1	1	0	[0]	1	1	1	1	1	1	0	1	0	0	1	1	1	0	1	1	1	1	1	0	0	1	1	1	1	1	1	1	1
11	1	[0]	1	1	[0]	0	[2]	1	0	1	[0]	0	1	1	0	2	1	1	0	1	1	0	1	0	1	1	1	1	1	1	1	1	1	1	1	1
12	1	1	0	1	[2]	1	0	1	1	0	[2]	1	0	0	1	0	0	1	1	0	0	1	1	1	1	0	1	1	0	1	1	1	1	0	1	1
13	0	1	1	0	0	[2]	1	0	1	1	0	1	1	1	0	0	1	0	1	1	1	1	1	1	1	0	1	0	1	1	0	1	1	1	1	0
14	1	1	1	1	1	0	1	1	1	1	1	1	0	0	1	1	1	1	1	0	0	1	1	1	1	0	1	1	1	1	1	0	1	1	1	1
15	1	[0]	1	1	1	1	1	1	1	1	[1]	0	1	1	1	1	1	1	0	2	1	0	1	1	1	1	0	1	1	0	1	1	1	0	0	1
16	1	1	0	1	1	1	[0]	1	1	0	1	1	0	0	1	0	0	1	1	0	1	1	1	1	1	1	1	0	1	1	1	0	2	1	1	1
17	[0]	1	1	0	0	1	1	0	1	1	0	0	1	1	1	1	1	0	1	1	1	0	1	0	1	1	0	1	0	1	1	1	1	0	1	1
18	1	1	1	1	0	0	[0]	1	1	[0]	1	1	1	0	1	1	0	0	1	1	0	1	1	1	1	0	0	0	1	1	1	2	1	1	1	1
19	1	[0]	1	1	1	1	1	0	0	[2]	0	0	1	1	0	1	1	1	0	1	1	0	0	0	1	1	1	1	1	1	0	1	1	0	0	0
20	1	1	[0]	1	1	[0]	0	1	1	0	1	1	0	0	0	0	0	1	1	0	1	1	1	1	0	1	1	1	1	1	0	1	1	1	1	0	1
21	[0]	1	1	0	0	1	1	0	1	1	0	[0]	1	2	1	1	1	0	1	0	1	0	1	1	1	1	0	1	1	1	1	0	1	0	1	1
22	1	1	1	1	1	0	1	1	1	0	1	[2]	1	0	1	0	1	1	1	0	0	2	1	0	1	1	1	1	1	1	1	2	0	1	1	1
23	1	[0]	1	[0]	[0]	1	1	[0]	0	1	1	0	1	1	0	1	1	1	0	1	1	0	1	1	1	1	1	1	0	0	1	1	1	0	1	0
24	1	1	0	1	1	1	0	[2]	1	0	1	1	0	1	0	0	0	1	1	0	1	1	0	1	1	0	1	0	1	1	0	1	0	1	1	0
25	[0]	1	1	0	0	1	1	0	0	1	0	1	1	1	1	1	1	1	0	1	1	1	1	1	1	0	1	1	1	1	1	2	1	0	0	1
26	1	1	0	1	1	0	[0]	1	1	[0]	1	1	1	0	2	1	0	1	1	0	0	1	1	0	1	1	1	1	1	0	1	1	1	1	0	0
27	1	[0]	1	1	1	1	1	[0]	0	1	[0]	0	1	1	0	1	1	1	0	2	1	0	1	1	1	1	0	1	1	1	1	1	1	1	0	1
28	1	1	0	1	1	1	0	1	1	0	[2]	1	0	1	0	0	0	1	1	0	1	1	1	1	0	0	1	1	1	1	1	1	1	1	1	0
29	[0]	[0]	1		0	1	1	0	1	0	0	1	1	1	1		1	0	0	1	1	1	0	1	1	0	0	1	0	1	1	0	1	0	1	1	
30	1	1	1		1	0	1	1	1	1	1	1	1	0	1		1	1	1	0	0	1	1	1	0	1	1		1	1	1	1	1	1	1		
31		[0]	1		1		1		0	1		0		1	0		1		0		1	1		1		1	1		1		0		0	1		

3.8 Comparison of Full-Disk Ca-K Line Measurements and NIMBUS-7 UV Flux Measurements

Meiqing Gao

Comparisons of White and Livingston's (1986) ground-based measurements of the Ca II K line at the National Solar Observatory on Kitt Peak near Tucson, Arizona, and solar UV spectral irradiance measurements from the NIMBUS-7 satellite were made for the period November 7, 1978 to October 29, 1984, using linear regression analysis, scatter plots and the correlation coefficient. Both a center of line measurement (Ca K3) and a central 1A band flux (Ca K-1A) were used to represent the Ca K line observations. The NIMBUS-7 solar UV measurements that were used (approximately 1nm bandpass) included the center of the Mg II H and K lines (unresolved) at 280nm, the flux at 205nm in the Al I absorption continuum, the center of the Ca K line at 393.5nm, and two flux ratios, namely the center-to-wing ratio for the Mg II H and K lines near 280nm and a short-wavelength to long-wavelength ratio for the Al I absorption edge near 208nm. These UV ratios are the same as those described by Heath and Schlesinger (1986) and are used here because they are expected to be much less sensitive in unknown drifts in the satellite instruments.

The Ca K II line measurements were made typically in groups of a few consecutive days with the start of the groups separated by about one month. The NIMBUS-7 measurements were made on three out of four days most of the time. Only the daily measurements when both the National Solar Observatory Ca K data and the NIMBUS-7 data were available were included in the analyses.

Scatter plots indicate, and the values in table 3.8.1 confirm that the UV data correlates well with both Ca K line measurements.

Table 3.8.1

Independent Variable X	Dependent Variable Y	Correlation Coefficient
Full disk Ca K 1A	Mg II ratio	0.9495
Full disk Ca K3	Mg II ratio	0.9690
Full disk Ca K 1A	Mg II 280nm	0.9292
Full disk Ca K 1A	Al I edge ratio	0.8291
Full disk Ca K3	Al I edge ratio	0.8518
Full disk Ca K 1A	Al I 205nm	0.8316
Full disk Ca K 1A	Ca K H&K (393.5nm)	0.8496

The Mg II center-to-wing ratio, not surprisingly, correlates the best with both the Ca K3 and the Ca K 1A data. This is likely due to the Mg II center-to-wing ratio being much less sensitive to instrument drift; the Mg II center-to-wing ratio is computed using an average of the continuum so that the change in flux represented by the ratio is a relative measurement and not an absolute measurement. In addition, the Al I edge ratio is a measure of a much less dramatic change in flux than the Mg II, the resolution of the UV measurements at the Ca K H & K line 393.5nm average is not as good as for the Mg II ratio-wavelength jitter introduces inaccuracies to the 393.5 average because it is such a narrow band. The Ca K line measured by White and Livingston is mostly chromospheric in origin, so the Mg II ratio, which is also nearly all chromospheric, naturally correlates better. The Al I edge ratio and the 205nm

data, on the other hand, are mostly photospheric and so would not be expected to correlate as well as the Mg II ratio, and they don't.

This analysis illustrates the value of ground-based measurements such as the Ca K line. These measurements can be used to show relative changes in the UV flux, which are predominantly satellite measurements for long time periods, which originates in the chromosphere with a fair degree of accuracy. The correlations with the other UV flux measurements suggest the possibility of a component model of the UV, with the Ca K line measurements as a major component.

4. PROBLEMS IN ANALYSES

The primary method of statistical comparisons made on the various data sets used by the Sun-Climate Staff for the past several years has been the time series analyses developed by Tom Repoff and described in Heath et. al., (1984). Unfortunately any specialized analyses require certain restrictions on the data being used, and there is a degree of uncertainty caused by the untested nature of the analyses. In addition there are other problems specific to individual data sets which must be addressed before analyses can be performed on the data sets. The following discussions will attempt to answer a number of questions which arose in our statistical manipulations the past two years.

4.1 Differences in Analyses Methods

L. C. Puga

One problem in the time series analysis program written by Tom Repoff is that the cross-correlation function at lag zero does not exactly equal the correlation coefficient computed for any particular data set, even though it should. Due to the sophisticated nature of the time series analysis, we believed initially that there might be some small error in calculations within the time series computations. Because the difference between the correlation coefficients and the value for the cross-correlation function at zero lag is small, (usually less than .5%, but up to 4%), any error would have to be very small. The calculation of the cross-correlation function itself involves summing a considerable number of values; that also means an error built into the equation would be minute. With this in mind, and since the equation for cross-correlation functions are straight forward despite their sophisticated applications, it becomes more likely that the difference between the two correlation values must be due to something that happens in the data set before the calculations are made. This would be very unusual if it were not for the fact that in the time series analysis points which lay outside certain parameters are eliminated as questionable data, the normal correlation coefficient calculations do not do this of course. This partially explains the results in table 4.1.1 which shows a comparison of 280nm NIMBUS-7 measured UV values with AE-E measurements of the EUV for the time period November 6, 1978 to November 2, 1980.

This particular comparison also illustrates other problems in the data sets themselves which affect the results of statistical procedures. The NIMBUS-7 data for this time period has an error every fourth day of data measurements due to a diffuser problem within the instrument. Thus, every fourth day's measurements had to be removed in order to have an accurate data set. Table 4.1.1 shows the effects the fourth day error had on statistical comparisons before it was discovered and removed. Though the differences between the data before and after the fourth day error was removed are not extremely large, they are certainly significant. Perhaps of more importance however, is the considerable difference in the results found using the two

different correlation techniques. The last two columns of table 4.1.1 show the percentage difference in the correlation coefficients before and after the removal of the fourth day error; the two columns should agree fairly closely and they obviously do not. This appeared to be a serious problem until we realized that the two correlation techniques are in fact dealing with two different data sets. Both use the residuals of the data set after the twelfth order polynomial have removed the long-term trends from the data. The cross-correlation, however, also accounts for missing data in the time series where the correlation coefficient calculations use only matching pairs of data. In addition the cross-correlation analysis uses an "N-1" term in the denominator of the equation while the correlation coefficient calculations use just "N" in the same place. This produces a larger and larger difference the smaller the data sets become, and quick checks showed differences of 1-1.5% can exist simply because of the difference in the denominator of the equations. Further work is needed to determine if there are other factors which effect the data set built into the cross-correlation analysis, but the differences in the two calculations are small enough that with the discussion above taken into consideration the cross-correlation value at zero lag is an accurate measure of the correlation coefficient for the data sets. However, R.F. Donnelly concludes that Tom Repoff's program should not be used to determine the commonly used correlation coefficient.

TABLE 4.1.1

EFFECTS OF THE FOURTH DAY ERROR IN 280nm DATA ON THE CROSS CORRELATION AND LINEAR LEAST SQUARES CORRELATION COEFFICIENTS
(Nov. 6, 1978 to Nov. 2, 1980)

Wave-lengths A	Ions Lines	With fourth day error still in r value	# points	With fourth day error removed r value	# points	Cross Correlations zero lag values w/ 4day	w/o 4day	Percentage difference r	lag=0
335	Fe XVI	.74316	387	.75663	340	.73546	.73731	1.78	.25
284	Fe XV	.77090	387	.78313	339	.76137	.76366	1.56	.42
255-300	-	.79592	385	.80610	338	.79184	.78847	1.26	- .43
200-204	(Fe XIII)	.77672	322	.77897	273	.78196	.76224	.29	2.52
190-206	-	.76098	323	.76413	274	.76762	.74545	.41	-2.89
206-255	-	.76039	383	.76883	335	.76217	.75276	1.10	-1.23
178-183	-	.70057	324	.70682	275	.71916	.69667	.88	-3.13
168-190	-	.69498	324	.70469	275	.69938	.67326	1.38	-3.73
169-173	(Fe IX)	.61408	324	.61351	276	.61568	.58384	- .09	-5.17
304	He II (Si XI)	.77614	378	.80249	334	.77503	.79200	3.28	2.14
584	He I	.77614	320	.79737	273	.81344	.82469	2.66	1.36
1026	H Lyman Beta	.86982	385	.89487	338	.87471	.88719	2.80	1.41
590-660	-	.58463	324	.57471	273	.60648	.59759	-1.70	-1.47
510-580	-	.64784	323	.65551	274	.65948	.66445	1.17	.75
1216	H Lyman Alpha	.85141	384	.88617	338	.81682	.84426	3.92	3.25
F10	10.7 Radio Flux	.72449	559	.74746	497	.73305	.74517	3.07	1.63
R	Sunspot Number	.69108	558	.72194	496	.69951	.72008	4.27	2.86
P	Plage Index	.74699	409	.76661	369	.75836	.78436	2.72	3.31
10830	He I	.8432	364	.85667	321	.85198	.84295	1.57	-1.06
205nm	NIMBUS-7 UV	.9330	498	.93792	498	.91065	.93951	.52	3.07
280nm	NIMBUS-7UV	1	568	1	503	1	1	0	0

4.2 The Effect on Linear Regression Analysis Results of Converting the AE-E EUV Data to 1 AU

K. Pfendt

Donnelly et al., (1986) reported linear regression comparisons made between solar EUV flux measurements from the AE-E satellite and ground based measures of solar activity. The ground based measures include the equivalent width (EW) of the He I absorption line at 10830A and the Ottawa 10.7cm solar radio flux (F10). These ground based measurements and the solar UV flux measurements from the NIMBUS-7 satellite have values adjusted to the fixed Sun-Earth distance of 1 AU. However, the EUV data was not similarly corrected, and in the present work these data were adjusted to 1 AU to take out the variation in the Sun-Earth distance. Linear regression comparisons of the revised EUV data against the ground based indicies were then conducted to compare revised results with the previous results. The time interval studied is that for which EUV measurements were taken by the AE-E satellite: July 1, 1977 to December 30, 1980.

Two EUV wavelengths were chosen as test cases for the revision: a representative coronal wavelength (Fe XVI 335A flux ratio) and a representative chromospheric wavelength (H Lyman beta 1026A flux ratio). To revise the EUV data to the fixed distance of 1 AU, all the old uncorrected flux ratios (FR_{old}) were first multiplied by the square of the distance from the sun $(distance/1AU)^2$. The EUV data were reported as flux ratios relative to the EUV average reference flux from July 13-28, 1976. During this reference period, the value of the square of the distance from the Earth to the Sun had the average value of 1.0329. Therefore, the old results were then divided by this value and FR_{1AU} is given by the following equation based on Smith and Gottlieb (1974):

$$FR_{1AU} = FR_{old} \times [1.0004 + 0.0334 \times \sin[(DOY - 94) \times 360°/365.25]]/(1.0329)$$

The linear regression analyses were run using corrected and uncorrected EUV data in comparison to each of the two ground based measures. The correlation line used had the equation Y = A + B *X, where the independent variable is X and the dependent variable is Y. The two data sets compared were switched back and forth as independent and dependent variables in order to get two regression lines for the same two variables. Table 4.X shows old and revised results.

The table shows that the percent changes in the correlation coefficients are quite small; the revised results are on average only 0.2% higher than the old results. Donnelly et al., (1986a) used only the correlation coefficients so the effect of these revisions on that paper is negligible. The effect on all the studies of short-term variations by Donnelly et al., (1986a,b) is also negligible because the correction is approximately an annual sinusoid and those studies of short-term variations first removed all such long-term trends from the data anyway. The changes in the coefficients of the regression lines, particularly the 4 to 5% decrease in slope, are large enough that they are not negligible. Those changes affect the "long-term" (not the "short-term") regression parameters in Tables 7.1-7.3 of Donnelly (1986b). Since the correlations in Table 7.3 are too low to be useful and only the Fe XVI result

in Table 7.2 (see Table 4.2) is superior to that for the 10830 A data, then the long-term columns in Table 7.1 are the main ones that should be revised.

TABLE 4.2 Comparison of Old and Revised Regression Analysis Results

Y = A + BX, r = correlation coefficient

Data Compared	Parameter	Old Value	Revised Value	Revised-Old Value / Revised Value
X = F10	r	0.934	0.936	+0.2%
Y = FR(Fe XVI)	A	-38.26	-36.41	+ 5%
	B	0.574	0.552	- 4%
X = F10	r	0.900	0.902	+0.2%
Y = FR(H Ly beta)	A	0.893	0.897	+0.5%
	B	0.00892	0.00849	- 5%
X = EW(10830Å)	r	0.909	0.911	+0.2%
Y = FR(Fe XVI)	A	-85.06	-81.61	+ 4%
	B	2.44	2.35	- 4%
X = EW(10830Å)	r	0.927	0.930	+0.3%
Y = FR(H Ly beta)	A	0.095	0.140	+ 32%
	B	0.0389	0.0371	- 5%

4.3 Comparison of Old and Revised 10830A Ground-Based Measurements

Joan Barrett

The 10830A equivalent-width (EW) data is a full disk ground based chromospheric emission covering the extended period of 1974 to 1986. Because of the longevity of the data set, it is very useful for comparisons with satellite data sets to search for changes in instrumentation. Members of the group have also used the data in conjunction with other ground based data such as the 10.7 cm flux, CaII plage index, and the sunspot number, as well as other satellite data like the AE-E and NIMBUS 7 UV measurements, to study temporal variations in the solar UV.

In January 1986, the group received a revised 10830A data set from Dr. Jack Harvey with recalibration based on more extensive comparisons with Dr. Bill Livingston's absolute equivalent width measurements. Since the old data had been used in studies (Donnelly et al., 1985, 1986a, b) conducted by the group for several years, a test of correlation between the data sets was conducted to determine how results from those studies could be reevaluated in reference to the new data.

Two linear regression analyses were performed using the method of ordinary least squares, first using the old data set values as the independent variable, and then the new data set values as the independent variable. The correlation coefficient was also calculated as a measure of the agreement in

the two sets. The correlation coefficient was .9998, indicating a nearly perfect linear relationship between the two sets. This is presumably a consequence of the revisions to the data being a linear revision as a function of intensity.

Since a high linear fit was established, the following formula can be used to adjust numerical results from studies using the old set:

New Data Point = Intercept + Slope x Old Data Point

by substituting -9.6179 for the intercept, 1.1606 for the slope. To compare work using the new data sets with results from studies using the old data set, the following equation to adjust those values to the ones used is:

Old 10830 A Data Point = Intercept + Slope x Revised Data Point

substituting 8.3053 for the intercept and .8612 for the slope.

The findings of this short comparison of the two data sets indicates that the results from the previous studies should not be affected by the changes in the revised data set since the two sets show such a high linear relationship and time series analysis techniques were used in the studies. However, adjusting the values using the above derived formulas should make results equivalent with new data set values for future work.

Harvey (1986, private communication) also reported identifying some problems in the 10830A EW data caused by terrestrial water-vapor induced complications. These problems occur mainly in the Arizona monsoon; the EW values may be systemmatically too large particularly in the summer months. The revisions discussed above do not include complete corrections for these water-vapor problems.

4.4 Tests of Time Series Analyses

D. Stevens and R.F. Donnelly

The computer programs for the numerical analyses now used extensively by the ARL Sun-Climate Staff, including autocorrelations, cross-correlations, power spectra, co-spectra, cross-spectra and complex demodulation for data sets with missing data analyses were developed for us by Tom Repoff in 1983. The most detailed descriptions of these analyses were published in Chapters 4-8 of Heath et al., (1984) for the NIMBUS-7 data, which has about one day missing out of every four days of data. Presumably Tom tested his software before the analyses reported in Heath et al., (1984) but he did not document the details of such tests before departing in December 1984. Some of these analyses use standard subroutines, which are well-tested. However, several tests of Repoff's analysis programs have been conducted to assure the staff their performance with test-case data was as expected. Some of these results are discussed below.

Because of the extensive use of the normalized power spectra results, several periodic input data sets were used, namely:

(1) Half-Wave Rectified Cosine with Average Removed

$$F_1(t) = \cos\left(\frac{2\pi t}{32}\right) - \frac{1}{\pi} \qquad \text{for } 0 \le t \le 8 \text{ days},$$

$$= -\frac{1}{\pi} \qquad \text{for } 8 \le t \le 24 \text{ days},$$

$$= \cos\left(\frac{2\pi t}{32}\right) - \frac{1}{\pi} \qquad \text{for } 24 \le t \le 40 \text{ days},$$

where the $-\frac{1}{\pi}$ term makes the average value zero, i.e., it removes the average of the half-wave rectified cosine.

(2) Sinusoidal Series with Fundamental and Even Harmonics

$$F_2(t) = \sin\left(\frac{2\pi t}{32}\right) + \frac{1}{2}\sin\left(\frac{2\pi t}{16}\right) + \frac{1}{4}\sin\left(\frac{2\pi t}{8}\right) + \frac{1}{8}\sin\left(\frac{2\pi t}{4}\right) + \frac{1}{16}\sin\left(\frac{2\pi t}{2}\right) .$$

The harmonics include the second, fourth, eighth and sixteenth harmonics.

(3) Sinusoid Series with Four Strong Even Harmonics

$$F_3(t) = 10\sin\left(\frac{2\pi t}{32}\right) + 9\sin\left(\frac{2\pi t}{16}\right) + 8\sin\left(\frac{2\pi t}{8}\right) + 7\sin\left(\frac{2\pi t}{4}\right) + 6\sin\left(\frac{2\pi t}{2}\right) .$$

The harmonics again include the second, fourth, eighth and sixteenth harmonics.

(4) Six-Sinusoid Series

$$F_4(t) = 10\sin\left(\frac{2\pi t}{32}\right) + 9\sin\left(\frac{2\pi t}{16}\right) + 8\sin\left(\frac{2\pi t}{8}\right) + 7\sin\left(\frac{2\pi t}{16/3}\right) + 6\sin\left(\frac{2\pi t}{4}\right) + 5\sin\left(\frac{2\pi t}{16/5}\right) .$$

Here, the harmonics are the second, fourth, sixth, eighth and tenth. In each case, the numerical analyses were conducted using daily samples (t = 1, 2, 3, ...) for twenty two cycles of the 32-day fundamental.

For an infinite series of continuous data, the power in each harmonic for cases 2-4 above are given by the square of the amplitude of the corresponding sinusoid term. So the power ratio with respect to that in the fundamental is given, for example, for F_3 for the ratio of the second harmonic to the fundamental $P_2/P_1 = 9^2/10^2 = 81/100 = 0.81$. For an infinite series of continuous half-wave rectified cosines of unity amplitude, the infinite-term Fourier Series is given by the following:

$$F_1(t) = \frac{1}{2}\cos\left(\frac{2\pi t}{T}\right) + \frac{2}{3\pi}\cos\left(\frac{2\pi t}{T/2}\right) +$$
$$-\frac{2}{15\pi}\cos\left(\frac{2\pi t}{T/4}\right) + \ldots. - (-1)^n \frac{2}{\pi(4n^2-1)}\cos\left(\frac{2\pi t}{T/2n}\right) + \ldots,$$

where T is 32 days and n = 3, 4, 5, ...∞. Only cosines are present because $F_1(t)$ is an even function ($F_1(t) = F_1(-t)$). Furthermore, only even harmonics are present. Again the ratio of power for the even harmonics relative to that of the fundamental is given by the ratio of the squares of the corresponding cosine amplitudes.

For example $P_2/P_1 = \left(\frac{2}{3\pi}\right)^2 / \left(\frac{1}{2}\right)^2 = 0.18$. Indeed, the power in the harmonics drops off rather quickly for the half-wave rectified cosine.

The comparison of the power ratios derived from Fourier Series (column labeled "Theory") with those derived from the numerical analysis program are given in Table 4.4.1. The results in the table show good agreement, where the percent error in the numerical analysis results increases as the peak line intensity becomes small, comparable to the background continuum.

Table 4.4.1 Power Ratios for Test Cases

Test Function	Ratio of Power in a Harmonic to Power in the Fundamental							
	P_2/P_1		P_4/P_1		P_6/P_1		P_8/P_1	
	Num. Anal.	Theory	Num. Anal.	Theory	Num. Anal.	Theory	Num. Anal.	Theory
F_1	0.183	0.180	0.0086	0.0072	0.00143	0.00132	S	0.00040
F_2	0.250	0.250	0.0623	0.0625	NL	0	S	0.0156
F_3	0.809	0.810	0.639	0.640	NL	0	0.489	0.490
F_4	0.808	0.810	0.639	0.640	0.489	0.490	0.359	0.360
Harmonic Period =	16 days		8 days		5.33 days		4 days	

S = small relative to the broad-band background. Small difference calculation causes large relative errors due to the uncertainty in the estimate of the background continuum.

NL = No distinct line just a smooth continuum.

The above values were computed from $(P_n - P_b)/(P_1 - P_b)$ where subscript n denotes the harmonic number, 1 denotes the fundamental at 32 days period and P_b is the background continuum usually estimated from results at periods between 4 and 5 days. A 32-day fundamental was selected as a value near the solar rotation period of 28 days where its even harmonics (16, 8, 5.33, 4 days, etc.) fit the grid of frequencies used in the numerical analysis.

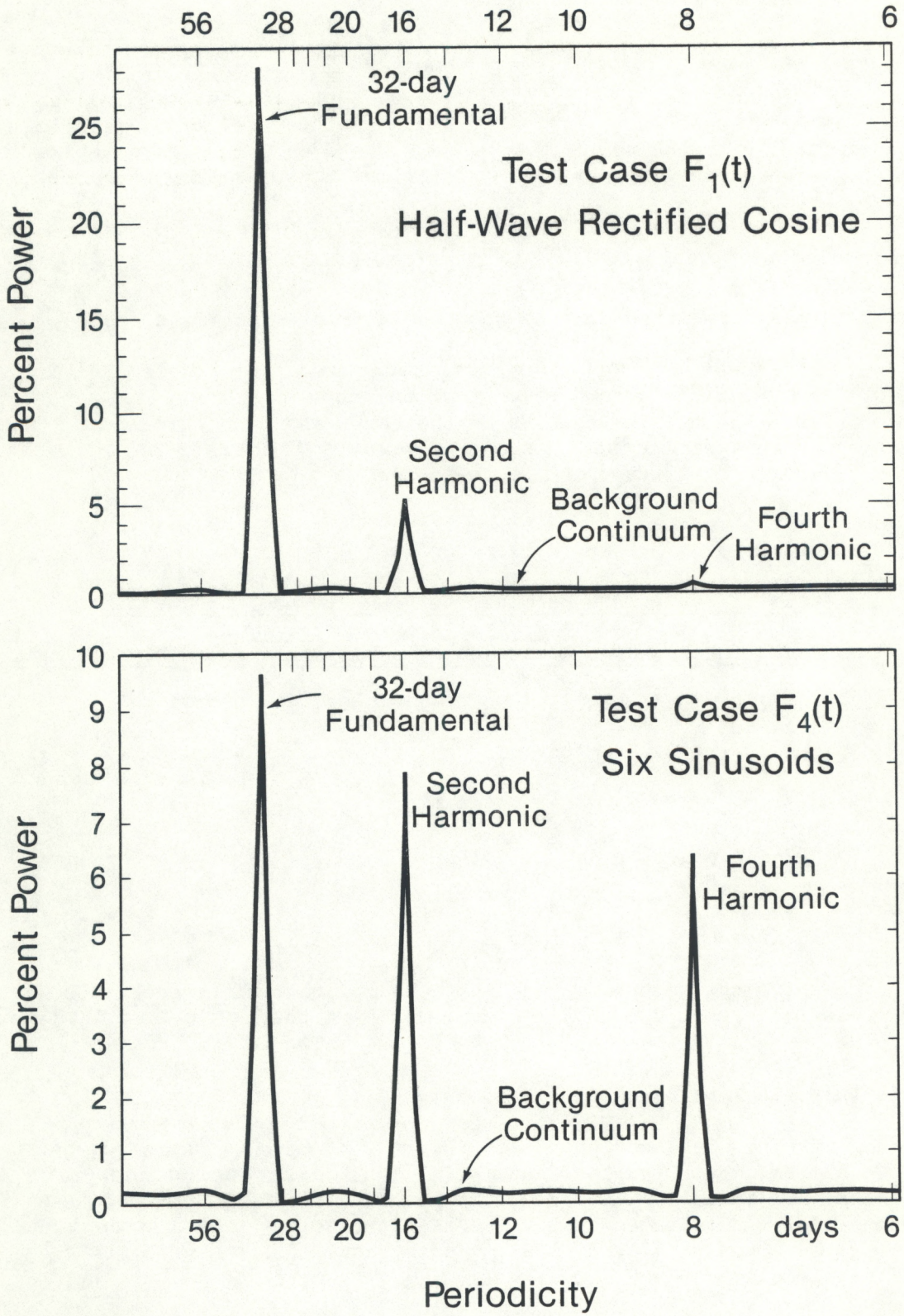

Figure 4.4.1 Power spectra for F_1 (top) and F_4 (bottom).

Figure 4.4.1 shows the power spectra for $F_1(t)$ at the top and F_4 at the bottom for periods in the range 6 - 256 days. These spectra have been normalized so the sum of the power over all frequencies used in the grid was 100%. Note that the lines in the numerical analysis are about four frequency steps wide at their base, or have half-max widths a little less than two frequency intervals. The infinite continuous periodic series have infinitesimally thin lines and no background continuum. The finite truncated time series, the daily sample rate and computational errors contribute both the low level background continuum and the thickness of the lines. The thickening of these lines by the numerical analysis programs should be taken into consideration when interpreting the results of similar analyses of solar-flux time series. The removal of the estimated background continuum for the results in Table 4.4.1 gave better agreement with the theoretical results than if the background were neglected.

In summary, the above tests show the numerical analysis results agree well with the theoretical values for ratios of peak values of spectral lines, with estimates of the background continuum removed, as long as the line intensity is larger than the background continuum. A little line-broadening and a small background continuum are artifacts of the numerical analysis.

5. ATMOSPHERIC PHYSICS

L.C. PUGA

To establish a definite link between solar UV irradiance varitions and climatic events on the earth's surface, it is necessary to develop a complete understanding of the chemistry and dynamics involved in UV induced changes in the lower mesosphere, the stratosphere, and the troposphere. Mechanisms for the transfer of solar UV energy into the weather systems of the world on a global, hemispheric and more localized level must be developed and verified. The nature of the general circulation in the stratosphere means there are few mechanisms to consider; the levels of energy available in the UV to power such mechanisms limits them even more. Development of a model of the stratosphere and troposphere which can accurately use such mechanisms necessitates a clear and complete working knowledge of the solar UV variability, stratospheric variations and their causes, and the coupling of the stratosphere and troposphere.

5.1 Responses to Solar UV Variability in the Stratosphere

Donnelly et al., (1984a) presented a general review of solar variability in the stratosphere up to about 1983. Hudson (1986) gave a complete and concise discussion of solar variability, rotational modulation and total solar irradiance. A very thorough review of solar UV irradiance is discussed in Lean (1987); note that the reviews of stratospheric effects of solar UV induced variations, in the same collection of papers, by Hood (1987) and Brasseur et al. (1987) do not discuss coupling of these effects into the troposphere.

The subject of middle atmospheric responses to solar variability, especially the UV, is no longer controversial. Eckman (1986a,b), Hood (1986,1985,1984), Donnelly and Heath (1985), Dameris et al., (1985), and Keating et al., (1985a,b) as well as others have documented very well the response of the middle atmosphere, changes in the temperature and ozone density in the stratosphere in particular, caused by solar UV variability. Changes in the dynamics and chemical processes in the stratosphere have also been linked to other modes of solar activity as unlikely as proton events, Jackman and McPeters (1985); these effects must be considered in the long-term changes in the ozone as they relate to climate.

Previous evidence for solar-rotational UV induced variations in the stratosphere, Ebel et al., (1981,1985) is supported by a number of models, Brassuer and Simon (1981), Callis et al., (1985), as well as observational evidence as seen in studies by Ebel and Batz (1977), Ebel et al., (1985), Donnelly and Heath (1985), Donnelly et al., (1984a,1985), Gille et al., (1984), Heath and Schlesinger (1985), Hood (1984,1985), Eckman (1986b), and Keating et al., (1985a,b). Calculations of temperature and ozone density in the one-dimensional model of Brasseur et al., (1985), and the three-dimensional model of Dameris et al., (1985) both show strong 13.5 and 27-day periodicities in the coherency spectra, but they lack the strength of these variations seen in observations, indicating the models need refinement. These models are valuable for studies of past temperature and ozone variations; advances in satellite measurements will allow observations to replace the models for future studies as shown by Keating et al., (1985) using seven individual data sets from satellite observations for their study of short-term solar UV variations in the middle atmosphere, (three ozone data sets, two

temperature data sets, and two UV data sets).

Chandra (1984) showed the anti-correlation of temperature and ozone in the middle latitudes, indicating a phase lag in the ozone changes with respect to the solar UV variability. Temperature varies in phase with solar activity and ozone varies out of phase; the maximum ozone density leads the UV maximum on both a short and long-term basis. Hood (1984,1985,1986) has compared satellite UV observations with traditional measures of solar activity, such as the 10.7cm radio flux, which have often been used as proxies of UV variations. Hood shows that the 10.7cm radio flux does not accurately reflect UV variations and their effects on the middle atmosphere. Maximum changes in ozone density of .5% for a 1% change in UV flux at 205nm at 3mbar found by Hood and not seen using the 10.7cm radio flux are corroborated by Keating et al., (1985).

The various studies discussed here have confirmed a number of previously controversial hypotheses. The ozone density and temperature fluctuations in the stratosphere and lower mesosphere are indeed tied to short-term and long-term variations of solar activity as seen in rotational and cyclic variations of the UV. There is a high correlation of ozone and temperature responses to UV variations at low latitudes, these correlations decrease with increasing latitude probably due to an increase of stratospheric response to dynamic effects of planetary waves at higher latitudes. Temperature increases tend to increase the size of response time to UV variability of ozone. General circulation models of the atmosphere reflect fairly well the UV caused variations in the ozone density and temperature profile of the stratosphere. Although the solar UV important to photochemical processes in the stratosphere makes up a small percentage (1.05%, Lean 1984a) of the total photon energy emitted from the sun, it plays a very important role in modulation of the stratospheric ozone and temperature. The maximum sensitivity of ozone appears to be at about 3mbar, and shows a ratio of 1/2 with variations of the UV at 205nm. Tropical oscillations in the ozone mixing ratios and temperature profile imply a 3-4% change over an eleven year solar cycle (Chandra, 1984), but there is still some disagreement about whether the ozone eleven year cycle is nearly in phase with the UV cycle, or if there are significant lags between the two.

Although the above discussion shows there are significant changes in the stratospheric ozone and temperature values related to UV variability, both in the short-term UV variations caused by rotational modulation of active regions and in the long-term variations that coincide with the solar cycle, there is still a need to translate these variations from the low energy environment of the stratosphere into significant changes in the high energy troposphere where the weather which creates the local, hemispheric and global climate takes place.

5.2 Coupling Between the Stratosphere and Troposphere

A variety of proposals for coupling mechanisms between the stratosphere and troposphere using radiative, dynamical and chemical processes exist; few are likely to stand up to the harsh criticism suggested mechanisms must face. Still it is probable a number of coupling mechanismstaken collectively will be the answer to connecting solar variability to weather and climate.

-

++ We will summarize a number of mechanisms, both direct and indirect, which

might link the variations of the stratosphereic meteorological parameters with those of the troposphere with solar variability as the driving force; then we will discuss a number of mechanisms in more detail. Several of these mechanisms have been discussed briefly in Donnelly et al., (1984a), but it is necessary to include all mechanisms if we are to address the idea of several mechanisms operating at the same time, even if they are not working in connection with each other.

STRATOSPHERIC - TROPOSPHERIC COUPLING MECHANISMS

Planetary Waves-
The vertical propagation of westerly (wintertime) planetary waves (1 and 2) can be altered by changes in the stratospheric wind distribution modifying the refectivity and transmission of planetary waves in the stratophere. Variability in the solar UV can effect the stratospheric flow, this tends to be a modification of poleward transportation of heat; the higher in latitude this happens, the greater the heighth in the stratosphere the changes can take place and still be felt in the troposphere. This mechanism by itself is best suited to explain long-term changes in weather patterns because of the slow nature (7-10 days) of planetary wave distribution of energy changes.

Radiative Coupling-
Solar radiation which reaches the troposphere is modulated by the absorption (or not) of solar radiation in the stratosphere. This alters the IR radiation in the troposphere and so changes the temperature profile in the troposphere on a short-term basis (1-3 days). Hadley cell and eddy transport of the energy is likely; by itself this mechanism cannot significantly alter atmospheric energy enough to change the weather, but in conjunction with planetary waves could do so.

Turbulent mixing-
Mixing of the atmosphere between the stratosphere and troposphere takes place at various latitudes where the heighth of the tropopause is not well defined and the stratophere loses some of its rigid stratification. Tropopause folding is another form of turbulent mixing which generally takes place near jet-streams in the form of clear air turbulence.

Convection-
A positive gradient from troposphere to stratosphere could be important to convective growth of very large cumulus clouds, which enter the tropopause/stratosphere. Since thousands of convective storms take place globally everyday, this is a possible mechanism for affecting short-term weather patterns. This mechanism probably needs to be considered in conjunction with turbulent mixing through tropopause which folds can affect the density of condensation nuclei and other chemically important particulates and elements in both the stratosphere and troposphere.

In addition to the mechanisms suggested here, things such as solar activity induced variations of cosmic ray fluxes and proton fluctuations have been put forth as possibly affecting weather and climate. These in fact probably are important, especially to long-term changes on the order of solar cycle variations. Chamberlain (1982) saw solar induced variations on the ozone as possibly affecting the greenhouse effect in the upper atmosphere, and

thus contributing to long term climate variation. The cumulative product of all of these mechanisms (and probably some not yet suggested) are more likely to cause variations we would consider significant than would any single mechanism.

5.2.1 Planetary Waves

Charney and Drazin (1961) were two of the first researchers to propose that planetary waves could transfer stratospheric energy to tropospheric weather systems, this mechanism has become the most widely accepted and scrutinized of all coupling mechanisms. They found that westerly (which means mostly winter-time in the northern hemisphere) wave numbers m = 1 and 2 could modulate tropospheric pressure systems by the variation of reflectivity and absorption of vertically propagating planetary waves. They found the effects to be latitude and height dependent; a great deal of research has been done on planetary waves since their studies. Hines (1974) suggested that planetary wave reflective variability in the atmosphere produces interference patterns in the lower atmosphere which can be manifested in changing weather patterns. King et al., (1977), indicated that oscillating large amplitude standing waves can modulate surface pressure, and they claimed to observe 11-year and 27.5-day solar cycle effects in surface pressure modulation. Green (1979), while dismissing the majority of statistical studies which found correlations between solar activity and meteorological phenomena, suggested that standing waves, propagating waves and tidal action in the lower atmosphere respond to stratopheric solar caused variations on a diurnal time scale. Larsen and Kelley (1979) also saw tidal action as modulating tropospheric parameters, as well as neutral atmospheric waves in the upper and middle atmosphere through a downward velocity component. Through these waves they claim the free energy of the atmosphere is enough to alter tropospheric circulation.

Starting with Volland (1979), planetary wave studies began including attempts to show solar variability effects in the troposphere, through planetary wave coupling, in a more quantitative manner. Volland found that wave numbers m = 1 and 2 account for a big percentage of the total poleward transport of heat in mid-latitude winter, and that solar UV variability can directly effect planetary waves by altering stratospheric reflectivity and transmissivity through ozone modification of the wind and temperature profiles. Volland found changes at the 500mb level of 0.5 a geopotential meter for solar radiation variation of 0.1% with a period of 27-days. Geller and Alpert (1980) also found positive evidence of solar UV irradiance manifesting itself in the stratospheric variations through changes in the mean zonal wind flows and temperature profile. They only believed long term weather and climate changes in conjunction with the 11 and 22-year solar cycles with a minimum of 20% change in mean zonal wind flow at 35km. Bates (1981) found a causal relationship between solar variability and changes in the steady state interference pattern in the atmosphere. This would affect the poleward heat transfer in particular. Finally, Callis (1985) computed wind field changes related to the 11-year cycle of solar UV variability; he found changes of 2% in wind field in the lower troposphere, 43% change in the vicinity of the stratopause due to planetary waves; significant changes in the thermal structure of the stratosphere was found in the summer as well as the winter in the northern hemisphere.

5.2.2 Turbulence and other Possible Mechanisms

In addition to planetary waves a number of other mechanisms are important to the connection of solar variability (the UV in particular) with the troposphere. Heating of the stratosphere is a chemical, radiative and dynamic process which can be transported to the troposphere by those means as well. Air and its chemical and radiative constituents can be transferred between the stratosphere and troposphere, in either direction, by Hadley cell circulation, tropopause height and potential temperature seasonal variations, tropopause potential temperature and upward displacement caused by radiative cooling in conjunction with the jet stream and cumulonimbus cirrus clouds, mass circulation around subtropical jet streams, mass exchange through tropopause folding associated with extratropical cyclonic systems, thunderstorms which penetrate the tropical and extratropical tropopause, clear air turbulence (CAT) in the vicinity of jet streams (due to wind shear within tropopause folds), and weak eddy diffusion across the tropopause (Shapiro 1979). All of these processes in conjunction with turbulent mixing and tropopause folding can carry solar induced stratospheric variations into the troposphere, affecting weather on a predominantly short-term basis. Danielsen (1968) suggested tropopause folding transferred stratospheric variations southward and into the troposphere at low latitudes in the northern hemisphere. Danielsen used potential vorticity to illustrate this and to show an increase of tropospheric inflow to the stratosphere as well. Goldberg (1979) proposed that the stratosphere serves as a regulating region for solar cycle variations being transported into the troposphere by many of the suggested methods, due to evidence of solar cycle variations of 27-days and 11-years for high latitude wintertime ozone measurements.

Hale (1983) implied a sun-weather connection between the conductivity of the lower atmosphere and radiation. Thunderstorms, particularly night-time storms at high latitudes, are modulated through the global electric circuit. If electrical fields in the stratosphere and troposphere are altered due to solar radiation affecting changes in the stratospheric field as a whole, then this mechanism must also be considered a component of the whole.

5.2.3 One Way Exchange?

It has often been assumed that in order for solar variability to manifest itself in the tropospheric weather systems, energy transfer must move from the stratosphere into the troposphere. The complexity of the processes taking place in the atmosphere suggests that a number of different modes of transport between the stratosphere and troposphere probably carry changes caused by solar variability. Any process which uses solar variability as its driving force becomes a component of the whole. Thus a transfer of energy out of the troposphere into the stratosphere caused by changes in the stratosphere which are due to solar variability are as important as the opposite. Movement of condensation nuclei and trace chemicals, radiation loss and modulation of dynamic flow through the modes outlined in section 5.2.2, can be due to both positive and negative temperature and pressure changes in the stratosphere caused by solar variability.

It becomes apparent from the discussion here that the next step in determining a real sun-weather, sun-climate connection will necessitate combining several mechanisms, as they are studied and tested, for coupling of the stratosphere and troposphere.

6. PUBLICATIONS AND PRESENTATIONS

The last report in this series (Donnelly et al., 1984a) reported on the publications and presentations of the NOAA-ERL-ARL Solar UV Radiation and Climate Project through fiscal year 1983. The present report covers fiscal years 1984-1986. The publications listed below include items authored or coauthored by scientists at institutions other than NOAA when their work was partially funded by this project.

6.1 FY 84 Publications

See Baker-Blocker and Bouwer (1984), Baker-Blocker et al. (1984), Donnelly et al. (1983, 1984 a,b) Heath et al. (1984), Lean (1984b), Lean et al. (1984a,b) and Skumanich et al. (1984) in the list of references in Chapter 8. FY 84 included the analysis of the second year of NIMBUS-7 data. Only short-term variations were included because corrections for long-term instrumentation drift were not yet available. The whole group started using improved analysis techniques under the guidance of mathematician and statistician Tom Repoff (Chapters 4-7, Heath et al., 1984), which has become a permanent feature of the group's later work. Modeling based on Ca-K plage data was extended to the Ca-K full-disk flux measurements (Skumanich et al., 1984).

6.2 FY 85 Publications

See Donnelly and Heath (1985), Donnelly et al. (1985), Lean (1984a, 1985). This research included our first comparisons of the temporal variations of the solar UV flux ground-based measurements of the HeI absorption line at 10830A (Donnelly et al., 1985), which led to our first estimates of the solar cycle variation of the UV flux based on full-disk 10830A data, namely: 13% for 205 nm for daily values, 10% for monthly averages and 8% for annual averages (Donnelly, 1985).

6.3 FY 86 Publications

See Donnelly et al. (1986a,b), Foukal and Lean (1986) and Kostkowski et al. (1986). The latter paper is the first publication from the program to develop UV spectroradiometers. It also involves the first intercomparison of irradiance standards from two different groups at the National Bureau of Standards (NBS), namely the Synchrotron Ultraviolet Radiation Facility and the visible radiation group with their tungster spectral irradiance lamps. The other papers involve comparisons of the temporal variations of solar ultraviolet radiation with the rest of the solar spectrum, including the total solar irradiance (Foukal and Lean, 1986) and the solar extreme ultraviolet flux (Donnelly et al., 1986a,b). Papers now in progress include Donnelly (1987), Lean (1987a,b) and Lean and Repoff (1987).

6.4 FY 86 Seminars

Donnelly, R. F., Temporal Variations of Solar UV, EUV and Total Irradiance, ARL Sun-Climate Seminar, Bldg. RL3, Rm. 620, Boulder, Colo., Sept. 10, 1986.

6.5 FY 86 Conference Presentations

Donnelly, R. F. and L. C. Puga, Solar EUV and UF Flux Variations, 1986 Spring Meeting of the American Geophysical Union, Baltimore, Maryland, May 21, 1986.

Donnelly, R. F., Temporal Changes of the Solar EUV, UV and 10830A Flux, 1985 Fall Meeting of the American Geophysical Union, San Francisco, November 12, 1986.

Donnelly, R. F., Temporal Variations of Solar EUV and UV Spectral Irradiances, 168th Meeting of the American Astronomical Society, Iowa State University, Ames, Iowa, Paper 2.07, June 23, 1986.

Falcon, G. D. and R. F. Donnelly, Selected Topics in the Analysis of NIMBUS-7 Satellite Solar UV Spectral Irradiance Data, 1986 Spring Meeting of the American Geophysical Union, Baltimore, Maryland, May 21, 1986.

Lean, J., Solar Ultraviolet Irradiance Variations, 1985 Fall Meeting of the American Geophysical Union, San Francisco, November 12, 1986.

Lean, J., Solar EUV Irradiances and Indices, Symposium XV, Presentation of CIRA 1986 and Comparisons with Other Models, Data and Theories, COSPARR XXVI Plenary Meeting, Toulouse, France, July 9, 1986.

Puga, L. and J. L. Lean, Short and Long Term Variations in the Solar EUV Flux and Solar Activity Indices, 1985 Fall Meeting of the American Geophysical Union, San Francisco, November 12, 1986.

Puga, L. C. and R. F. Donnelly, Average Center to Limb Variation of UV Plage Emissions, 1986 Spring Meeting of the American Geophysical Union, Baltimore, Maryland, May, 21, 1986.

7. CONCLUSIONS -- SUMMATION OF PROJECT ACCOMPLISHMENTS AND PLANS

7.1 Report Summation

As previously noted, the research presented in this technical memorandum represents a rather disparate group of studies which were not published elsewhere, but were considered of importance to the overall research of solar-terrestrial relationships, and thus needed to be made available to the scientific community.

On an individual basis the various UV studies make small but important impacts on our search for a consistent data base for examining the UV temporal variations over past solar cycles and in the future. We have found there is no current model of the UV or ground based observations of other solar indices which allow us to study UV short-term, intermediate, or long-term variations with complete accuracy for times prior to satellite observations; we are encouraged by our results, however. The satellite measurements of the UV are themselves subject to certain doubts, as illustrated by the disagreement between measurements made by the NIMBUS-7 and SME instruments.

Problems in methods used in the various analyses discussed in chapter 4 are certainly to be expected given the resolution needed to competently pursue the project as it currently exists, we have made every effort to identify possible areas where problems exist, and are confident corrections have been made for all discrepancies.

The project has begun the process of identifying possible mechanisms for converting variations in the solar UV into changes in weather and climate at the earth's surface. The complexity of this problem requires a number of stages, with the understanding of UV caused variations in stratospheric ozone densities and temperature profiles, and their subsequent effect on the troposphere through coupling mechanisms the second goal of the project after the first one of monitoring and describing solar UV variability. The first step towards this second goal is presented in chapter five where we have identified research into mechanisms of stratospheric-tropospheric exchange, and discussed those most appropriate to our research.

7.2 Research Accomplishments of the Sun-Climate Staff

The main research accomplishments of this project, since the last report in this series (Donnelly et al., 1984), include many results that are not discussed here in Chapters 1-5 but have been published elsewhere. These research accomplishments include the following:

Time-Series Analyses. Tom Repoff showed the research group how to conduct time-series analyses for daily solar observations like the NIMBUS-7 UV flux measurements, which have missing data about every fourth day, including the following: autocorrelations, cross-correlations, power spectra, squared coherency CO- and quad-amplitude and phase spectra, and complex-demodulation analyses. These analyses were described in Chapters 4-8 of Heath et al. (1984) and analyses are now used by all members of the group and were essential in determining most of the results listed below.

Short-Term Solar UV Variations. Heath et al. (1984) showed that the

ratio of the power-spectra line intensity of 13 days periodicity to that at 27 days was higher for the photospheric UV fluxes (205 nm Al I continuum and the Mg I absorption line at 285 nm) than for the UV fluxes that are partially from the chromosphere (Mg II H and K absorption lines at 280 nm and Si II emission lines at 182 nm). Because of the good agreement in power ratios for these UV chromospheric fluxes with those of chromospheric EUV emission lines, we thought the 13- to 27-day power ratios were in good agreement for all chromospheric fluxes. However, from section 3.3, we now know that the chromospheric Si II lines near 182 nm by themselves, with the photospheric Al I background continuum removed, have a very low ratio of 13- to 27-day periodicity. This suggests that the Si II lines (also the H Lyman alpha line at 121.6 nm) have a broader central-meridian-distance (CMD) dependence for their active region emissions than the chromospheric emission lines at shorter EUV wavelengths and longer wavelength UV absorption lines.

Solar UV Flux and the He I Line at 10830A. Because the common indices of solar activity, like the 10.7 cm flux (F10), the sunspot number (R) and Ca-II K-line plage index (P), have marked differences in their temporal variations with respect to those of the solar UV flux observations, (Donnelly et al., 1983), we wanted to compare the temporal variations of the solar UV observations with those of a ground-based measure of a full-disk chromospheric absorption line. A chromospheric line was preferred over photospheric fluxes, despite the fact the UV flux at most wavelengths in the 170-300 nm range is from the photosphere and rarely from the chromosphere, because the percent variation in a chromospheric line is much larger and easier to measure as a relative measurement, relative to photospheric fluxes at nearby wavelengths where the solar variation is very small. The Ca-II K line or H line would be excellent choices, but the UV data from the NIMBUS-7 satellite available for study up to the spring of 1986, namely data for Nov. 7, 1978 - Nov. 1, 1980, without long-term instrument drift corrections, corresponded to a time when Ca-II full-disk flux measurements were not available on a daily basis. NIMBUS-7 measurements at the one wavelength of 205 nm were available through November 6, 1982, with most of the long-term drift correction included. Daily measurements of the equivalent width (EW) of the chromospheric He I absorption line at 10830A were available from Jack Harvey at the National Solar Observatory. Comparisons of daily EW measurements (about 1/3 missing) with the four years of 205 nm data (Donnelly et al., 1985) showed the following: (a) The variation of 205 nm solar flux during solar cycle 21 estimated from the linear correlation of 205 nm flux with respect to the 10830A EW and the rise in EW from minimum to maximum in late 1981 (two years after the sunspot cycle maximum) was 13% for daily values (includes short-term, intermediate term and long-term variations combined), 10% for monthly averages (includes intermediate- and long-term variations) and 8% for annual averages (includes only long-term variations) (Donnelly, 1985). (b) The 13-day periodicity is not simply a second harmonic related to a fundamental of 27-day periodicity. Some episodes of activity are dominated by 13-day periodicity, other episodes are dominated by 27-day periodicity, and some are a mixture of 13- and 27-day periodicity (Donnelly et al., 1985) (c) The 10.7cm solar radio flux F10 and the sunspot number R have temporal variations that differ from those of the UV flux or He I absorption line in several ways. F10 is nearly devoid and R is weak in 13-day periodicity. The power in the 27-day periodic signal is weaker in F10 and R in relation to the background nonperiodic noise than in the UV and He I line because of thier greater persistence of plages than sunspots and the coronal active region sources of 10cm radio emission. The episodic variation of R and F10 rises, peaks, and decays earlier than the UV or He I

data and sometimes includes a second enhancement or resurgence of R and F10 during what appears to be one episode in the UV or He I line. Finally the solar cycle variation of R maximized in late 1979 with a secondary peak in late 1981 while the converse occurs in the UV and He I line. (Donnelly et al., 1985).

Solar EUV and UV Flux Comparisons. Measurements of the extreme ultraviolet (EUV) flux by the AE-E satellite (Hinteregger et al., 1981) were compared with the solar UV measurements from the NIMBUS-7 satellite and the He I 10830A data (Donnelly et al., 1986a,b) and the results were as follows: (a) The amplitude of the long-term EUV flux variation relative to that of the short-term temporal variations of the Fe XV and XVI lines agree fairly well with those of F10. These coronal Fe lines and the 10.7cm flux tend to peak and decay early in a series of rotational peaks of an episode of major activity. They also have very weak or negligible 13-day periodicity, like F10 but unlike the coronal 1- to 8-A solar X-ray flux. The average CMD dependence of these EUV Fe lines is more like that of the 10cm curve than like the soft X-ray curve. These Fe XV and XVI lines are not optically thin but suffer some absorption of occultation in solar active regions near the solar limb. (c) The 13-day periodicity of the various chromospheric EUV lines (H Lyman beta 1026A, He I 584A, and He II 304A) has a similar strength to that of the chromospheric 10830A He I line, which is weaker than that of the photospheric 2050A flux, but much stronger than that of the coronal EUV lines. This was interpreted to mean that the average CMD dependence for the chromospheric EUV flux must be more like cos(CMD) or the CMD curve for R than like the UV curves or the 10cm curve versus CMD. (d) Considering the combined results from analyses of episodic variations, 13-day periodicity, correlation, and the ratio of long-term to short-term variations, the 10830A data were concluded to be better than F10 for estimating daily values of chromospheric EUV fluxes. Conversely, F10 may be better than 10830A data for estimating the daily coronal EUV fluxes like those of Fe XVI.

7.3 Future Project Plans

The comparison of the temporal variations of EUV and UV fluxes is interesting from the viewpoint of the solar physics involved. The EUV results are also interesting for ionospheric and thermospheric physics. The results are of minor interest to the middle atmosphere through solar EUV modulation of downward moving NO_x, so EUV variations are not likely to be important to climate. Therefore, we are discontinuing further studies of solar EUV radiation except for the completion of several journal papers now in progress. We are now emphasizing completing our research of NIMBUS-7 and SME observations of solar UV radiation variations and enhancing our work on NOAA-9 measurements of the solar spectral irradiance.

UV Spectroradiometer Development. Progress has been slow and has now essentially stopped with the loss of our expert on UV-optics, cryogenic vacuum systems and rocket flight experiments, namely Dr. J.L. Lean, now at the Naval Research Laboratories. We are therefore closing down this portion of our program as an inhouse activity and hope to continue the instruments through future collaborations with other groups. As a first step toward developing future collaborations the recent development work and status of the instruments are reviewed in the appendices of this report.

Stratospheric Effects of Solar UV Variations. Research of the

stratospheric effects of solar UV variations has recently been aggressively pursued by many research groups. Our role in research of the stratospheric effects has been two-fold: (a) to review (Chapter 5) the outpouring of new results and (b) to promote and organize conference sessions on this subject, including two special sessions at the 1985 Fall AGU Meeting, and conference proceedings, like that published in the January 1987 issue of JGR-Atmosphere.

Stratosphere-Troposphere Coupling. If solar UV variations influence climate, their effects in the stratosphere must be transferred to the troposphere. This area of research will be our predominant target for growth. The funds freed by the departure of Dr. J.L. Lean and the closure of the rocket flight UV spectroradiometer program will be used for a new grant to CIRES for research of possible stratosphere-troposphere coupling. Two years from now, this project will involve two main area of research: (a) the analysis of SBUV/2 measurements from the NOAA satellites of solar spectral irradiance and their stratospheric effects, and (b) research of the coupling of stratospheric effects into the troposphere and their effects on regional climate.

8. References

Baker-Blocker, A. and S. D. Bouwer, El Nino: Evidence for Climate Nondeterminism?, Arch. Met Geoph. Biocl., Ser. B34, 65-73, 1984.

Baker-Blocker, A., J. J. DeLuisi and E. Dutton, Received Ultraviolet Radiation at the South Pole, Solar Energy, 32, 659-662, 1984.

Bates, J. R., A Dynamical Mechanism through which Variations in Solar Ultraviolet Radiation can influence Tropospheric Climate, Solar Physics, 74, 399-415, 1979.

Brasseur, G, and P. C. Simon, Stratospheric Chemical and Thermal Response to Long-Term Variability in Solar UV Irradiance, J. Geophys. Res., 86, 7343-7362, 1981.

Brasseur, G., G. M. Keating and M. C. Pitts, Response of Middle Atmosphere to Short-term Solar Ultraviolet Variations: 2. Theory, J. Geophys. Res., 92, 903-914, 1987.

Callis, L. B., J. C. Alpert and M. A. Geller, An Assessment of Thermal, Wind, and Planetary Wave Changes in the Middle and Lower Atmosphere Due to 11-year UV Flux Variations, J. Geophys. Res., V90, #d1, 2273-2282, 2/20/85.

Chamberlain, J. W., The Influence of Solar Ultraviolet Variability on Climate, Planet. Space Sci., V30, #2, 147-150, 1982.

Chandra, S., Solar-Induced Oscillations in the Stratosphere: A Myth or Reality?, J. Geophys. Res., 90, 2331-2339, 1984.

Charney, J. G. and P. G. Drazin, Propagation of Planetary-Scale Disturbances from the Lower into the Upper Atmosphere, J. Geophys. Res., V66, #1, 83-109, 1/61.

Dameris, M., A. Ebel, and H.J. Jakobs, 3-Dimensional Simulation of Quasi-periodic Perturbations attributed to Solar Activity Effects in the Middle Atmosphere, Ann. Geophys. Gauthier-Villars, 4(A), 287-296, 1986.

Dameris, M., A. Ebel, H. Hass, A. H. Manson, C. E. Meek and K. Petzoldt, Vertical Change of the Response to Solar Activity Oscillations with Periods Around 13.6 and 27 days in the Middle Atmosphere, Ann. Geophys. Gauthier Villars, in press, 1986.

Danielsen, E. F., Stratospheric-Tropospheric Exchange Based on Radioactivity, Ozone and Potential Vorticity, J. Atm. Sci., V25, 502-518, 5/68.

Donnelly, R. F., The NOAA-ERL-SEL Solar UV Radiation Research Project, Program Description and Progress Report, NOAA Tech. Memo. ERL SEL-58, NOAA Space Environment Laboratory, Boulder, Colorado 80303, 76pp., 1981.

Donnelly, R. F., A. Baker-Blocker, S. D. Bouwer, and J. Lean, The NOAA-ERL UV Radiation and Climate Research Project, Program Description and Progress Report, NOAA Tech. Memo ERL SEL-64, Sun-Climate Staff, ARL, NOAA ERL, Boulder, CO, 76 pp., 1982.

Donnelly, R. F., D. F. Heath, J. L. Lean and G. J. Rottman, Differences in the Temporal Variations of Solar UV Flux, 10.7-cm Solar RAdio Flux, Sunspot Numbers, and the Ca-K Plage Data Caused by Solar Rotation and Active Region Evolution, J. Geophys. Res., 88, 9883-9888, 1983.

Donnelly, R. F., L. C. Puga, T. P. Repoff and J. L. Lean, The NOAA-ERL-ARL Solar UV Radiation and Climate Research Project Program Description and Progress Report, NOAA Tech. Memo. ERL ARL-126, Sun-Climate Staff, ARL, NOAA-ERL, Boulder, CO, 142 pp, 1984a.

Donnelly, R. F., D. F. Heath, J. L. Lean and G. J. Rottman, Temporal Variations of Solar UV Spectral Irradiance Caused by Solar Rotation and Active Region Evolution, Solar Irradiance Variations on Active Region Time Scales, ed. B. J. LaBonte et al., NASA Conf. Publ. 2310, 233-249, 1984b.

Donnelly, R. F., Short-Term Variations of UV Solar Spectral Irradiance from Satellite Observations and Indices of Solar Activity, Presented at the MAP Workshop on Climatic Ozone Variations, held in Salzburg, Austria, August 19-22, 1985, (to be published in a MAP Handbook).

Donnelly, R. F. and D. F. Heath, Solar UV Radiation Variations and Their Stratospheric and Climatic Effects, Adv. Space Res. V5, #6, 145-148, 1985.

Donnelly, R. F., J. W. Harvey, D. F. Heath, AND T. P. Repoff, Temporal Characteristics of the Solar UV Flux and He I Line at 1083 nm, J. Geophys. Res., 90, 6267-6273, 1985.

Donnelly, R. F., H. E. Hinteregger and D. F. Heath, Temporal Variations of Solar EUV, UV, and 10830A Radiations, J. Geophys. Res., 91,5567-5578, 1986a.

Donnelly, R. F., L. C. Puga and W. S. Busby, Temporal Characteristics of Solar EUV, UV and 10830-A Full-Disk Fluxes, NOAA Tech. Memo. ERL ARL-146, Sun-Climate Staff, ARL, NOAA ERL, Boulder, CO, 1986b.

Donnelly, R. F., Temporal Trends of Solar EUV and UV Full-Disk Fluxes, Submitted for Publication in Solar Phys. J., 1987.

Ebel, A., and W. Batz, Response of Stratospheric Circulation at 10mb to Solar Activity Oscillations Resulting from the Sun's Rotation, Tellus, 29, 41-47, 1977.

Ebel, A., B. Schwister and K. Labitzke, Planetary Waves and Solar Activity in the Stratosphere between 50 and 10 mbar, J. Geophys. Res., 86, 9729-9738, 1981.

Eckman, R., Response of Ozone to Short-Term Variations in the Solar Ultraviolet Irradiance: 1. Observations and Interpretation, J. Geophys. Res., 91, 6705-6721, 1986.

Falcon, G., and J. Taylor, Electronics Control System for an Ultraviolet Spectroradiometer, NOAA Tech. Memo. ERL ARL, to be published, (contact R.

F. Donnelly, NOAA ERL ARL, Boulder, Colorado, 80303)

Fleming, R. J., RD Plan for Climate System Research (1982-1986), NOAA Office of Research and Development, Special Research Programs Office, Rockville, Maryland 20852, 1982.

Foukal, P. and J. L. Lean, The Influence of Faculate on Total Solar Irradiance and Luminosity, Astrophys. J., 302, 826-835, March 15, 1986.

Gellar, M. A., and J. C. Alpert, Planetary Wave Coupling Between the Troposphere and the Middle Atmosphere as a Possible Sun-Weather Mechanism, J. Atm. Sci., 37, 1197-1215, June 1980.

Gille, J. C., C. M. Smythe and D. F. Heath, Observed Ozone Response to Variations in Solar Ultraviolet Radiation, Science, 225, 315-317, 1984.

Goldberg, R. A., An Experimental Search for Causal Mechanisms in Sun-Weather Climatic Relationships, Solar-Terrestrial Influences on Weather and Climate, eds. B. M. McCormac and T. A. Seliga, Reidel Publ., Dordrecht, Holland, 161-173, 1979.

Green, J. S. A., Possible Mechanisms through which Variations in Solar Ultraviolet Radiation can Influence Tropospheric Climate, Solar Physics, 74, 399-415, 1979.

Hale, L. C., Experimentally Determined Factors Influencing Electrical Coupling Mechanisms, Weather and Climate Responses to solar Variations, ed. B. M. McCormac, Colorado Associated University Press, 309-322, 1983.

Heath, D. F., A. J. Krueger, H. A. Roeder, and B. D. Henderson, The Solar Backscatter Ultraviolet and Total Ozone Mapping Spectrometer (SBUV/TOMS) for NIMBUS G., Optical Eng., 14, 323-331, 1975.

Heath, D. F. and B. M. Schlesinger, Temporal Variability of UV Solar Spectral Irradiance from 160-400nm Over Periods of the Evolution and Rotation of Active Regions from Maximum to Minimum Phases of the Sunspot Cycle, IRS '84: Current Problems in Atmospheric Radiation, Deepak Publ., Hampton, VA, p315, 1984.

Heath, D. F., T. P. Repoff and R. F. Donnelly, NIMBUS-7 Observations of Solar UV Spectral Irradiance Variations Caused By Solar Rotation and Active-Region Evolution for the Period November 7, 1978 - November 1, 1980, NOAA Tech. Memo. ERL ARL-129, ARL, NOAA ERL, Boulder, CO, 75 pp, 1984.

Herman, J. R., and R. A. Goldberg, Sun, Weather, and Climate, NASA SP-426, Superintendent of Documents, U. S. Gov't. Printing Office, Washington, D.C. 20402, Stock #033-000-00747-7, 360pp., 1978.

Hines, C. O., A Possible Mechanism for the Production of Sun-Weather Correlations, J. Atm. Sci., 31, 589-591, March 1974.

Hood, L. L., The Temporal Behavior of Upper Stratospheric Ozone at Low Latitudes: Evidence from NIMBUS-4 BUV Data for Short-Term Responses to Solar Ultraviolet Variability, J. Geophys. Res., 89, 9557-9568, 1984.

Hood, L. L., Coupled Stratospheric Ozone and Termperature Responses to Short-term Changes in Solar Ultraviolet Flux: An Analysis of NIMBUS-7 SBUV and SAMS Data, J. Geophys. Res., 91, 5264-5276, 1986.

Hood, L. L., Solar Ultraviolet Radiation Induced Variations in the Stratosphere and Mesosphere, J. Geophys. Res., 92, 876-888, 1987.

Hoyt, D. V., and J. A. Eddy, An Atlas of Variations in the Solar Constant Caused by Sunspot Blocking and Facular Emissions from 1874 to 1981, NCAR Technical Note - 194+STR, High Altitude Observatory, National Center for Atmospheric Research, Boulder, Colorado, 80303.

Hudson, H. S., Solar Variability and Oscillations, accepted for publication in Reviews of Geophysics, 1987.

Jackman, C. H. and R. D. McPeters, The Response of Ozone to Solar Proton Events During Solar Cycle 21: A Theoretical Interpretation, J. Geophys. Res., 90, 7955-7966, 1985.

Keating, G. M., G. P. Brasseur, J. Y. Nicholson III, AND A. De Rudder, Detection of the Response of Ozone in the Middle Atmosphere to Short-term Solar Ultraviolet Variations, Geophys. Res. Ltrs., 12, 449-452, 1985.

Keating, G. M., M. C. Pitts and G. Brasseur, Response of Middle Atmosphere to Short-term Solar Ultraviolet Variations: 1. Observations, J. Geophys. Res., 92, 889-902, 1987.

King, J. W., A. J. Slater A. D. Stevens, P. A. Smith and D. M. Willis, Large Amplitude Standing Planetary Waves Induced in the Troposphere by the Sun, J. Atm. Terr. Phys., 39, 1357-1367, 1977.

Kostkowski, J. J., J. L. Lean, R. D. Saunders and L. R. Hughey, Comparison of the NBS SURF and Tungsten Ultraviolet Irradiance Standards, Applied Optics, 25, 3297-3306, September, 1986.

Larsen, M. F. and M. C. Kelley, Available Potential Energy in the Middle Atmosphere as it Relates to the Sun-Weather Effect, Solar-Terrestrial Influences on Weather and Climate, eds. B. M. McCormac and T. A. Seliga, D. Reidel Publ., Dordrecht, Holland, 145-147, 1979.

Lean, J. L., O. R. White, W. C. Livingston, D. F. Heath, R. F. Donnelly, and A. Skumanich, A Three Component Model of the Variability of the Solar Ultraviolet Flux: 145-200 nm, J. Geophys. Res., 87, p10307, 1982.

Lean, J. L., Estimating the Variability of the Solar Flux Between 200 and 300 nm, J. Geophys. Res., 89, 1-9, 1984a.

Lean, J. L., Solar Ulatraviolet Irradiance Variations and the Earth's Atmosphere, Climatic Changes on a Yearly to Millennial Basis, eds. N. A. Morner and W. Karlan, D. Reidel Publ. Co., Dordrecht, Holland, 449-471, 1984b.

Lean, J. L., T. P. Repoff and D. F. Heath, Statistical Comparison of Observed and Modeled Solar UV Irradiance Variations with Solar Activity Parameters

During the Maximum of Solar Cycle 21, in IRS '84: Current Problems in Atmospheric Radiation, ed. G. Fiocco, A. Deepak Publ., Hampton, VA, 325-328, 1984a.

Lean, J. L., W. C. Livingston, O. R. White and A. Skumanich, Modeling Solar Spectral Irradiance Variations at Ultraviolet Wavelengths, in Solar Irradiance Variations on Active Region Time Scales, NASA Conf. Publ. 2310, ed. B. J. LaBonte et al., Sci. & Tech. Info. Branch, NASA, Washington, DC, 253-288, 1984b.

Lean, J. L., Calculations of Lyman Alpha Absorption in the Mesosphere, in Atmospheric Ozone, eds. C. S. Zerefos and A. Ghazi, D. Reidel Publ. Co., Dordrecht, Holland, 697-701, 1985.

Lean, J. L., and T. P. Repoff A Statistical Analysis of Solar Flux Variations over Time Scales of Solar Rotation: 1978-1982, submitted for publication in J. Geophys. Res., 1987.

Lean, J. L., Solar Ultraviolet Irradiance Variations: A Review, J. Geophys. Res., 92, 839-868, January 1987.

Lean, J. L., Solar EUV Irradiances and Indices, accepted for publication in Advances in Space Res., Pergamon Press, Oxford, England, 1987.

Shapiro, M. A., Turbulent Mixing within Tropopause Folds as a Mechanism for the Exchange of Chemical Constituents between the Stratosphere and Troposphere, J. Atm. Sci., 37, 994-1004, 1980.

Skumanich, A., J. L. Lean, O. R. White and W. C. Livingston, The Sun as a Star: Three-component Analysis of Chromospheric Variability in the Calcium K Line, Astrophys. J., 282, 776-783, 1984.

Smith, E. V. P. and D. M. Gottlieb, Solar Flux and Its Variations, Space Science Rev., 771-802, 1974.

Volland, H., Possible Mechanisms of Solar Activity- Weather Effects Involving Planetary Waves, olar-Terrestrial Influences on Weather and Climate, eds. B. M. McCormac and T. A. Seliga, 263-274, 1979.

Webb, D. F., J. M. Davis, and P. S. McIntosh, Observations of the Reappearance of Polar Coronal Holes and the Reversal of the Polar Magnetic Field, Solar Physics, 92, 109-132, 1984.

White, O. R., W. C. Livingston, and L. Wallace, Variability of chromospheric and photospheric lines in solar cycle 21, J. Geophys. Res., 92, 823-827, 1987.

APPENDIX I

Solar UV Spectroradiometers

by

Richard F. Donnelly

November 26, 1986

1. Introduction

The portion of the Solar UV Radiation and Climate Research Project called the Rocket-Flight Solar UV Spectroradiometer Development Program is being discontinued as a NOAA in-house activity. The causes of this action are the following: (1) irreplaceable loss of key personnel, (2) low progress, (3) decreased flight opportunities for new research groups because of the shuttle Challenger disaster and the consequent increased demand for the few remaining rocket flights, and (4) declining funding caused partly by budget cuts, rises in expenses, and the rising importance of research of stratosphere-troposphere coupling to determine whether the stratospheric effects of solar UV variations can affect regional climate. Additional influences are that the group is now being buried in data from the daily solar UV irradiance measurements from the NOAA-9 satellite and have been quite busy studying six years of NIMBUS-7 data. The excellent SUSIM shuttle-flight instrument of NRL, which is a direct competitor of our rocket-flight instruments, has now had one successful flight and hopefully will fly again in the 1990's when the shuttles fly again.

The original intent of the rocket-flight instruments was to recalibrate the satellite instruments that used to suffer from large drifts in instrumentation while in the harsh environment of space. However, improvements in satellite instruments have greatly reduced these drifts; and relative measurements, like Heath's center-to-wing ratio for the Mg II H & K lines (Heath and Schlesinger, 1986) are much less sensitive to instrumentation drifts. Intercomparisons of NIMBUS-7 solar UV measurements and mountain-top measurements of the He I absorption line at 10830 Å (Donnelly et al., 1985) and also the Ca-II K line (Gao, Section 3.4 of this report) means that future such intercomparisons will help test whether the satellite measurements, especially those of the Mg II H & K lines, drift relative to the ground-based measurements. Consequently, the need for rocket-flight measurements has diminished.

Shuttle and/or rocket-flight measurements are still important for determining the absolute solar UV spectral irradiance, especially during solar minimum. (The next solar cycle minimum should be about (1997.) Rocket-flight measurements are still important for satellite recalibration purposes if apparent problems develop in the satellite measurements and also for time scales greater than two years, if SUSIM measurements are not being made successfully frequently enough.

Two spectroradiometers have been developed, a long-wavelength monochromator (LWM) for 200 to 400 nm range and a short-wavelength monochromator (SWM) for the 120 to 200 nm wavelength range. They have some problems that need to be fixed yet but they are still a very valuable asset worthy of further consideration. Whereas most rocket-flight solar spectrometers have been single monochromators, these are double monochromators with an exquisite inner coating of Ball-Black, painstakingly applied by Dr. J.L. Lean, and consequently have very low scattered light levels. They were also built to be evacuated before flight and to maintain a very good vacuum throughout the flight via a fly-along cryogenic pump system. We hope the development work will be continued through collaborations with other research groups. Possible opportunities for further collaborations include any of the following goals: (1) solar spectral irradiance measurements with minor repairs for high absolute accuracy and/or recalibration of satellite instruments, (2) solar spectral irradiance measurements with very high absolute accuracy with major modifications, e.g. replacing each photomultiplier with a cryogenically-cooled cavity radiometers for shuttle flights with long-duration exposures (a few minutes) per wavelength step, and (3) UV radiation levels as a function of altitude in the stratosphere. We may also simply keep them for a rainy day in case the satellite instruments change from their current long-life and low-drift behavior to short-lives or high drifts or the shuttle flights of SUSIM are too infrequent. In order to develop collaborations, the first step is to document the current status of the instruments.

2. Research Results

Several important research results have been achieved with these instruments. Kostkowski et al., (1986) used these two spectroradiometers to compare the spectral irradiance of the NBS Synchrotron Ultraviolet Radiation Facility II and tungsten FEL lamps at 297 and 254 nm and showed that the spectral irradiances assigned to these standards are consistent to within 1%. Comparisons were also made with the argon-arc and we still hope those results will be published by J.L. Lean, H.J. Kostkowski and their associates. These intercomparisons are important because two major sources of error in absolute solar flux measurements are the accuracy of the NBS reference irradiance standards and the accuracy to which one can relate or transfer the accuracy of the reference standards to their spectroradiometer for use in measuring the solar irradiance, (or some other irradiance), where the intensity of the solar irradiance is usually much different than that of the irradiance reference standard.

3. Development Results

Dr. H.J. Kostkowski worked under a personal services contract that included the following parts: (1) an investigation and evaluation of existing spectroradiometers, (2) an investigation of transmission diffusers at UV wavelengths, (3) design of our UV spectroradiometers, (4) tests and calibrations of the UV spectroradiometers, (5) experiments using the UV spectroradiometers to intercompare NBS radiation standards at UV wavelengths, and (6) tutoring of a NOAA representative, Dr. J.L. Lean, on conducting calibrations and tests of the spectroradiometers. The results of Kostkowski's

work on the above parts are published respectively as follows: (1) Appendix I of Donnelly et al., (1982), (2) see Appendix II of this report, (3) Appendix II of Donnelly et al., (1982), Appendix II of Donnelly et al.,(1984a), (4) Appendix III of this report, (5) and (6) Kostkowski et al., (1986).

While Dr. J.L. Lean was a Research Associate at CIRES, University of Colorado (1981-1986), she worked on developing and testing the UV spectroradiometers. Her work also included applying the Ball-Black coating to reduce scattered light and developing the cryogenic pumping systems for maintaining a high quality vacuum inside the spectroradiometers both during ground tests, prelaunch, and during a rocket flight.

The electronic control systems and data amplification, telemetry and processing systems were designed and developed in the electronics laboratory of the NOAA-ERL Space Environmental Laboratory with continued development work by G.D. Falcon. These systems and their current status are described by Falcon and Taylor (1987).

4. Equipment

As an aid to promoting future collaboration, we list below some of the equipment currently on hand in our UV spectroradiometer development program:

1. Long Wavelength Monochromator (200-400 nm), Property No. NOAA/ERL 28348. (See sections 2 and 3 above.)

2. Short Wavelength Monochromator (120-200 nm), Property No. NOAA/ERL 49270. (See sections 2 and 3 above.)

3. CTI - Cryogenics Model 350 cP cryogenics system and helium refrigerator unit. Property No. NOAA/ERL 48906.

4. Argon mini arc and associated systems.

5. Tungsten lamps and power supply.

6. Zinc and mercury pen-ray lamps and power supplies.

7. SURF interface system.

8. Rotary indexing tables for holding and moving standard lamps.

9. Apple computer and disk drives for electronics control and data processing during laboratory tests.

5. Problems for Further Development

1. Low Through-Put
   The through-put is lower in both monochromators than expected in the design. Optical design is not a precise art compared to most engineering design fields because some of the reflectance and

transmission coefficients can't be guaranteed in single item purchase without prohibitive prices. See item 7 on p. A3-3.

2. Shutter Mechanism
The shutter mechanism will need to be improved before being used in space. The shutter has three positions, where one of them is for a filter, a second position is open and the third is closed. It appears the filters haven't really been used and therefore may not be needed in the revised shutter.

3. Oil Contamination
See the bottom paragraph on p. A3-1

4. Photomultiplier Drift
See items 11 and 14

5. HV Power Supply
The high voltage supply was designed to be able to be set at many different voltages. It has problems with noise and also a transient response when the voltage is changed. For rocket-flight measurements, a fixed value HV source, where the voltage is accurately known, should be considered.

References for this appendix are listed in Section 8.

APPENDIX II

Roughened Quartz Surfaces and Teflon as Small-Angle Diffusers and Depolarizers Between 200 and 400 nm.

Henry J. Kostkowski
Spectroradiometry Consulting
Route 1, Box 69
Charlotte Hall, Maryland 20622

and

Robert D. Saunders
National Bureau of Standards
Gaithersburg, Maryland 20899

March 19, 1984
NOAA Contract NA82RAC0028

Laboratory tests of transmission diffusers are reported for quartz and teflon. These tests were conducted in order to select transmission diffusers for the NOAA rocket-flight UV spectroradiometers.

1. Introduction

As part of a NOAA program to improve UV spectral irradiance rocket measurements of the sun, a suitable diffuser is being sought for the 200-400 nm region. Its purpose is to eliminate significant differences in the irradiance responsivity (1) of our spectroradiometer when viewing the sun and source standards such as a tungsten FEL-type lamp, an argon arc and the NBS Synchrotron (SURF II). Differences in the irradiance responsivity arise because of differences in the angle of incidence and of polarization of the radiation from these sources and of the strong sensitivity of our spectroradiometer, without a diffuser at its entrance aperture, to these quantities.

Selection of a suitable diffuser will depend on the range of angles of incidence and on the polarization of the incident radiation, on the maximum exiting angle from the diffuser and on the attenuation, stability and uniformity of the diffuser. The angle of incidence of the radiation from the above mentioned sources varies from 0° to about 2°, and the exiting angle (from the diffuser) for our f/5 system varies from 0° to 5.7° as indicated in Figure 1. The degree of polarization of the radiation from the above sources varies from zero for the argon arc to 3% for an FEL tungsten irradiance standard (2) and is almost 100% for SURF II (3). Therefore, we are seeking diffusers that obey the cosine saw for incident angles up to 2° and exiting angles up to 5.7° and that depolarize the incident radiation to a high degree. Because of signal-to-noise limitations, the diffuser must have a receiving area of at least a square centimeter, and its attenuation should not be greater than about 500. Because of our goal of limiting the uncertainty of the solar spectral irradiance measurements to a few percent, a stability of about 1% between calibration and use in solar measurements is required. Since the irradiance over a square centimeter from the above sources is highly uniform at the distances normally used, uniformity of the diffuser is not a critical requirement.

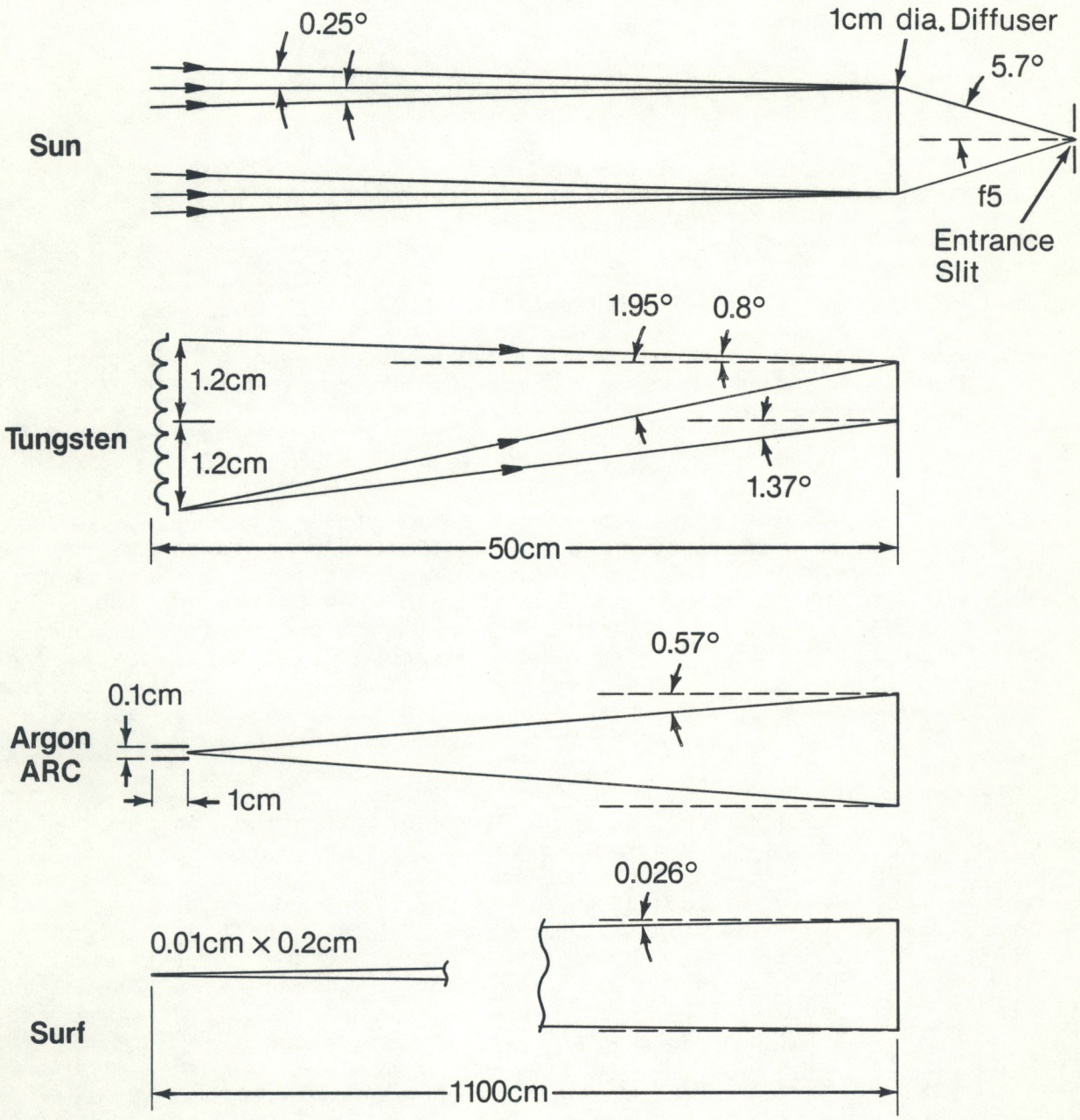

Figure 1. Angular configurations for the sun and various source standards.

We have not been able to obtain information from the archival literature or our colleagues that is needed to select a suitable diffuser. From our own limited experience, there are three possibilities: (1) an averaging/integrating sphere, (2) a roughened quartz surface or a stack of such surfaces and (3) sheet teflon. The averaging/integrating sphere is expected to have too high an attenuation, particularly at the shorter wavelengths. Therefore, we have concentrated on the remaining two possibilities. The current paper reports on an investigation of the diffusing, depolarizing and attenuating properties of roughened quartz surfaces and sheet teflon between about 200 nm and 400 nm. Stability measurements will be conducted later during the characterization and calibration of the rocket-bourne instrument.

2. Experimental Set-Up

Figure 2 is a schematic drawing of our experimental set-up. the spectroradiometer includes an f/5 Ebert-Fastie double monochromator with a 0.1 mm x 5.0 mm entrance slit, a spectral bandpass of 0.2 nm and bialkali photomultiplier operating in a photon counting mode (1).

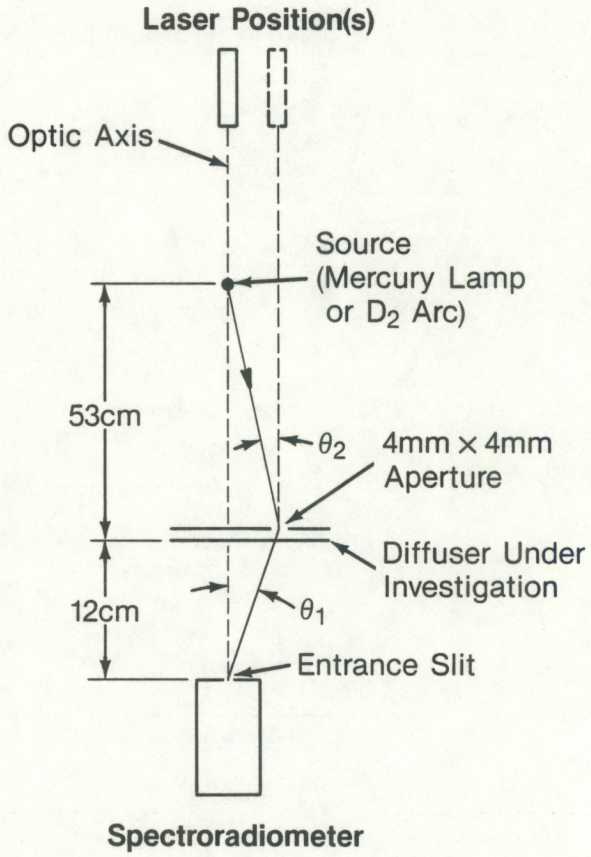

Figure 2. Schematic drawing of experimental set-up.

A low power He/Ne laser (shown in Figure 2) is used in setting the position of the 4x4 mm aperture for a particular value of θ_1 and in setting the position of the source so that $\theta_2 = 0^0$ for that aperture setting. The laser

itself is positioned so that its beam is on the optic axis or parallel to the optic axis striking the diffuser under investigation at the point where the 4mm by 4mm aperture is placed. A laser mount with micrometer-type translational and angular motions provides the required adjustments.

The sources used consist of either a 12 mm long section of a 1/4 inch diameter by 2 1/8 inch long low pressure cold cathode mercury discharge lamp or a 30 W deuterium arc lamp with a 1 mm diameter discharge-constriction aperture. The deuterium lamp is used primarily for measurements below 250 nm. The irradiance (at the slit and with no diffuser) of the UV spectral lines of the mercury lamp has the angular variation (about the lamp axis) shown in Figure 3. Before each measurement, the mercury lamp is rotated about is own axis so that the irradiance at the 4mm x 4mm aperture is always at the minimum value indicated in Figure 3.

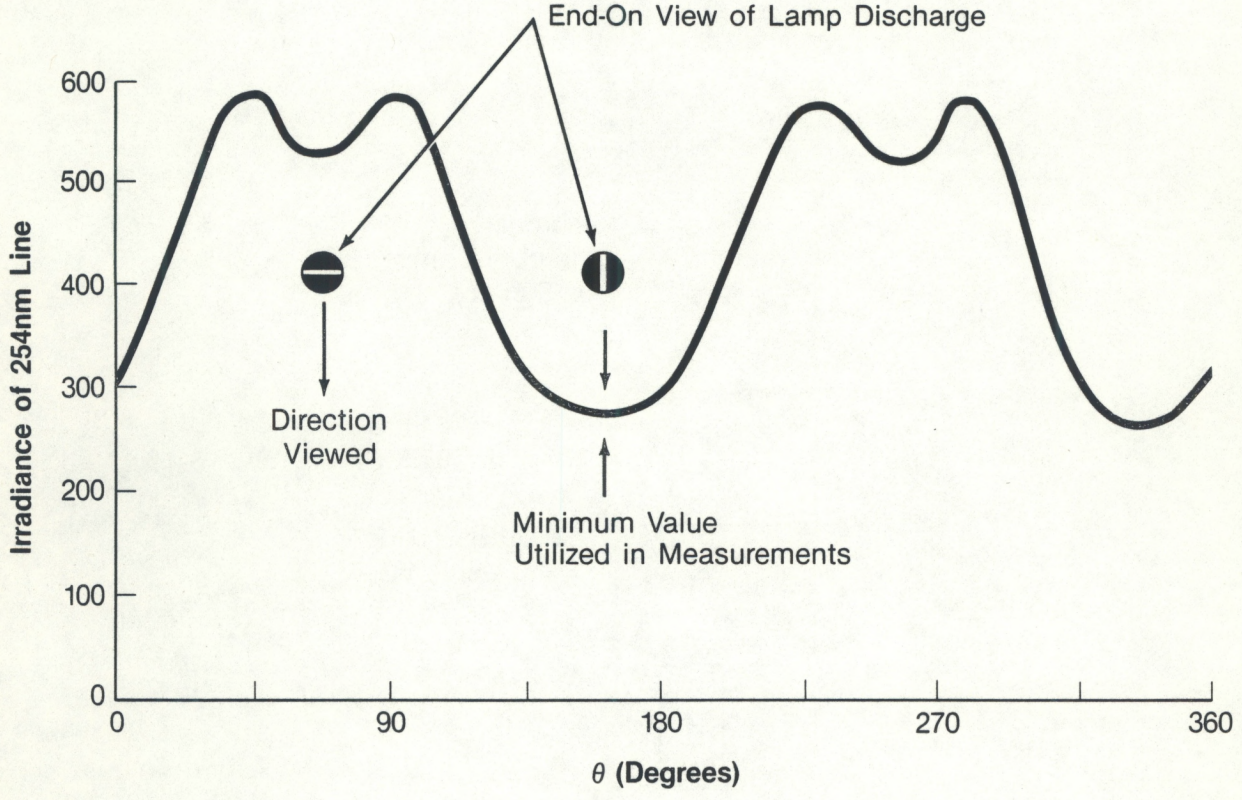

Figure 3. Variation of irradiance of 254 nm mercury spectral line as a function of angle of rotation θ about axis of lamp envelope.

3. Transmission Diffusers

The quartz elements being investigated consist of Supracil II disks either 2 or 2.5 mm thick and 25 mm in diameter. One or both surfaces of the disks have been ground so that they have an 8μ, 30μ, or 100μ (pit-size) finish. In use, the disks are stacked so as to produce 1 to 3 surfaces with the same finish, each 2 to 2.5 mm apart. The teflon disks being investigated are also about 25 mm in diameter with thickness of 0.003, 0.005, 0.01, 0.014 and 0.031 inches. The above disks are positioned and oriented so that their center is on the optic axis and their surfaces are normal to the optic axis as indicated in Figure 2. In order to test for the desired normality, the laser beam is retroreflected off a piece of microscope glass placed on the upper disk.

A 4mm x 4mm aperture, made from black matte paper, together with the entrance slit or the source fix the angles θ_1 and θ_2 in the measurements involving the cosine law. The 4x4 aperture is replaced by a one centimeter diameter aperture, with its center on the optic axis, for the attenuation measurements. For polarization measurements, the full f/5 system is used along with a dichroic polarizer having an extinction coefficient (when polarization axes are crossed) of a few percent at 254 nm.

4. Measurements and Results

Since the attenuation has to be limited to about 500, and approximate measurements of attenuation are easy to make, this measurement was carried out first. Attenuation for this investigation is defined as the ratio of the output signal of the spectroradiometer without a diffuser to that with a diffuser, keeping (or correcting) the irradiance at the entrance slit when the diffuser is not used to be the same as the irradiance at the diffuser when the latter is used.

Table 1 gives the results of the attenuation measurements, corrected for an f/5 system, for a number of roughened quartz surfaces and various thicknesses of teflon. The uncertainty of the values in Table 1 is very large, about 25%. The reason for this is that the irradiance responsivity without a diffuser depends greatly on the angle of the incident radiation as mentioned earlier. However, the large uncertainty is not a problem because the major purpose for the attenuation measurements is only to rule out some of the diffusers and reduce the number of time consuming cosine law experiments that has to be conducted. Based on the results shown in Table 1, Teflon with a thickness greater than 0.010 inches was excluded from further measurements.

Table 1. Sample attenuations for f/5 system.

Diffuser type		Wavelength (nm) 201	210	220	254	365
Quartz surfaces						
1 side	8μ pit size				7	
	30μ				10	
2 sides	8μ				21	
	30μ				32	
3 sides	8μ				57	
	30μ				94	
	100μ				159	135
Teflon sheet						
.031" thickness					1012	431
.014"		2301	1399	988	547	
.010"		860	625		374	278
.005"		643	441		263	
.003"					228	

For checking how well the cosine law is obeyed for the range of incident and exiting angles that exist in our case (see Figure 1), two sets of values were assigned to θ_1 and θ_2. These are shown in Figures 4a and 4b.

For the measurement configuration shown in Fig. 4a where $\theta_1 = 0°$ and $\theta_2 = +2°$ and $-2°$, the percent deviation from the cosine law, designated D(4a), is defined by the expression

$$D(4a) = 100 \cdot \left[\left(\frac{S_{+2}}{\cos^2 2°} - S_0 \cos 2°\right) + \left(\frac{S_{-2}}{\cos^2 2°} - S_0 \cos 2°\right)\right]/2S_0$$

where Si is the output signal for the i^{th} angular position. The cosine-squared term is an inverse square law correction because the source was at a greater distance when in the +2° or -2° position. Results for roughened quartz surfaces in configuration Figure 4a are given in Table 2 for the 254 nm and 365 nm mercury spectral lines. Without any diffuser present, the deviation is -28%. A few measurements were also made for $\theta_2 = \pm 5°$ in order to observe how rapidly D(4a) increased with θ_2.

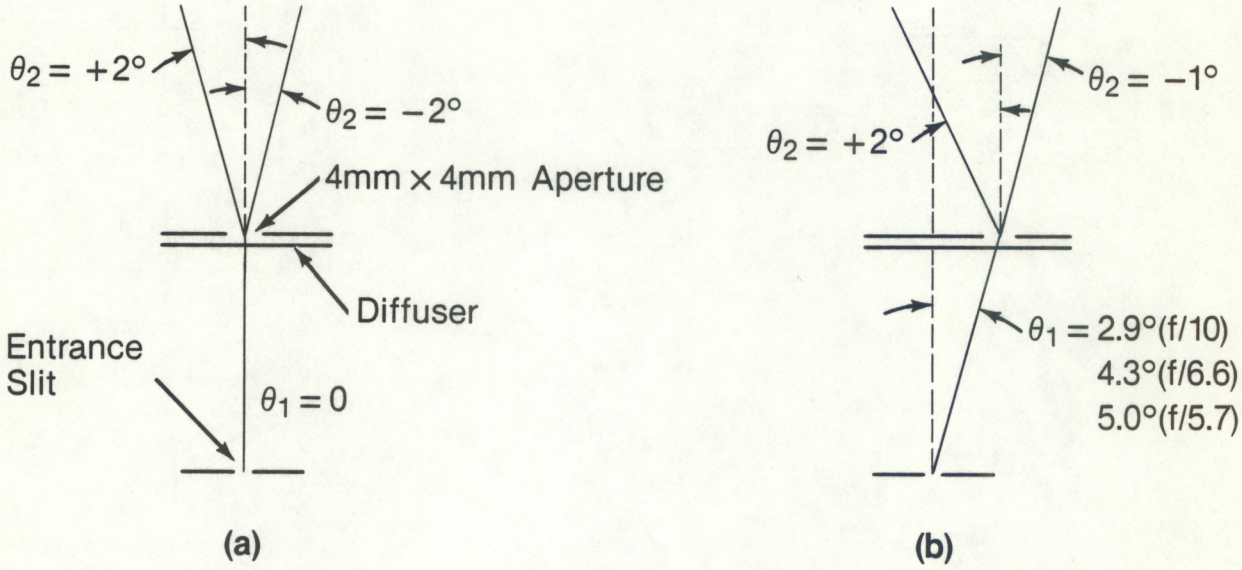

Figure 4. Configurations for measurements on deviation from cosine law.

Results for the second group (Figure 4b) where θ_2 = +2° and −1° for each of three values of θ_1 are presented in Table 3. Here, θ_1 has the value 2.9°, 4.3° and 5° corresponding to the maximum θ_1 for an f/10, f/6.6 and f/5.7 system. The percent deviation in this case is calculated by the equation:

$$Di(4b) = 100 \cdot \left(\frac{Si}{\cos^2 i} - S_0 \cos i\right)/S_0$$

where i is either 2° or −1°. Again Si is the output signal in the i^{th} degree position and $\cos^2 i$ term is an inverse square law correction. For this case, it is seen that the cosine law deviation is greater than 1% for all the quartz configurations. Teflon is a significant improvement, but even here the maximum deviation for an f/5.7 system is −1.7%.

The major source of uncertainty for the results in Tables 2 and 3 is the drift (due to temperature) of the mercury lamp output. The drift averaged about 0.7% per 5 minutes which was about the maximum time interval between repeats at the same angle position. Enough data was taken so that the uncertainty of the results in Table 2 and 3 is estimated to not exceed a few tenths of a percent.

Table 2. Sample deviations from cosine law for roughened quartz surfaces; $\theta_1 = 0°$, $\theta_2 = \pm 2°$ and $\pm 5°$ (See Figure 4a).

θ_2	Number of Surfaces	Roughness (pit size)	Percent Deviation 254 nm	Percent Deviation 365 nm
±2°	none	-		-28.0%
	1	8μ	-4.7%	-5.0
		30μ	-4.3	-3.7
	2	8μ	-1.3	-2.8
		30μ	-1.0	-1.4
	3	8μ	-1.0	-1.1
		30μ	-0.1	-0.8
±5°	1	8μ	-19.0	
		30μ	-21.0	
	3	8μ	-5.0	
		30μ	-3.3	

Table 4 gives the results of the polarization measurements. The polarization responsivity for the spectroradiometer is defined as

$$P = \left(\frac{S(max) - S(min)}{S(max) + S(max)}\right) \times 100$$

where S(max) is the maximum output signal and S(min) is the minimum output signal relative to the rotation of the dichroic polarizer. One sees from Table 4 that the roughened quartz surfaces are very poor depolarizes and that the Teflon is significantly better. The uncertainty of the values in Table 4 is a few percent.

Table 3. Sample deviations from cosine law at 254 nm for roughened quartz surfaces and teflon; $\theta_1 = 2.9°(f/10)$ to $5.0°(f/5.7)$, $\theta_2 = 2°$ and $-1°$; (See Figure 4b).

Diffuser type	θ_1	Percent Deviation $\theta_2=2°$	Percent Deviation $\theta_2=-1°$
Quartz surfaces			
3 sides/30μ	2.9°(f/10)	-4.8%	+2.2%
3 sides/30μ	4.3°(f/6.6)	-6.2	+3.0
3 sides/100μ	4.3°(f/6.6)	-3.9	+1.6
Teflon sheet			
0.010" thickness	4.3°(f/6.6)	-0.9	+0.7
	5.0°(f/5.7)	-1.7	+1.5

Table 4. Polarization responsivity of spectroradiometer with and without various roughened quartz and teflon diffusers.

Diffuser	Percent Polarization Responsivity 254 nm	365 nm
none	89%	84%
Quartz Surfaces		
8μ, 3 sides		81%
30μ, 3 sides	84	78
4 sides		72
100μ, 3 sides	52	
Teflon sheet		
0.031" thickness	4.3	3.5
0.014"	5.7	
0.01"	4.3	1.2

5. Summary and Conclusions

Tables 1 to 4 give the measured attenuations, cosine law departures, and depolarizations for a number of roughened quartz diffusers and for several thicknesses of sheet teflon. It is seen that one to three stacked roughened quartz surfaces with pit sizes varying from 8μ to 100μ are not suitable diffusers for our application relative to either the cosine law or to depolarization in the wavelength range 200 nm to 400 nm. Sheet Teflon is significantly better. A 0.01 inch thick sheet of Teflon obeys the cosine law at 254 nm to better than 1% for incident angles of 2° and exit angles of 4.3° (f/6.6), and it depolarizes plane polarized radiation at 254 nm by about 95%. The attenuation is significantly greater for Teflon than for roughened quartz but is acceptable in our application for Teflon thicknesses of 0.005 inches and possibly 0.010 inches.

6. Acknowledgements

The experimental work performed in this investigation was carried out at the National Bureau of Standards, Gaithersburg, Maryland and was supported by the National Oceanographic and Atmospheric Administration, Boulder, Colorado, under contract NA82RAC00028.

7. References

1. Henry J. Kostkowski, Robert D. Saunders, John F. Ward, Charles H. Popenoe and A.E. S. Green, "Measurement of Solar Terrestrial Spectral Irradiance in the Ozone Cut-Off Region", Chapter 1 of "Self-Study Manual on Optical Radiation Measurements: Part III-Applications", Nat. Bur. Stand. (U.S.), Tech. Note 910-5, 80 pages (1982).

2. Appl. Opt. 20, 2181, 1981.

3. Optical Eng., 21, 951, 1982.

APPENDIX III

Tests and Calibrations of Spectroradiometers

by

Henry J. Kostkowski
Route 1, Box 69
Charlotte Hall, Maryland 20622

Report for Part IV
NOAA ERL Contract No. NA82RAC00028

December 24, 1984

This report summarizes the status, repairs, modifications, calibrations and tests made during the summer of 1984, and investigations and results obtained at the National Bureau of Standards (NBS) from October 1 through December 10, 1984. It completes Part 4 of contract NA82RAC00028.

1. Current Status

Radiometric characterizations were made of the NOAA spectroradiometers relative to NBS' tungsten FEL, Synchrotron Ultraviolet Radiation Facility (SURF) and argon-arc standards in order to determine how tests to intercompare these standards should be designed and responsivity corrections made relative to source geometry, anode current, temperature, time of observation, time of darkness (shutter), scattering, and electrometer and integrator parameters. Preliminary radiometric comparison were made between SURF and a tungsten FEL standard at 254 nm and 296 nm with the result that these standards agree within their combined estimated uncertainties of about 6%. In the next comparison planned in January, the uncertainty of the comparison between SURF and the argon arc at 200 nm should have an uncertainty no greater than about 3%.

We are not currently able to estimate the accuracy that will be realized in comparing SURF and argon at wavelengths between 120 nm and 200 nm. The presence of an oil-like substance on a small area of the back cover plate of the SWM has not been explained. This has not affected the stability of the optics between 200 nm and 300 nm, but we have not yet determined that the optics has not been affected at shorter wavelengths. The major suspect for the oil is the wavelength drive stepping motor. Its manufacturer says it has not been designed for vacuum use, but RSI says that their tests show it can be used in vacuum. I recommend changing the motor if one designed for vacuum can be obtained by March 1 and can be used without extensive mechanical modification to the monochromators. Otherwise, I recommend determining if the current short-wavelength monochromator (SWM) can be used accurately in argon; and, if not, attempt to use the system as is in vacuum.

2. Repairs and Modifications During the Summer of 1984

1. The power supply for the argon mini-arc was repaired by the manufacturer, but it broke down again after a few hours of use. It has been returned to the manufacturer. A similar power supply that we were able to borrow at NBS is working very well.

2. It has not yet been possible to obtain a commercial photomultiplier (PMT) with the low dark current originally specified for the long-wavelength monochromator (LWM). EMR is still trying to select one that will meet these specifications. However, we are able to operate with an adequate signal-to-noise ratio with the currently available PMT as long as a diffuser is not used below about 290 nm.

3. The kinematic mount for the FEL tungsten standard and the bracket and baffle required for this mount were designed and fabricated. They are working well.

4. Obtaining the mirror mount and mirror for the feed-through on the SURF interface was postponed. The feed-through must now be utilized for holding either a 2 mm aperture during radiometric mapping or a shutter for use with the SWM. A method of operating satisfactorily without the mirror was developed.

5. RSI improved the operation of the shutter system on the SWM but it is still not reliable. I believe by very careful adjustments, it can be made adequate for laboratory use. However, because of time limitations, it has been removed and for the time being a gate valve on SURF will be used as a shutter for the SWM. The shutter system on the LWM continues to operate satisfactorily.

6. Light leakage in the LWM has been eliminated by RSI.

7. Modification of the alignment ports by RSI has been completed. They now are vacuum tight.

8. Items numbered 11 through 20 relating to electronics or computer software that I requested from NOAA in my Technical Report of 7-6-84 have not been received. This has reduced our research efficiency. Fortunately, NBS collaborator Bob Saunders was able to provide adequate substitutes for the most pressing needs. These will be described later.

9. A second draft of the diffuser paper was completed.

10. Chapter 6 of the NBS Self-Study Manual on Polarization was reviewed to determine any purchases required for addressing polarization effects. A quarter waveplate at 250 nm is required in order to determine R(04) in the Mueller responsivity matrix of our monochromators. This term is only significant if circularly polarized light is present in the incident beam. In our experiments, ignoring this term should result in an error of less than about 0.5%. Because of tightness in funds, it was decided not to purchase or at least postpone the ordering of this $1100 item.

3. Investigations and Results in the Period October 1 Through December 10, 1984

1. Experiments and calculations were carried out to determine the dynode resistors to be used with the photomultiplier now being selected by EMR. The one megaohm resistors originally specified would result in neglible nonlinearity but in significant thermal effects which were recently discovered. It was decided to use 3.9 megaohm resistors because non-linearity effects can be corrected much easier than thermal effects.

2. A variety of experiments were conducted relative to wavelength. It was found that the LWM had a reproducibility of 1 step (.025 nm) when resetting on the short wavelength fiducial. Disconnecting and reconnecting power to the stepping motor also has a maximum effect of 1 step. Finally, the temperature effect produced by running the stepping motor is -.0055nm/deg C using sensor T15 in the LWM.

3. Procedures recommended by NBS for operating the argon arc with optimum reproducibility were investigated. It was found that changes in spectral irradiance as large as 3% (at 300 nm) were obtained when a new electrode was used. Relighting a used electrode was better, but changes as large as 2% were noted. NBS is investigating the use of round rather than pointed electrodes relative to reducing the magnitude of these changes. After a "burn-in" period of about 15 minutes, the spectral irradiance at 300 nm drifted downward at a rate of about 1% per hour. These tests were done without an arc window which may be omitted above 200 nm. Window contamination is expected to make the drift larger. The half-irradiance diameter of the arc at 35 amperes was determined to be 2.0 mm.

4. The ratio of the responsivity of the LWM when observing an FEL tungsten standard to that when observing an argon arc was determined by making measurements as a function of angle of a carefully positioned and oriented argon arc. The ratio was .99 at 300 nm and .98 at 254 nm.

5. The stability of the LWM was determined as a function of anode current. At 8 X E-7 amps, the drift rate was 2.5% per hour. At 1.7 X E-7 and 3.7 X E-8 amperes, it was 0.2% per hour.

6. The effect of temperature changes of the electrometer/PMT housing (T1 sensor) on responsivity was investigated and found to be -.057%/deg C for a gain of 1xE+7 V/A and +.051%/deg C for a gain of 1xE+9 V/A.

7. The relative spectral responsivity of the LWM was determined from 400 nm to 200 nm. A large unexpected fall-off of approximately a factor of 30 was observed in going from 300 to 250 nm. This, in addition to the high dark current, prevents the use of a diffuser at 250 nm. The fall-off is probably due to the grating blaze being at 300 nm rather than the requested 250 nm or to insufficiently pure aluminum being used when the optics were aluminized. This will be investigated at a later date. When it is corrected, a diffuser can be used through much of the wavelength range of the LWM and scattering which is now about 0.6% at 250 nm when using a tungsten lamp will be completely negligible.

8. The FEL 1000 watt tungsten lamp standard was investigated relative to emission from the quartz bead in the lower part of the lamp and the seal at the top of the lamp. As a result of reflection and scattering, the bead contributes 1.0% and the seal 0.4% to the irradiance of the lamp. The entrance slit baffle system in the monochromators limits the monochromators from seeing all of this light. We will take this into account in our measurements and in what we request relative to NBS' calibration of these lamps.

9. NBS performed a preliminary calibration on two FEL lamps that we are using. One of these lamps (F156) has been used extensively. The other (F174) is used infrequently in order that the changes in F156 may be determined when this is pertinent. The irradiance of F156 at 280 nm is increasing at a rate of 0.04% per hour of burning time. The effect of small displacements of the lamps when viewed by the LWM was also determined. Changes in signal as large as 1% per 1 mm of displacement perpendicular to the optic axis was noted. This means careful laser-positioning of the lamps is required for optimum repeatability.

10. Preliminary measurements of the ratio of output signal when changing from the E+7 to the E+9 electrometer gains was 92.7 rather than the anticipated 100.0. Smaller but significant differences were also obtained for the integrator gain ratios. These ratios will have to be checked as a function of time and temperature.

11. The effect on the responsivity of the LWM after the PMT has been dark for various lengths of time has been determined. The responsivity returns to its original value in a few minutes after the tube has been dark for a minute. When the tube is dark for 30 minutes, the responsivity is still different by .3% after a few minutes and requires about 10 minutes of irradiation to return to its original value.

12. The SWM has higher drift rates than the LWM. At an anode current of 4.6 X E-10 amps and 1.2 X E-8 amps, the responsivity of the SWM decreases at a rate of 1.4% per hour and at 1.9 X E-7 amps the decrease is 4% per hour. It is expected that these rates will decrease as the PMT is aged.

13. The effect on the responsivity of the SWM when its PMT is dark for various lengths of time is about the same as that for the LWM in spite of the fact that the PMT's are quite different.

14. Preliminary measurements have been made on the change of responsivity after a PMT voltage change. Immediately after a 1300 V to 1000 V change in the LWM, the responsivity is .3% lower than its "normal" value at 1000 V. It takes about 15 minutes to return to the normal value. In general, for optimum precision, one must determine changes in responsivity as a function of time during irradiation and after being dark or the voltage is changed. Ideally, one should determine the responsivity changes for the specific conditions and time sequences used in every calibration or measurement.

15. Fixtures required for precise use of the tungsten lamp and argon arc including laser alignment at the SURF facility were fabricated and installed.

16. R. Saunders of NBS developed the hardware and software required for utilizing an auxiliary NBS computer with our system. This enables us to perform various calculations as the data are taken so that decisions can be made during the course of an experiment. For example, the mean and standard deviation of successive sets of twenty data points, corrected means and standard deviations after particularly noisy points are deleted, the time data is taken, and the ratio of the mean signal to SURF beam current are all printed out. It is also possible to have this data recorded on a floppy disk for computer calculations at a later time. Without this capability, data reduction would be much more time consuming.

17. The SURF beam was scanned radiometrically with the LWM relative to translation and angle. The results of these scans are used to precisely position and align the monochromators which is of great importance when a diffuser is not used.

18. The first complete radiometric comparison was made between SURF and an FEL tungsten standard. The spectral irradiance of SURF at 254 was 2% higher that that of the FEL and at 296 nm SURF was 5% higher. The uncertainty of these preliminary results are at least several percent because various responsivity corrections have not yet been determined and applied. In fact, beyond telling us that the results are "in the ballpark", the major usefulness of the comparison is to provide us with the electrometer and integrator parameters, PMT voltages, and the times required for various parts of the comparison so that responsivity corrections can be determined for these conditions and time sequence.

19. A stainless steel bracket and an associated 2 mm aperture to be mounted on the linear motion feed-through were designed and fabricated. The 2 mm diameter SURF beam that this will provide will make it possible to determine the ratio of the responsivities of the two monochromators when viewing SURF and an FEL lamp.

APPENDIX IV

Coronal Holes

by

Larry C. Puga

March 26, 1987

1. Introduction

The modeled values of the UV for wavelengths between 140-300nm, (modeled from Ca K plage data, see Lean et al., 1982 and Lean et al., 1984b), have consistently correlated well with the NIMBUS-7 observed UV irradiance for short-term temporal variations, with the exception of peak values on a number of solar rotations showing a discrepancy between the modeled and NIMBUS-7 observed UV variations for the magnitude of the peak value. One possible explanation of these differences between modeled and observed UV, is that the presence of coronal holes is a factor in these discrepancies. Through the use of ratios of power spectra for the short-term variations, the presence and effect of coronal holes is investigated.

2. Data and Methods

To determine if the presence of coronal holes affects the peak variation ratio of modeled UV irradiance versus observed UV irradiance at a wavelength of 205nm, it was first necessary to assemble an accurate list of coronal hole occurrences and their position on the solar disk. Table 1 is a listing of coronal holes; to compile such a list for the time period 10/7/78 to 8/31/82 required using three different sets of photographs and charts;

1.) **SGD** synoptic charts, created from 10830A He I photographs, for the period October 1978 to July 15, 1979.

2.) **SGD** 10830A He I photographs from July 15, 1979 to December 1981

3.) H-alpha synoptic charts from December 1981 to November 1982 (P. McIntosh of the Space Environment Lab, NOAA/ERL supplied these charts.)

A comparison of H-alpha charts that indicate the location of coronal holes for the same time periods as the 10830A He I photographs indicates coronal holes found using the photographs are often smaller than those indicated on the H-alpha synoptic charts, and the fine structure patterns of the H-alpha charts sometimes indicate coronal holes where the 10830A photographs do not; the photographs are **the only** available data for most of the time period, thus the list of coronal holes, which despite their somewhat arbitrary identification, is as accurate as possble.

A total of 1366 days of observations were used to obtain the data set;

Table 1

CORONAL HOLES FROM 10830A SYNOPTIC MAPS

DATE(S) OF OCCURRENCE	NORTH LAT. BOUND.	SOUTH LAT. BOUND.	EAST CARR. BOUND.	WEST CARR. BOUND.
10/17/78 (Possible)	+25°	+16°	353°	360°
10/18-10/20/78 (Possible)	57°	21°	326°	341°
10/22-10/23/78	+25°	- 2°	274°	296°
10/16-11/17/78	90°	55°	140°	360°
10/26-11/1/78	55°	41°	160°	235°
10/30-11/5/78 (Polar)	-36°	-90°	135°	200°
11/5-11/7/78	43°	33°	97°	118°
11/8-11/12/78	-20°	-41°	43°	67°
11/9/78 (Possible)	24°	17°	55°	63°
11/14-11/21/78 (Polar)	90°	40°	260°	346°
11/28-12/2/78 (Polar)	90°	40°	115°	177°
11/26-12/5/78 (Polar)	-38°	-90°	46°	186°
11/18/78 (Possible)	13°	5°	302°	311°
11/19/78	-20°	-35°	283°	295°
11/20/78	14°	4°	272°	283°
11/22/78	40°	30°	235°	252°
12/1/78 (Possible)	34°	21°	127°	141°
12/2/78 (Possible)	33°	22°	117°	123°
12/1/78	-16°	30°	123°	137°
12/19/78	52°	27°	85°	98°
12/1-12/27/78	high level Polar hole above or equal to 70°			
12/1-12/18/78	high level Polar hole above or equal to -70°			

DATE(S) OF OCCURRENCE	NORTH LAT. BOUND.	SOUTH LAT. BOUND.	EAST CARR. BOUND.	WEST CARR. BOUND.
12/14/78 (Possible)	28°	6°	318°	318°
12/15-12/16/78	11°	-30°	287°	303°
12/18/78 (Possible)	8°	- 4°	250°	266°
12/19/78 (Possible)	28°	12°	246°	253°
12/21-12/22/78	41°	16°	209°	228°
12/25-12/26/78	35°	20°	156°	179°
12/26/78-1/1/79	-18°	-90°	80°	160°
			(90-140°	major)
12/31/78-1/1/79	42°	26°	85°	109°
1/2/79 (Possible)	43°	37°	68°	76°
1/2/79 (Possible)	23°	17°	67°	72°
1/4-1/6/79 (Polar)	90°	62°	15°	48°
1/11/79	- 7°	-24°	307°	322°
1/13-1/16/79 (Polar)	90°	48°	241°	317°
1/17-1/23/79 (Begins Polar)	90°	17°	145° (160°-232°	232° major)
1/24-1/28/79	-20°	-60°	80°	136°
1/24-2/3/79 (Polar)	-60°	-90°	0°	140°
2/5/79	-13°	-28°	338°	349°
2/6-2/7/79	19°	8°	303°	316°
2/14-2/15/79	36°	15°	212°	231°
2/17/79	21°	12°	183°	194°
2/22/79	16°	-6°	117°	129°

DATES OF OCCURRENCE	NORTH LAT. BOUND.	SOUTH LAT. BOUND.	EAST CARR. BOUND.	WEST CARR. BOUND.
2/22-2/26/79	-22°	-50°	65°	118°
2/23-3/3/79 (Polar)	-50°	-90°	0°	90°
2/28/79	14°	8°	39°	46°
3/3-3/6/79 (Polar)	-60°	-90°	320°	36°
3/7-3/8/79	37°	25°	300°	310°
3/12-3/13/79	35°	27°	233°	239°
3/14/79	-30°	-41°	213°	233°
3/14-3/16/79	31°	0°	186°	218°
3/16-3/17/79 (Polar)	90°	50°	157°	188°
3/22-3/26/79	-26°	-48°	57°	111°
3/24-3/30/79 (Polar)	-60°	-90°	0°	80°
4/4/79	-28°	-46°	283°	298°
4/6-4/7/79	0°	-10°	263°	275°
4/10-4/12/79	24°	- 8°	182°	213°
4/12/79	-33°	-42°	186°	201°
4/16/79	5°	- 6°	117°	132°
4/16-4/17/79	30°	8°	110° (combo two	127° holes)
4/17-4/24/79	-21°	-53°	38°	117°
4/24/79	37°	16°	22°	38°
4/25-4/27/79 (Polar)	-60°	-90°	0°	27°
4/25-4/27/79	-38°	-52°	0°	20°
4/27/79	- 6°	-20°	0°	6°
4/26-5/2/79 (Polar)	-60°	-90°	280°	360°
4/26-4/29/79	-30	-55°	317°	-360°
4/26/79	-12°	-21°	353°	360°

Table 1 (continued)

CORONAL HOLES FROM 10830Å SYNOPTIC MAPS

DATE(S) OF OCCURRENCE	NORTH LAT. BOUND.	SOUTH LAT. BOUND.	EAST CARR. BOUND.	WEST CARR. BOUND.
4/26-4/28/79 (Poss. Polar)	90°	50°	330°	357°
5/3-5/5/79	42°	23°	246°	271°
5/3-5/5/79	-26°	-40°	248°	267°
5/9-5/11/79	20°	- 4°	176°	205°
5/11-5/12/79	-33°	-51°	153°	177°
5/15/79	22°	8°	110°	123°
5/21/79 (Possible)	14°	4°	74°	81°
5/22-5/27/79	-17°	-90°	0°	63°
5/22-5/29/79 (Polar)	90°	62°	270°	360° (+10°)
5/27-5/29/79	-25°	-90° (300°-360° major)	290°	360°
6/1/79	33°	18°	253°	270°
6/2/79	-23°	-45°	229°	247°
6/4-6/5/79	10°	- 5°	197°	220°
6/8-6/9/79	-29°	-41°	143°	154°
6/11/79	11°	- 1°	114°	128°
6/13-6/14/79	40°	23°	78°	102°
6/17/79	-28°	-40°	34°	51°
6/18-6/19/79	-15°	-45°	0°	20°
6/20-6/27/79	90°	+60°	275°	360°
6/20-6/22/79	-23°	-57°	330°	360°
6/22-6/26/79	-43°	-90°	280°	330°
6/29-7/1/79	-27°	-37°	215°	245°
7/1-7/2/79	18°	-11°	194°	217°
7/11/79	35°	25°	87°	92°
7/11/79	18°	5°	77°	92°
7/14-7/16/79	-12°	-30°	0°	46°
Begin use of Synoptic Maps composed of actual photos				
7/18-7/20/79	-22°	-60°	310d	335°
7/20-7/29/79	-71°	-90°	210°	300°
7/22-7/31/79	90°	60°	165°	280°
7/28/79	-24°	-38°	205°	213°
7/27-7/28/79	18°	-11°	198°	217°
8/8/79	-40°	-52°	56°	63°
8/8-8/9/79	42°	37°	35°	60°
8/13/79	-22°	-30°	0°	10°
7/30-8/2/79 (Polar)	65°	57°	140°	180°
8/15-8/24/79 (Polar)	-70°	-90°	200°	320°
8/16-8/19/79	-26°	-50°	270°	320°
8/20-8/22/79	1°	- 5°	236°	262°
8/23-8/24/79	22°	5°	210°	231°
8/24-8/29/79 (Polar)	90°	45°	140°	215°
9/1-9/2/79	-22°	-40°	93°	120°
9/1/79 (Possible)	-52°	-57°	102°	111°
9/5/79	40°	30°	42°	54°
9/5-9/9/79 (Possible)	70°	55°	5°	50°
9/8-9/9/79	10°	- 8°	0°	15°
9/10-9/13/79	-14°	-40°	296°	350°
9/13/79	51°	40°	290°	310°
9/19/79 (Possible)	15°	9°	222°	229°
9/21-9/24/79	60°	20°	160°	205°
9/24-9/28/79 (Polar)	90°	60°	100°	160°
9/24/79	21°	17°	165°	169°
9/30/79 (Possible)	65°	45°	67°	78°
10/4-10/6/79 (Possible)	60°	50°	0°	35°
10/5-10/6/79	35°	24°	0°	15°
10/5-10/6/79	3°	-11°	0°	16°
10/11-10/14/79	52°	28°	248°	303°
10/7-10/10/79 (Highly possible)	10°	-30°	300°	357°
10/11-10/12/79	-34°	-41°	279°	297°
10/13/79	30°	20°	274°	287°
10/20/79 (Probable)	8°	- 7°	174°	185°
10/18-10/25/79 (Polar)	-47°	-90°	110°	200°
10/28/79	-33°	-43°	63°	79°
10/28-10/29/79 (Polar)	90°	+65°	50°	70°
10/29-11/2/79 (Probable)	90°	40°	0°	60°
10/30/79	- 3°	-11°	37°	43°
11/1-11/2/79	35°	30°	0°	20°
10/31-11/2/79	10°	-20°	0°	30°
10/7-10/8/79	40°	28°	287°	300°
11/10/79 (Probable)	11°	3°	248°	257°
11/11/79 (Possible)	-40°	-30°	233°	241°
11/13-11/14/79	-40°	-48°	203°	225°
11/17/79	9°	5°	164°	170°
11/18/79	15°	7°	152°	165°
11/18/79	60°	54°	142°	161°

Table 1 (continued)

CORONAL HOLES FROM 10830Å SYNOPTIC MAPS

DATE(S) OF OCCURRENCE	NORTH LAT. BOUND.	SOUTH LAT. BOUND.	EAST CARR. BOUND.	WEST CARR. BOUND.
11/21/79	-13°	2°	105°	115°
11/26/79	-27°	-38°	49°	60°
11/26/79	2°	- 7°	44°	52°
11/28-11/30/79	10°	-27°	0°	30°
12/5/79	20°	-10°	286°	293°
12/7/79	30°	20°	267°	271°
12/12/79	20°	13°	194°	203°
12/20-12/21/79 (Possible)	60°	57°	80°	97°
12/26/79	23°	17°	9°	20°
12/27/79	-30°	-40°	0°	14°
12/28-12/31/79 (Polar)	90°	70°	310°	350°
12/29-12/30/79 (Polar)	-70°	-90°	305°	327°
1/1/80	13°	-11°	284°	298°
1/2/80	33°	27°	279°	285°
1/4/80 (Possible)	32°	28°	256°	263°
1/8/80	13°	10°	202°	206°
1/11-1/12/80	-39°	-47°	140°	162°
1/17-1/24/80 (Polar)	90°	56°	0°	82°
1/23-1/24/80	33°	-12°	0°	15°
1/24/80	-20°	-60°	0°	6°
1/8/80 (Polar)	90°	60°	191°	208°
No Data for February 1980				
3/19/80 (Highly Possible)	30°	-12°	344°	357°
3/19-3/20-80	60°	48°	239°	360°
3/24/80	10°	- 8°	282°	295°
3/27/80	21°	15°	236°	242°
3/28-3/30/80 (Possible)	41°	29°	210°	241°
3/30-4/1/80 (Polar)	90°	60°	180°	193°
3/31-4/1/80	11°	- 2°	174°	190°
4/5-4/8/80 (Polar)	90°	60°	90°	121°
4/9-4/10/80 (Polar)	-70°	-90°	50°	67°
4/10/80	40°	-10°	47°	55°
4/11-4/14/80	30°	-10°	0°	46°
4/13-4/14/80	-35°	-70°	0°	21°
4/13-4/14/80	90°	23°	0°	22°
4/15-4/18/80	60°	46°	310°	360°
4/20/80	-30°	-37°	285°	293°
4/20-4/21/80 (Polar)	-70°	-90°	276°	290°
4/23-4/24/80	21°	9°	238°	249°
4/29/80	40°	29°	165°	179°
4/29/80 (Possible)	-30°	-40°	160°	176°
5/7-5/8/80	10°	-10°	44°	58°
5/11/80	43°	40°	14°	20°
5/13-5/20/80	60°	43°	250°	358°
5/18/80	2°	- 7°	272°	282°
5/18/80	-16°	-32°	270°	291°
5/21/80 (Polar)	90°	60°	239°	251°
5/22/80	31°	19°	217°	233°
5/20/80	22°	3°		
5/29/80	-28°	-42°	124°	142°
5/28-5/29/80 (Polar)	90°	48°	128°	150°
6/2-6/3/80	50°	33°	62°	92°
6/6-6/8/80	90°	0°	0°	25°
6/12/80	57°	49°	293°	310°
6/17-6/18/80	30°	14°	224°	248°
6/18/80 (Possible)	2°	-4°	228°	231°
6/20/86	47°	41°	203°	210°
6/25/80	62°	49°	127°	142°
6/24-6/26/80 (Possible)	-36°	-47°	97°	147°
7/1/80	50°	40°	42°	67°
7/1/80	-20°	-10°	48°	66°
7/1/80	-40°	-53°	43°	63°
7/11/80	68°	56°	276°	293°
7/14-7/16/80 (Possible)	47°	24°	207°	246°
7/16/80 (Possible)	-10°	-23°	213°	222°
7/22-7/24/80	63°	44°	104°	147°
7/22/80	-30°	-38°	128°	137°
7/30/80	-38°	-50°	20°	32°
8/1/80	28°	-10°	0°	13°
8/2/80 (Possible)	-62°	-48°	346°	360°
8/2-8/3/80	63°	-41°	330°	360°
8/12-8/13/80	42°	31°	199°	227°
8/14/86	24°	19°	184°	191°
8/19-8/20/80	60°	39°	103°	136°
8/20-8/21/80	-30°	-47°	80°	117°

Table 1 (continued)

CORONAL HOLES FROM 10830A SYNOPTIC MAPS

DATE(S) OF OCCURRENCE	NORTH LAT. BOUND.	SOUTH LAT. BOUND.	EAST CARR. BOUND.	WEST CARR. BOUND.
8/26-8/28/80 (Probable)	60°	33°	0°	41°
8/27-8/28/79	-37°	-56°	0°	18°
8/29/80	-42°	-53°	344°	360°
8/31-9/2/80 (Polar)	90°	58°	296°	340°
9/9-9/10/80	40°	31°	186°	223°
9/12/80	8°	- 5°	163°	175°
9/17-9/18/80	-29°	-47°	73°	112°
9/17-9/25/80	68°	47°	0°	105°
9/23-9/24/80 (Probable)	-44°	-52°	0°	30°
9/23-9/24/80 (Probable)	11°	-10°	0°	26°
9/25-9/27/80 (Possible)	-44°	-53°	320°	360°
9/29/80	70°	64°	292°	302°
10/4/80	-20°	-31°	228°	237°
10/5/80	-18°	-24°	202°	211°
10/8-10/9/80	41°	24°	165°	182°
10/14/80	-25°	-33°	90°	102°
10/16-10/18/80 (Possible)	90°	54°	40°	80°
10/21/80	70°	59°	0°	17°
10/22-10/25	-36°	-67°	313°	360°
10/28/80	13°	- 8°	277°	295°
11/1-11/2/80	- 8°	-27°	199°	234°
11/6/80	-14°	-26°	159°	171°
11/12/80	-20°	-34°	77°	93°
11/14-11/15/80 (Probable)	48°	29°	32°	62°
11/17/80 (Possible)	3°	-12°	0°	18°
11/19-11/21/80 (Polar)	90°	56°	320°	360°
11/19-11/21/80	-42°	-57°	296°	351°
11/24/80	16°	4°	275°	284°
11/25/80	-33°	-48°	268°	278°
11/28-11/30/80	2°	-24°	203°	236°
12/2-12/4/80	-18°	-31°	144°	180°
12/5/80	-37°	-49°	123°	142°
12/9-12/10/80 (Polar)	90°	63°	71°	95°
12/10-12/12/80	-27°	-50°	45°	87°
12/10-12/11/80	55°	34°	0°	12°
12/16/80	8°	- 6°	356°	360°
12/16-12/18/80	90°	33°	314°	360°
12/18-12/19/80	-35°	-57°	303°	336°
12/22-12/23/80	-34°	-53°	252°	278°
12/31-1/1/81	26°	2°	143°	161°
1/1-1/2/81	-20°	-40°	127°	159°
1/7-1/9/81	-26°	-47°	30°	77°
1/10-1/11/81	42°	32°	0°	26°
1/14-1/16/81 (Polar)	90°	57°	293°	340°
1/16/81	40°	26°	297°	325°
1/16-1/21/81	-38°	-47°	230°	316°
1/28/81	28°	7°	143°	151°
1/30/81	-18°	-34°	107°	132°
1/31-2/4/81	-46°	-59°	52°	116°
2/2-2/3/81	54°	38°	58°	87°
2/4-2/8/81	-20°	-58°	0°	65°
2/6-2/8/81	90°	36°	0°	30°
3/9/81	-44°	-63°	345°	360°
3/9-3/11/81 (Polar)	90°	60°	298°	360°
2/14-2/18/81	-24°	-63°	225°	290°
2/19-2/20/81	- 5°	-25°	184°	216°
2/23/81	20°	- 8°	148°	173°
2/27/81	-24°	-37°	103°	128°
3/5/81	-22°	-38°	23°	39°
3/11/81	43°	25°	314°	325°
3/14-3/17/81	-31°	-57°	226°	293°
3/20/81	31°	21°	187°	193°
3/22/81	-10°	-36°	170°	177°
3/28-3/30/81 (Polar)	61°	58°	53°	106°
3/28-3/30/81	39°	36°	52°	98°
3/29/81	-30°	-34°	68°	78°
3/29-3/30/81	-45°	-52°	47°	87°
4/7-4/16/81	-31°	-75°	193°	325°
4/8/81	55°	19°	293°	318°
4/19/81	-13°	-41°	139°	170°
4/24/81	-22°	-30°	84°	98°
4/28-4/29/81	36°	25°	22°	48°
5/6-5/7/81	47°	28°	277°	307°
5/9-5/11/81	-27°	-71°	217°	266°
5/18/81	-28°	-41°	119°	151°
5/25/81	8°	1°	47°	53°
5/26-5/27/81	37°	21°	6°	44°

Table 1 (continued)

CORONAL HOLES FROM 10830A SYNOPTIC MAPS

DATE(S) OF OCCURRENCE	NORTH LAT. BOUND.	SOUTH LAT. BOUND.	EAST CARR. BOUND.	WEST CARR. BOUND.
5/29-6/12/81	-58°	158°	360°	
(Polar) (-8 -90° finger at 250°)				
6/4-6/8/81	53°	22°	208°	283°
6/12/81	- 6°	-26°	155°	172°
6/21/81	16°	4°	43°	64°
6/22-6/24/81	47°	21°	0°	44°
6/26/81	37°	18°	335°	354°
7/3/81	7°	-47°	234°	255°
7/3-7/7/81	75°	17°	185°	255°
7/14-7/17/81	90°	32°	53°	118°
7/17/81	-36°	-44°	48°	68°
7/31/81	-11°	-33°	233°	253°
8/2-8/5/81	56°	28°	176°	222°
8/10/81	40°	30°	89°	107°
8/31/81	17°	6°	61°	73°
8/14-8/16/81	35°	17°	19°	55°
8/17/81	-25°	-36°	5°	18°
8/26/81	9°	1°	253°	261°
8/26-8/29/81	- 6°	-90°	202°	253°
8/30-9/3/81	60°	24°	145°	207°
9/7-9/8/81 (Polar)	-52°	-90°	74°	103°

DATE(S) OF OCCURRENCE	NORTH LAT. BOUND.	SOUTH LAT. BOUND.	EAST CARR. BOUND.	WEST CARR. BOUND.
9/8/81	11°	- 6°	72°	85°
9/9/81	36°	19°	60°	67°
9/10-9/11/81	38°	21°	34°	57°
9/14/81	-30°	-40°	347°	360°
9/14-9/18/81 (Possible)	90°	56°	305°	360°
9/21/81	6°	-23°	248°	274°
9/26-10/2/81	90°	23°	130°	211°
9/30/81	37°	-22°	163°	173°
10/5/81	11°	- 5°	79°	93°
10/5-10/9/81	-26°	-90°	27°	91°
10/5-10/9/81	90°	44°	24°	83°
10/13/81	-26°	-45°	331°	343°
10/20/81	-19°	-30°	243°	252°
10/23-10/28/81	52°	23°	136°	212°
10/30-11/2/81	-22°	-49°	64°	115°
11/1/81	- 6°	-25°	89°	98°
10/4-10/5/81	-24°	-33°	27°	52°
10/5-10/6/81	73°	27°	16°	48°
11/8-11/11/81 (Polar Possible)	90°	53°	300°	360°
11/12-11/13/81	13°	-11°	288°	313°

DATES OF OCCURRENCE	NORTH LAT. BOUND.	SOUTH LAT. BOUND.	EAST CARR. BOUND.	WEST CARR. BOUND.
11/13-11/14/81	-24°	-40°	267°	293°
11/16/81	-22°	-32°	247°	257°
11/21/11/28/81	90°	23°	90°	197°
11/23/81	- 5°	- 9°	153°	158°
11/27/81	- 8°	-16°	98°	113°
11/28-12/1/81	52°	27°	34°	92°

From 12/1/81 Hα Synoptic maps from P. McIntosh are used to get coronal holes

(Carrington Rotation 1716)

Table 1 (continued)

CORONAL HOLES FROM Hα SYNOPTIC CHARTS (FROM 10830A PHOTOS)

DATE(S) OF OCCURRENCE	NORTH LATITUDE BOUNDARY	SOUTH LATITUDE BOUNDARY	EAST CARRINGTON BOUNDARY	WEST CARRINGTON BOUNDARY	ROTATION
On the Hα charts Coronal holes between the poles and 70° of latitude occur nearly at all times; thus only coronal holes between ±70° of latitude will be listed.					
12/15/81	-24°	-36°	228°	247°	1716
12/23-12/25/81	7°	-44°	012°	136°	1716
12/5-12/6/81 (Polar)	+70°	49°	338°	360°	1716
12/10-12/13/81 (Polar)	70°	47°	258°	313°	1716
12/31/81 (Polar)	-65°	-70°	250°	267°	1716
12/22-12/16/81	70°	25°	93°	155°	1716
12/27/81-1/1/82 (Polar)	-61°	-70°	0°	87°	1716
12/19-12/30/81	-23°	-38°	27°	48°	1716
12/31/81-1/1/82	70°	43°	0°	28°	1716
1/1-1/2/82	70°	35°	220°	360°	1717
1/3-1/4/82	-22°	-33°	330°	344°	1717
1/5/82	-28°	-43°	310°	324°	1717
1/5/82	-24°	-33°	227°	268°	1717
1/10-1/11/82	-31°	-37°	210°	221°	1717
1/13/82	15°	-24°	112°	143°	1717
1/21-1/26/82 (Polar)	70°	55°	38°	114°	1717
1/26-1/27/82	-10°	-40°	13°	41°	1717
1/29/82 (Polar)	-59°	-70°	0°	16°	1717
1/31-2/1/82	-22°	-41°	313°	339°	1718
1/31-2/10/82	70°	18°	193°	332°	1718
2/3-2/4/82	11°	1°	285°	292°	1718
2/7-2/10/82	-28°	-41°	190°	250°	1718
2/15-2/16/82	5°	-30°	116°	147°	1718
2/18-2/25/82	70°	40°	0°	101°	1718
2/23/82	6°	-23°	23°	44°	1718
2/23-2/24/82 (Polar)	-62°	-70°	13°	38°	1718
2/26-3/2/82 (Polar)	70°	58°	300°	360°	1719
3/6-3/12/82	70°	30°	160°	260°	1719
3/6-3/7/82	-29°	-36°	230°	250°	1719
3/8/82	-30°	-39°	210°	227°	1719
3/9-3/13/82	-25°	-47°	174°	208°	1719
3/13-3/14/82	8°	-26°	133°	155°	1719
3/20-3/22/82	14°	-27°	29°	68°	1719
3/24/82	-38°	-30°	12°	23°	1719
3/28-4/11/82	70°	33°	130°	315°	1720
4/7-4/13/82	-18°	-52°	97°	203°	1720
4/10-4/11/82	20°	- 3°	126°	153°	1720
4/13-4/15/82 (Polar)	-56°	-70°	62°	117°	1720
4/17-4/18/82	17°	-16°	31°	52°	1720
4/27/82	24°	-14°	274°	292°	1721
4/28/82	54°	29°	258°	276°	1721
4/29-1/30/82 (Polar)	70°	60°	220°	262°	1721
5/4-5/9/82	-21°	-47°	122°	203°	1721
5/4-5/7/82 (Polar)	70°	55°	174°	202°	1721
5/11-5/15/82	12°	-34°	40°	98°	1721
5/22-5/24/82 (Polar)	70°	57°	280°	320°	1722
5/25-5/28/82	57°	- 3°	220°	280°	all one 1722
5/29-6/1/82 (Polar)	70°	48°	165°	220°	1722

Table 1 (continued)

CORONAL HOLES FROM Hα SYNOPTIC CHARTS (FROM 10830A PHOTOS)

DATE(S) OF OCCURRENCE	NORTH LATITUDE BOUNDARY	SOUTH LATITUDE BOUNDARY	EAST CARRINGTON BOUNDARY	WEST CARRINGTON BOUNDARY		ROTATION
5/31-6/5/82	-30°	-53°	113°	193°	all	1722
6/6-6/8/82	13°	52°	83°	113°	one	1722
6/6-6/8/82 (Polar)	70°	62°	80°	117°		1722
6/9-6/10/82	-13°	-38°	50°	74°		1722
6/11-6/13/82	24°	- 3°	5°	50°		1722
6/19-6/25/82	70°	-10°	218°	307°		1723
7/1-7/9/82	-15°	-60°	25°	160°		1723
7/8-7/11/82	34°	- 5°	0°	60°		1723
7/9-7/11/82 (Polar)	70°	60°	3°	39°		1723
7/19-7/20/82	12°	-14°	238°	276°		1724
7/20-8/6/82	70°	23°	8°	263°		1724
7/26-8/7/82	-16°	-57°	8°	175°	all	1724
8/6-8/8/82 (Polar)	-57°	-70°	0°	30°	one	1724
7/29/82	16°	8°	134°	139°		1724
8/3/82	16°	6°	57°	66°		1724
8/7-8/8/82	27°	18°	0°	23°		1724
8/10/82	- 7°	-14°	325°	334°		1725
8/15/82	14°	6°	261°	276°		1725
8/17-8/26/82	70°	23°	112°	252°		1725
8/24-9/3/82	-17°	-60°	0°	162°	all	1725
8/31-9/3/82 (Polar)	-60°	-70°	0°	66°	one	1725
9/4/82	22°	13°	366°	4°		1725/1726
9/7/82	- 9°	-15°	321°	332°		1726
9/8-9/9/82	38°	27°	292°	317°		1726
9/11-9/12/92	27°	8°	254°	271°		1726
9/14-9/25/82	70°	25°	70°	240°		1726
9/14/82	- 6°	-21°	212°	235°		1726
9/20/82	-18°	-33°	142°	157°		1726
9/21-9/29/82	-15°	-56°	33°	138°		1726
9/28-10/1/82 (Polar)	-56°	-70°	0°	52°	all	1726
9/24-9/25/82 (Polar)	-56°	-70°	78°	101°	one	1726
10/4/82	-14°	-17°	325°	336°		1727
10/5-10/6/82	-10°	-18°	283°	317°		1727
10/2-10/7/82 (Polar)	-46°	-70°	285°	360°		1727
10/5/82	43°	38°	304°	311°		1727
10/8/82	25°	- 4°	283°	274°		1727
10/11-10/14/82	42°	20°	180°	243°	all	1727
10/14-10/28/82	70°	45°	0°	196°	one	1727
10/11/82	- 6°	-17°	222°	235°		1727
10/18-10/28/82	-20°	-60°	0°	153°	all	1727
10/23-10/28/82 (Polar)	-60°	-70°	0°	90°	one	1727
10/20/82	24°	17°	106°	113°		1727

the period covered is October 7, 1978 to November 11, 1982 (minus Feb. 1980 for which photographs were not available); only data through August 31, 1982 was used for comparison purposes, since the modeled UV data ends on that date. Out of these 1366 days, there were 649 days (48%) when coronal holes were positively identified; that number incresed to 828 days (61%) when holes which were classified as possible, probable or polar were included. Polar holes were identified as coronal holes which occurred between $\pm 70^{o}$ and $\pm 45^{o}$. They were not included with positively identified holes because it is assumed that coronal holes at those latitudes have less influence than those at lower latitudes; holes classified as polar ended at $+70^{o}$ because coronal holes exist above that latitude for very long periods of time (D.F. Webb, et al. 1984), but probably would have little influence on the UV peak variation ratio. Table 2 shows one possible effect of coronal holes; that these coronal holes might enhance the plage area seen and used in the modeled UV, thereby causing the model to over-estimate the observed UV, especially on solar rotations where large plages dominate the solar disk. The values in table 2 are a comparison between coronal hole occurrence and ratios of modeled UV flux to observed UV flux computed for days when large plages existed and possibly affected the UV model. There is no obvious indication from this that coronal holes enhance the effects of a large plage area in any way, but by looking at the the table another question arises--why are coronal holes conspicuously absent on days when the large plages dominate the solar disk? The very number of coronal holes found would suggest that their absence and appearance would be evenly distributed over these days if they are of no importance to the model; perhaps it is their absence which is the most important.

TABLE 2

Julian Date of modeled UV Peak	Ratio of Modeled UV/ Observed UV	Coronal Hole present
1978		
338	0.73/1	yes
1979		
51	2/1	no
77	1.75/1	no
156	1.24/1	no<PH>
187	1.23/1	no
237	1.71/1	no<PH>
268	0.95/1	no<PH>
317	1.44/1	no
343	1.44/1	no
1980		
127	2.44/1	no
173	1.98/1	no
283	3.76/1	yes<SM>
339	2.03/1	yes<LG>
349	1.48/1	no
1981		
208	1.38/1	no
292	2.19/1	no
316	1.90/1 questionable due to photo	yes, but
343	1.44/1	no
1982		
32	1.75/1	no<PH>
169	3.63/1	no
199	1.57/1	no
222	1.59/1	yes<VSM

* There is a coronal hole present which ends before Ca K observations were made; SGD reports indicate no plage at 200^{o} longitude.

<PH>=Polar Holes present
<SM>=Small hole
<VSM>=Very small hole

A comparison of dates of the occurrence of peaks on the observed UV and the modeled UV with the occurrence of coronal holes also does not conform to what would be expected, based on the number of coronal holes which were present during the entire study. Table 3 is a list of the dates when the NIMBUS-7

Table 3

	NIMBUS-7 OBSERVED UV PEAK DATE	CORONAL HOLE PRESENT	J.LEAN MODELED UV PEAK DATE	CORONAL HOLE PRESENT	PEAK VARIATION RATIO VALUE
1978					
	338	YES	346	NO	0.806241
1979					
	26	YES	26	YES<SMALL>	1.405483
	36	@NO	51	NO	2.125138
	62	NO<POLAR>	67	NO	--------
	78	NO	77	NO	1.537725
	90	NO	93	NO	0.606188
	106	*NO	104	NO	1.355198
	119	NO<POLAR>	119	NO<POLAR>	1.229608
	133	NO	131	YES	0.849280
	145	NO<POLAR>	147	NO<POLAR>	--------
	158	NO	156	NO	1.245862
	185	NO	187	NO	1.182551
	213	NO<POLAR>	211	YES<SMALL>	0.777566
	237	NO	237	NO	1.527462
	265	NO<POLAR>	268	NO	1.314539
	291	NO	291	NO	0.934612
	317	NO	317	NO	1.421165
	345	NO	342	NO	1.463972
1980					
	34	NO	35	NO	0.604275
	49	NO	NO DATA AVAILABLE		--------
	61	NO	64	NO	1.209065
	74	YES	73	NO	0.958785
	89	NO	89	NO	0.986207
	105	*NO	102	NO	1.574567
	116	NO	116	NO	0.876020
	130	NO	127	NO	2.039944
	146	NO	146	NO	1.162417
	174	NO	173	NO	1.968915
	202	NO<POLAR>	202	NO<POLAR>	1.239638
	229	NO	227	@NO	1.171299
	250	NO	245	NO<POLAR>	2.205961
	277	NO	268	YES	0.932098
	285	NO	283	YES	3.814159
1980(cont.)					
	310	NO	297	NO<POLAR>	1.625130
	325	NO<POLAR>	326	YES<SLIGHT>	0.771144
	338	YES	339	YES	2.021159
	353	YES<SLIGHT>	349	NO	1.452897
1981					
	12	NO	13	NO	0.841307
	27	NO	32	NO<POLAR>	1.378528
	60	NO	64	NO	1.288043
	88	*NO	84	NO	--------
	100	NO<POLAR>	100	NO<POLAR>	1.379913
	124	NO	136	NO	1.321302
	148	NO	151	NO<POLAR>	0.560816
	176	NO	164	NO	1.541610
	196	NO<POLAR>	195	NO<POLAR>	1.291961
	208	NO<BAD DATA>	208	NO<BAD DATA>	1.406158
	236	NO	239	YES	0.694730
	247	NO	250	NO<POLAR>	0.603193
	264	YES	263	NO	1.619956
	276	NO	273	YES	0.650861
	291	NO	292	NO	2.195279
	304	NO	316	YES	1.756951
	344	NO<POLAR>	343	NO	1.483193
1982					
	31	YES<SMALL>	32	YES	1.508909
	59	NO<POLAR>	63	NO<POLAR>	0.833382
	89	YES	88	NO<POLAR>	0.856853
	102	NO<POLAR>	102	NO<POLAR>	1.056986
	114	NO	115	NO	0.769998
	141	NO	142	NO<POLAR>	--------
	169	YES	169	YES	2.572222
	197	NO	199	NO	1.669886
	223	NO	222	YES<SMALL>	1.584921

* CORONAL HOLE APPEARS MUCH LATER IN THE DAY THAN UV OBSERVATIONS WERE MADE

@ UV OBSERVED LATE IN THE DAY; CORONAL HOLE DIED OUT VERY EARLY THAT DAY

<POLAR> MEANS A CORONAL HOLE EXISTED AT THE POLE(S) THAT DAY BUT NOT AT LATITUDES BELOW +45° OR ABOVE -45°

observed UV flux and the modeled UV flux peaked, the corresponding peak variation ratio for the approximately 27 day time period of minimum to peak to minimum temporal variations, and an indication of whether or not a coronal hole was present at the time of the peak. Since the date listed in the table of coronal holes indicates passage of a specific carrington longitude past CMD it is slightly misleading to suggest that no coronal holes existed on that date at all; it is appropriate, however, to assume that an influence of coronal holes would be greatest when they occur at low latitudes, towards the center of the sun (Webb, et al., 1984). Therefore if coronal holes were to influence the values obtained through the UV model, it would certainly be best to ascertain whether the hole was positioned above some area important to the model; converting the positions of the many coronal holes to fit the coordinates given for the many plages and then comparing their relative positions on the sun on a daily basis is not, however, a viable alternative within the limited time and scope of the present study.

3. Conclusions

The results of Table 3 can be summarized as follows:

1.) Four of the sixty-four time rotations have coronal holes present on the day(s) that both UV flux values peak; the two flux values peak together twice, and the observed UV peaks one day before the modeled UV twice. The ratio of peak variation for these four rotational periods all are greater than the mean of 1.356 and the median of 1.321 for the entire data set. This indicates that during these time periods the model is over-estimating the UV even more than normal, two of the cases have a ratio of variation greater than two.

2.) Five of the sixty-four time periods have coronal holes present on the day that the NIMBUS-7 observed UV peaks but not on the day of the model peak, of these the modeled UV peaks before the observed UV four times. The other rotation has the observed UV peak preceding the modeled peak by eight days, so must be disregarded for our purposes. Three of the five time periods have peak variation ratios less than one which indicates that the model is under-estimating the observed UV for that peak; the other two rotations have values greater than the mean and median for the data set, indicating greater over-estimation than normal.

3.) Nine of the sixty-four rotational periods have coronal holes in evidence on the day the modeled UV peaks but not on the day that the observed UV flux peaks. The peaks of the two UV data sets fall within three days of each other for all but two of these rotations. The two have a nine and twelve day separation between the peak values and so are likely exhibiting a thirteen day variability in one data set and not the other. Six of the nine cases have peak variation ratios less than one, so the model is under-estimating the UV in those cases, the others have ratios above one, all above the mean and median for the entire data set, and one rotation in 1980 has the largest ratio of variation in the entire data set. The model is vastly over-estimating the UV in that case.

4.) There are 44 cases out of the total of sixty-four where there is not a hole present for either of the two peaks. Of these 44 cases there are four with no peak variation ratios calculated because the minimums in the two data sets did not match up well enough. Ten of the other forty cases have values

less than one which means the model is under-estimating the peak at that point; thirty have the model over-estimating the observed UV flux. The thirty cases which are over-estimating the UV flux have a mean of 1.487; the group of forty rotations as a whole have a mean peak variation ratio of 1.306 which is slightly less than the mean for the entire data set, meaning a slightly better fit to the observed data. Three cases where the UV peaks much later than the modeled UV have a very large peak variation ratio, (>2.0/1), although all three cases represent over-estimation of the peak greater than the mean. Out of the remaining 37 rotations, nine have the peaks of both UV flux values occuring on the same day and all but one are cases of the model over-estimating the observed flux; the one that is not has the model very nearly matching the observed UV flux with a peak variation ratio of 0.986. The other 28 rotations have peak values separated with a variety of numbers of days.

(References for this appendix can be found in chapter 8.)